Imaging of Fuel Cell Diffusion Media Under Compressive Strain

By

Joseph Lechnyr

A THESIS

Submitted in partial fulfillment of the requirements

for the degree of

Master of Science in Mechanical Engineering

MICHIGAN TECHNOLOGICAL UNIVERSITY

2009

This thesis, "Imaging of Fuel Cell Diffusion Media Under Compressive Strain" is hereby approved in partial fulfillment of the requirements of the Degree of Master of Science in Mechanical Engineering.

Department of Mechanical Engineering - Engineering Mechanics

Advisor: ______________________________
Jeffrey Allen

Committee Member: ______________________________
Reza Shahbazian-Yassar

Committee Member: ______________________________
Jaroslaw Drelich

Department Chair: ______________________________
Professor William W. Predebon

Date: ______________________________

ABSTRACT

The gas diffusion layer (GDL) inside a proton exchange membrane fuel cell serves several functions including removal of water, conducting electrons, and protecting the membrane. These functions can be affected by the compression that fuel cells are subjected to during assembly. Compression can change the conductivity and damage the coating, reducing the water management capabilities. These changes may lead to flooding and lowered overall performance of the fuel cell. In order to study the physical damage caused to a GDL under compression, a test fixture was designed and fabricated which allows for a known pressure to be applied to the GDL while simultaneously imaging the GDL in a scanning electron microscope (SEM). This allows the compression effects on fibers and the coating materials to be observed at various strains. This fixture also allows for the stress and strain applied to the GDL to be measured. The measured stress appears to be heavily influenced by the friction between the GDL and the compressing plates.

ACKNOWLEDGMENTS

I would like to thank my advisor Dr. Jeffrey Allen for his assistance and guidance in completing this project. He has given me a deeper appreciation of the work involved in a reasearch project. I would also like to thank the MNiT research group for their assitance and Dave Fritz in particular for the help he provided in collecting the data and organizing the results.

CONTENTS

LIST OF FIGURES

LIST OF TABLES

1. INTRODUCTION

A proton exchange membrane fuel cell (PEMFC) is an electro-chemical device which uses hydrogen and oxygen to convert energy cleanly and efficiently. Before this next generation technology is ready for commercial markets as a viable power source, many concepts and improvements need to to be better understood. Characterizing the components inside fuel cells can lead to improvements, and of all the components inside the cell, none serve as many critical purposes as the gas diffusion layer (GDL). Figure 1.1 shows several types of GDL material imaged with a scanning electron microscope (SEM).

Components such as the bipolar flow field plates and electrolyte (membrane) have dual purposes, providing a path for the fuel and current, as well as facilitating the reaction of hydrogen and oxygen to release energy, respectively. The GDL, however, has multiple roles; it is a current collector; as the electrons are released by the hydrogen, the GDL must conduct them to the electrode and out through the circuit. The gas diffusion layer must distribute reactants to the catalyst layer, so porosity is an important factor. The GDL protects the membrane from damage by the bipolar plates, or the flowing reactants.

The diffusion layer also plays a large role in water management. The GDL must be hydrophobic to transport the product water out of the cell; if the water is not removed, the cell can begin to flood which limits the supply of reactants and lowers the overall output and efficiency of the fuel cell.

One area of interest in the literature is characterization of the mechanisms by

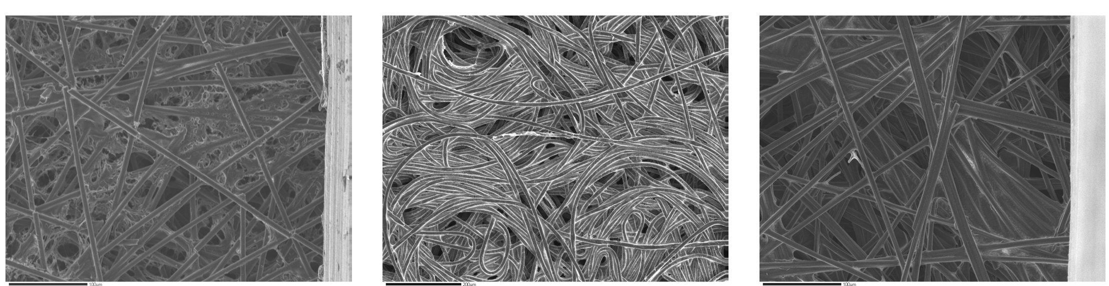

(a) (b) (c)

Figure 1.1. Examples of GDL structures imaged by SEM at 250x magnification; (a) Mitsubishi MRC 105 9% PTFE with MPL, (b) Freudenberg with MPL, and (c) Toray TGD-H-060 9% PTFE wet-proofed.

which a GDL is damaged from the compression of the fuel cell stack. Compression is necessary to seal the fuel cell and prevent leakage of the reactants. This compression may cause the GDL to intrude into the flow channels of the bipolar plates, reducing the cross-sectional area of the channels and increasing the presure drop and reducing the flow of reactants. Compression can also break fibers in the GDL; these fibers can intrude into the membrane damaging the material causing voltage loss and inefficiency due to fuel crossover.

The GDL is coated with polytetraflouroethylene (PTFE) which is used to give it a hydrophobic character. This coating can be damaged by compression, which changes the wettability. These changes can reduce the hydrophobicity of the material by damaging and removing the coating, and lead to less transport of water and eventually the flooding of the fuel cell.

GDL damage has been investigated by a number of researchers. Nitta et al. [1] tested several parameters of GDLs under compression and found that the conductivity under the channels increased, creating localized areas of increased conductivity across the GDL, which can affect the overall cell performance. Wang and Liu [2] also found that outside of the high current density region, the area under the rib structures conducts better due to compression. Damage of the GDL was shown by Su et al. [3], however, since the pressure used during this experimentation is not reported, it can be difficult to develop any sound conclusions about the damage that was reported. Several authors have studied the effect of compression damage on GDLs using compression ratios rather than pressures. [4, 5] Bazylak et al. [6] lists the pressure used and has images from the experiment, concluding that the damage caused holes in the hydrophobic coating which created pathways for water transport. Escribano et al. [7] began profiling the material characteristics of various GDLs and includes some stress response data among other characteristics, with his main conclusion being the need for further research into the material properties. Fekrazad [8] generated a 2-D model of the fuel cell, and concluded that the clamping pressure reduces electrical resistance and permeability and the pressure can affect the internal temperature difference of the fuel cell, this result is opposite of what the authors above have shown. Feser et al. [9] also experimentally tests the in-plane permeability and also notes the decrease with increased strain on the GDL. Cross-sectional images of the GDL compressed by the rib structure on a flow plate are shown in the work of Lim and Wang [10], the difference between the areas is quite severe. This work only looks at the cross-section and only lists the compression ratio applied. Lin et al. [11] look at MPL preperation and note that their new method of hot-rolling the MPL onto the GDL increases the mass transport through the layer, SEM imaging reveals that their new layer has more cracks and voids allowing tranport and better performance. Distribution of current density due to compression and contact resistance of the GDL and catalyst layer was studied by Nitta et al. [12], the conclusion being this resistance is more important then believed and the compression may cause large variations in resistance.

2. EXPERIMENTAL METHOD

The objective of this project is to compress the GDL and image the resulting damage. This damage can then be correlated to the pressure and strain applied to the sample. To achieve this correlation accurate force and strain measurements are necessary, as well as the ability to maintain the pressure while the sample is imaged.

In order to obtain the pressures and image the GDL, two fixtures were developed. The first fixture is the aluminum compression fixture, which applies a known load and allows for imaging inside the SEM, this will be referred to as the SEM mount. The SEM mounts are limited to a maximum diameter of 3.175 cm and height of 2.159 cm. This mount is shown in figure 2.1; it has a base plate where the GDL samples are placed. This base plate has a channel which runs across the plate in one direction. Above this plate is a ring which compresses the samples. The bottom face of this middle ring also has a channel running through in one direction. The ring can thus be oriented to either place this channel directly above the bottom channel or rotated so three combinations are created, one with no channel above or below the sample, one with a channel above the sample but not below, and one with a channel below the samplebut not above. This allows a more accurate modeling of the conditions inside a fuel cell. To apply a known force to the GDLs, springs are placed in insets on this ring with another ring placed on top of the springs. Six screws run through the assembly holding the rings and springs in place and allowing the whole assembly to be compressed. As the screws are tightened, the two rings will be displaced differently based on the displacements of the GDL samples and the springs. The displacement of the springs combined with known spring constants allows for the compressive force to be determined. This force is being applied evenly over the bottom ring and is as such, easily related to the force the GDL samples are receiving. The displacement of the middle ring is the displacement of the GDL directly.

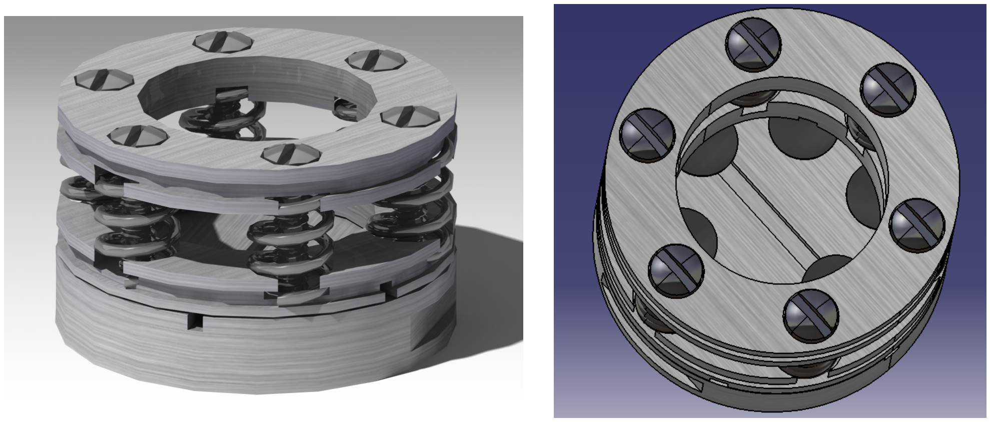

Side View Top View

Figure 2.1. CAD rendered views of the SEM mount

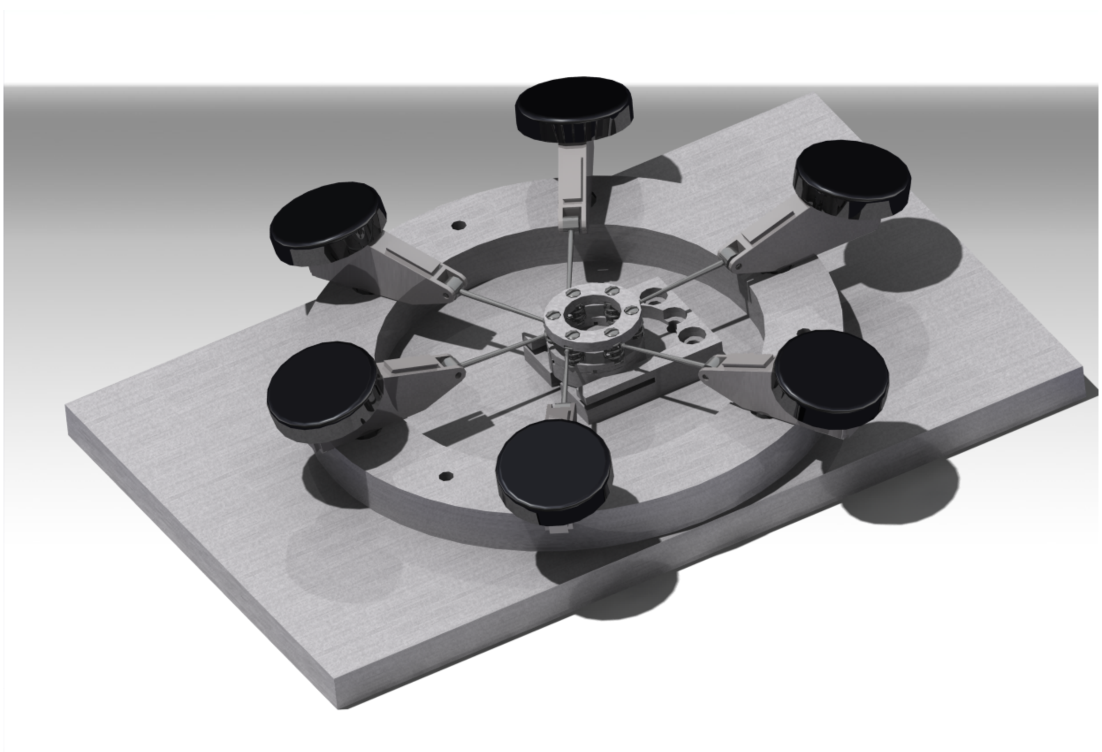

Figure 2.2. Test Dial indicator fixture with SEM mount located in middle.

A fixture to measure the displacements of the individual SEM mount rings was designed and built, this will be referred to as the measurement fixture. A CAD representation of the measurement fixture is shown in figure 2.2. This aluminum measurement fixture had a base with slots which allowed the SEM mount to slide in and be held in one alignment to prevent twisting. Around this base are a series of

Table 2.1. List of initial thicknesses and types of GDLs tested

GDL Type	Initial Thickness
Mitsubishi MRC 105 9% PTFE w/ MPL	257. μm
Freudenberg with MPL	290. μm
Toray TGD-H-060 9% PTFE	320. μm

dovetail mounts for six Starrett test dial indicators (model 709ALZ). These indicators are placed in contact with the rings of the SEM mount, with three indicators evenly spaced around each ring. As the screws are tightened, the dials are easily read and the displacements determined. This setup of dial indicators also ensures that the rings are being evenly compressed, to prevent excessive force on one side of the mount. A thin plastic shim is inserted under the SEM mount to prevent any motion laterally. This shim also allows for easy removal of the sample without applying pressure to the sides and possibly changing the effective forces on the GDL.

The goal of imaging samples on the SEM mount imposed several constraints, the most difficult being size. A large mount could not be inserted into the microscope. A maximum height constraint for the SEM mount prevents the use of larger springs. The springs selected were chosen due to small size and a high spring constant, to allow for higher forces and pressures to be applied to the samples. Up to six samples can be compressed at the same time. If all six GDL samples are placed on the mount a force of up to 67.8 N can be applied. The springs are currently calibrated using an Instra - MET/Sintech computer controlled tester.

The pressure can be varied on the samples by changing how much of the sample is under the compressing ring; the ring is wide enough to cover an entire GDL sample if desired. The GDL samples are prepared by taking a sheet of the bulk material and punching out small 6.35 mm diameter circles. This method of creating small samples keeps damage localized at the edges and produces less damage when compared to other separation techniques. The samples created this way have an average area of 30 mm^2. Table 2.1 lists the GDLs that were tested as well as their initial thicknesses.

A JEOL-6400 SEM was used for imaging and was set to 10keV accelerating voltage. The samples conduct well enough that no gold sputtering is needed to increase the conductivity. This also eliminates any error or false positives that the gold coating might provide. The size of the image is set at 1028 pixels, and at least 25 samples per pixel. Close imaging of the samples was done at 250x magnification, this magnification is close enough to see features of the fibers and binder, but provides a larger viewing area of the GDL.

3. COMPRESSION DAMAGE

Several points of interest have emerged through the testing. The first is that the damage being caused is easily visible at very low magnifications. The boundary of where the ring and channel edges pressed down onto the sample is shown in figure 3.1. The top shows the inside edge of the ring, while the channel can be seen running perpendicular to the ring's edge. The material on the left edge is carbon paint which is used to secure the sample and ensure good conductivity for imaging. The dark spots on the sample are caused by charging effects. This is likely dust which is highly non-conductive causing the material to charge and the contrast to hide the features in the surrounding areas of the particle. Another example is figure 3.2, which shows the same material, however this sample had no channels above or below and thus has only the curved interface from the ring running down the middle.

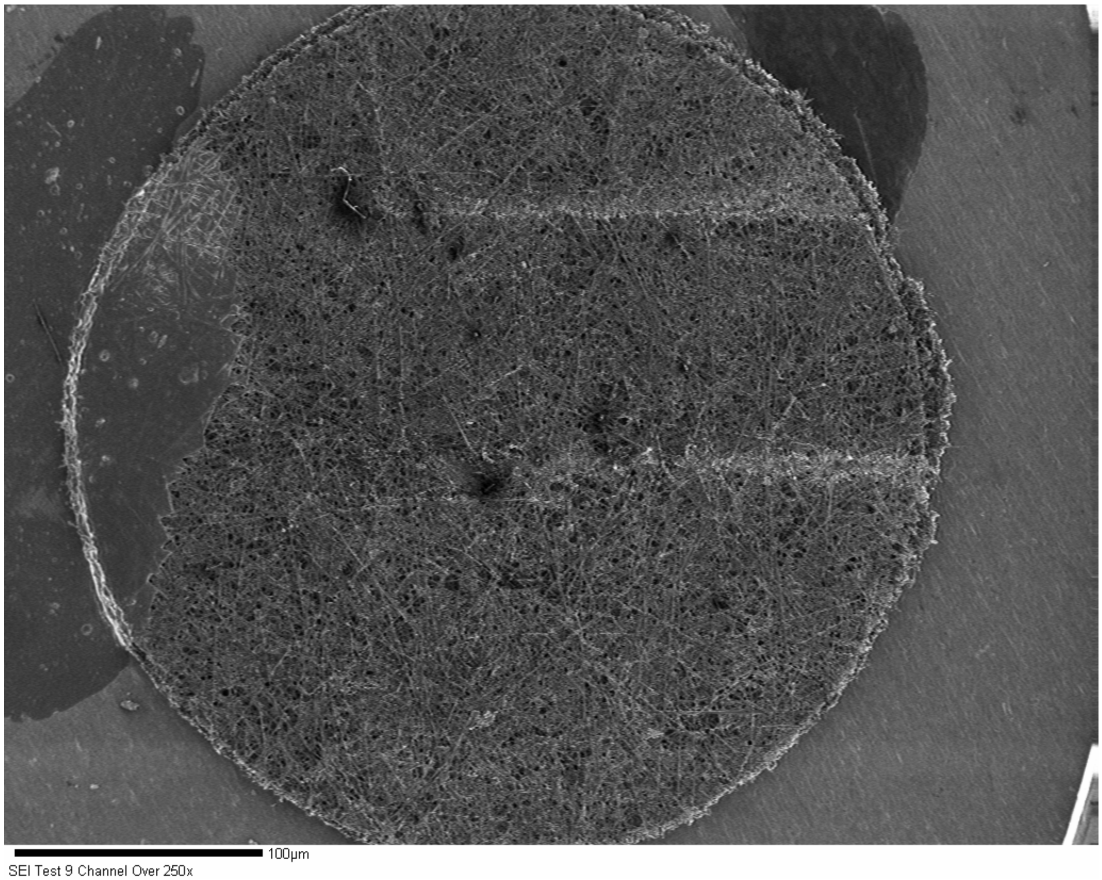

Figure 3.1. 14x view of Mitsubishi MRC 105 9% PTFE with MPL after compression. The channel location is visible on the sample.

Another noticeable result of the fibers being moved or destroyed is the change in conductivity. A charging pattern is observed in locations where a fiber pulled loose or was removed. Figure 3.3 shows a Freudenberg sample at the end of compression, with a channel above pressing onto the flat plate, imaged at 250x magnification, compared to figure 3.4 which is the same sample and area imaged at the same magnification after the compression ring was removed. Several fibers can be seen as missing with a charging remnant left behind where the fibers used to be located. The arrows indicate one such fiber that can be seen in figure 3.3 but is missing in figure 3.4. Another example is figure 3.5, where the fiber running vertically in the middle has shifted to the left, leaving behind charging in its previous location. This figure is a Freudenberg GDL with no channels above or below the sample.

Figure 3.6 shows another interesting feature, the damage appears more apparent approximately 70 microns inside from the edge of the ring. The left-most line in the image shows where the compressing ring edge was located, a line of damage is visible a small distance to the right of this edge, where the second line is located. The GDL in this image is one of the Mitsubishi MRC 105 samples and is imaged at 250x

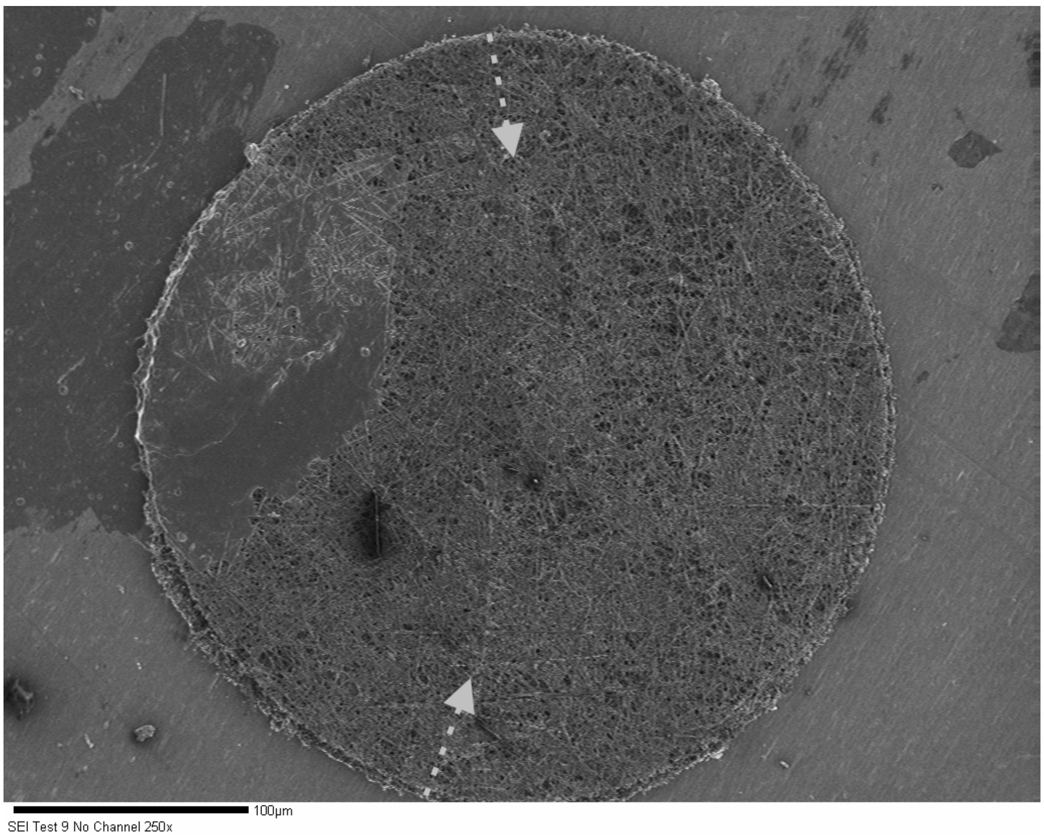

Figure 3.2. 14x view of Mitsubishi MRC 105 9% PTFE with MPL after compression, the sample was compressed with a solid surface (no channel), dashed line superimposed to highlight damaged boundary.

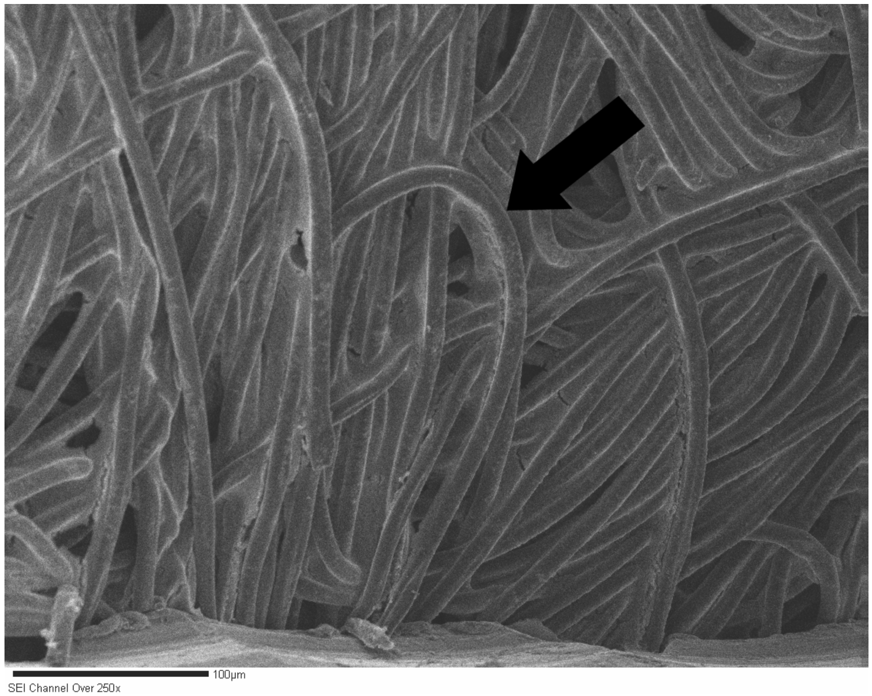

Figure 3.3. 250x view of Freudenberg with MPL during compression, the inside edge of the channel can be seen along the bottom.

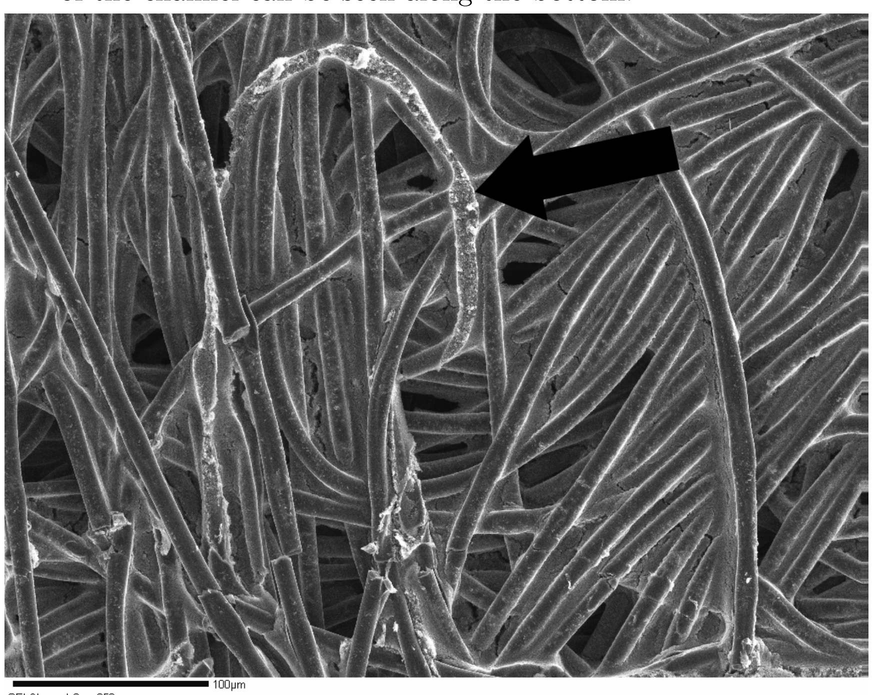

Figure 3.4. 250x view of Freudenberg with MPL after compression, the channel has been removed to release the pressure.

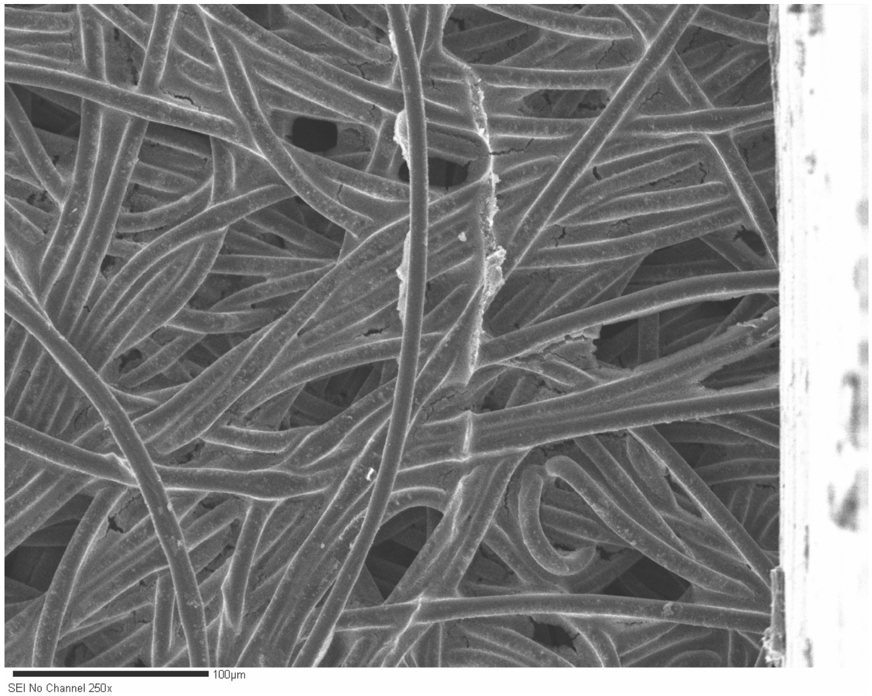

Figure 3.5. 250x view of Freudenberg with MPL during compression, the sample was compressed with a solid surface (no channel).

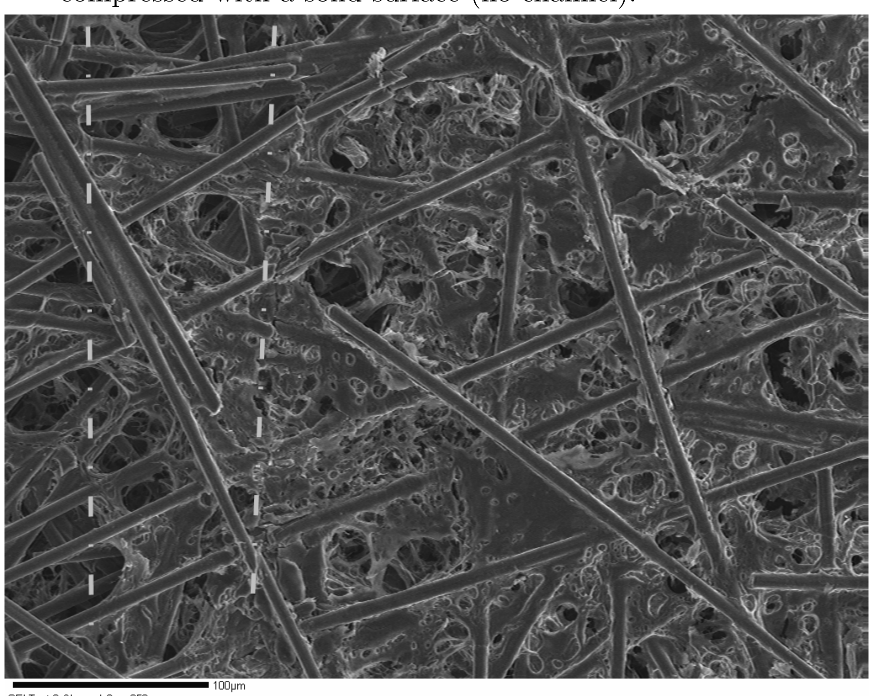

Figure 3.6. 250x view of Mitsubishi MRC 105 9% PTFE with MPL after compression, dashed lines superimposed to highlight areas of interest.

magnification, the sample is located on the mount with no channels above or below the GDL and imaged after releasing the pressure. Such damage as fibers fracturing or moving from one compression to another has been observed. In addition the binder and/or PTFE material between fibers appears less porous after the compression.

4. STRESS-STRAIN BEHAVIOR

The strain is determined by reading the test dial indicator measuring the middle ring's displacement. This displacement is then divided by the initial thickness of the GDL as measured using a micrometer. The stress is calculated using the force and area of the samples. The force is calculated using the difference in displacements of the test dial indicators, this difference is then multiplied by the calibrated effective stiffness of the springs. The area under compression is calculated from the images of the sample before compression and while under compression. The area that is uncompressed is then subtracted from the overall area of the whole sample to determine the compressed area.

Figure 4.1 shows the stress strain curves for four compression tests. The curve labeled 1 is the initial compression test, with six single samples arranged around the SEM mount and incrementally compressed. This curve is also when the Freudenberg images in Appendix E were captured. The six samples had approximately half their area under compression. In an effort to verify this data another compression test was performed, curve 2. This test used only four single samples arranged with no channels affecting the samples, and with the entire samples under compression. A significant difference is observed, but the overall slope of the curves are very similar.

Another set of compression tests was performed to check repeatability and these are curves 7 and 8. These tests were run again with four new single samples with the entire sample under compression. Curve 7 is the inital compression of the samples, the pressure was then relieved and reapplied to create curve 8. The curves fall on top of each other and curve 2. This would seem to indicate that either the edge of the ring caused the change or that the samples were pre-stressed unintentionally or an error in zeroing the strain for the first test caused the shift.

This data raised a concern about friction and how it may be affecting the stress data. As a plate presses down the areas in contact with the plates experience friction which prevents the free radial expansion of the material and extends a small distance into the sample. [13] In a thin material this area, known as a "dead zone", can run all the way through the sample. This causes the forces observed to be increased due to overcoming the friction in addition to compressing the material. Several of the common methods of reducing friction, such as hydraulic bulge testing and spherical indentation, could not be used due to the goal of imaging the samples while under compression. Another common method of reducing friction's role is to stack multiple layers of the material to provide a large height over diameter ratio, H/D. This allows

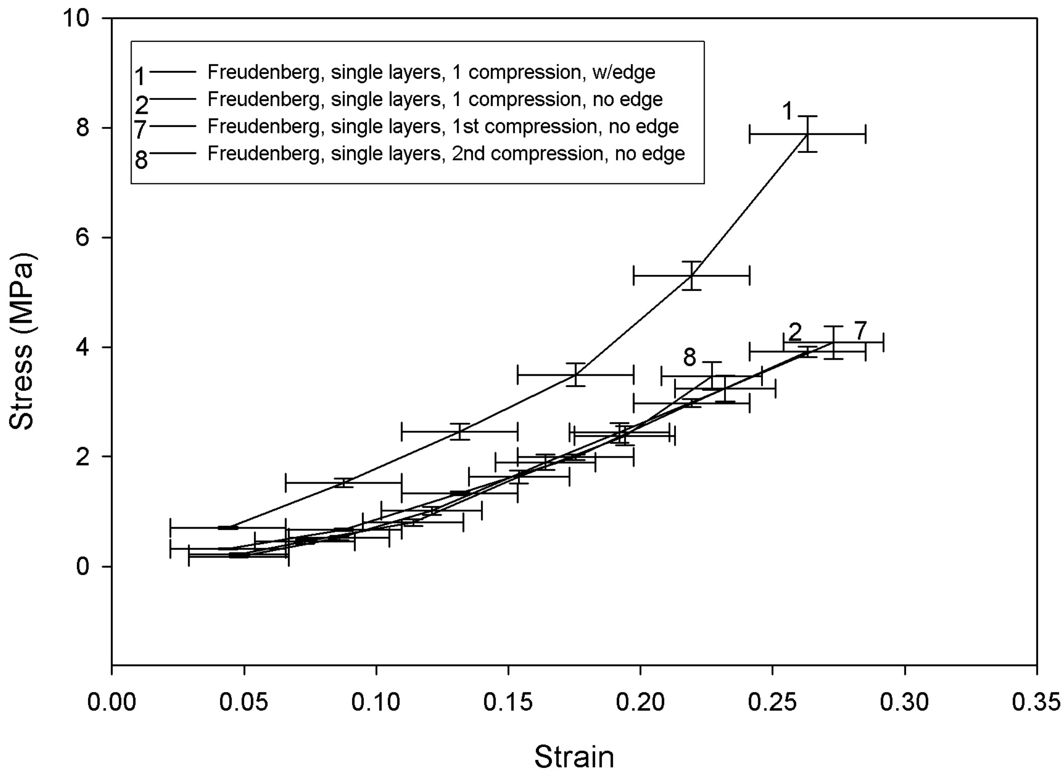

Figure 4.1. Stress-Strain curves of compression tests using a single layer of the Freudenberg with MPL.

the material to compress similar to large bulk material tests and prevents the "dead zone" from extending the entire distance through the sample. The target of stacking would be raising the H/D ratio to at least two or three, the constraints of the current system however limited this test to a ratio approximately equal to one.

Using four stacks of twenty Freudenberg GDLs each, the stress strain curves in Figure 4.2 were recorded. The curve marked 3 is the initial compression, with the other curves being recompressions in the labeled order. The last two compressions, labeled 5 and 6, had only half the area compressed compared to the whole area for the first two compressions. The re-compressed curves follow very similar trends while the first curve is very different from the others. This large difference is likely partly due to settling of the samples into each other as the initial force is applied to the samples. The stack of GDLs started with an overall height of 6.70 mm, or 0.335 mm for each GDL. After the first compression test was run the thickness was again measured and had decreased to a stack size of 4.9 mm, or 0.245 mm thick for each GDL. The following compressions did not change the thickness of the GDLs. The interesting result from this is that the stacked samples have a higher slope than the single layer of samples and can be seen in Figure 4.3. This is interesting as the elastic modulus would be expected to drop if the friction force was indeed reduced.

The stacked samples were examined in an effort to explain the increase in force required. It was observed that the samples held together without any external force when removed from the mount. This prompted an examination of the damaged GDLs inside the SEM. Most of the area appeared as previously discussed, fibers broken and shifted very similar to the single layer. Examination of the microporous layer (MPL) side however showed heavy damage. Figure 4.4 shows an image of an undamaged MPL on a Freudenberg GDL and Figure 4.5 shows the damage observed after the stacked compression. The majority of the lines are indentions created by the fibers in the sample below and this can be seen more clearly in Figure 4.6. This indenting and locking of the fibers can help explain the low slope in the initial compression as the fibers are embedded into the soft MPL, and the increase in stiffness. As with the fibers embedded, they are not free to expand laterally. Thus, rather then reduce friction this embedding may cause an increase in the friction between each sample.

A concern with the GDLs was that they may exhibit a tendency to creep when left under compression for a period of time. This is worrisome due to the desire to image while under compression. Four single samples of Freudenberg with MPL were left under a moderate compression for a twenty-four hour period with all the test dial indicators in place and zeroed. When checked after this period the dials still read zero, confirming that the Freudenberg GDLs did not creep while under compression. This also alleviates concerns that the rate of compression may affect the damage and pressures needed to compress the samples.

Figure 4.7 shows the preliminary results from a single incremental compression test performed on the Mitsubishi MRC 105 9% PTFE with MPL and Toray TGD-H-060 9% PTFE wet-proofed GDL materials. Both tests were performed with six single

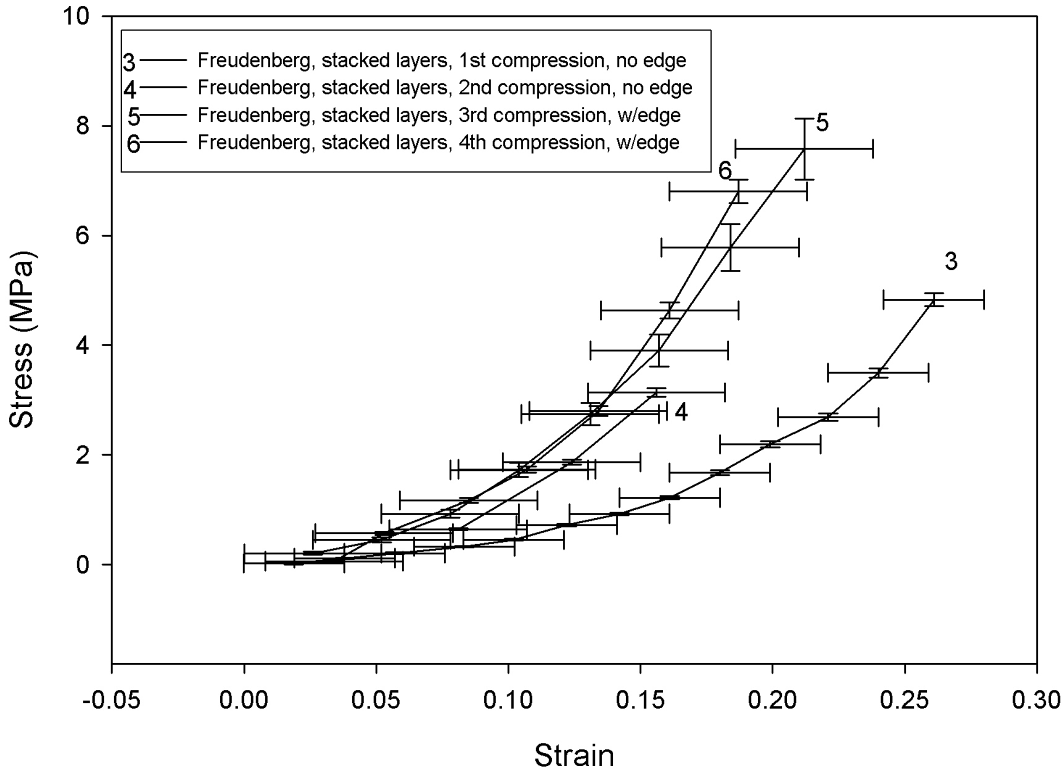

Figure 4.2. Stress-Strain curves of compression tests using stacked layers of the Freudenberg with MPL.

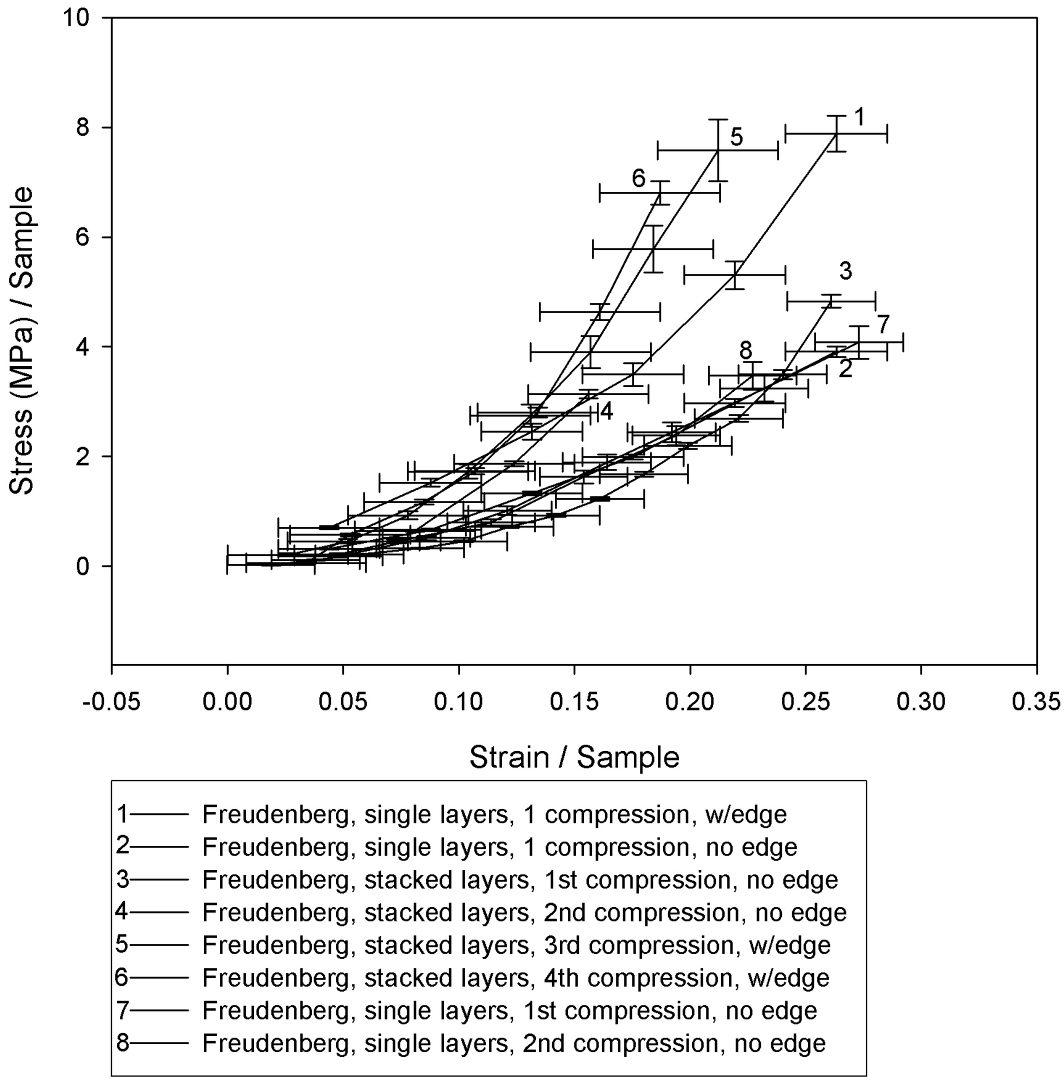

Figure 4.3. Stress-Strain curves of several compression tests using the Freudenberg with MPL.

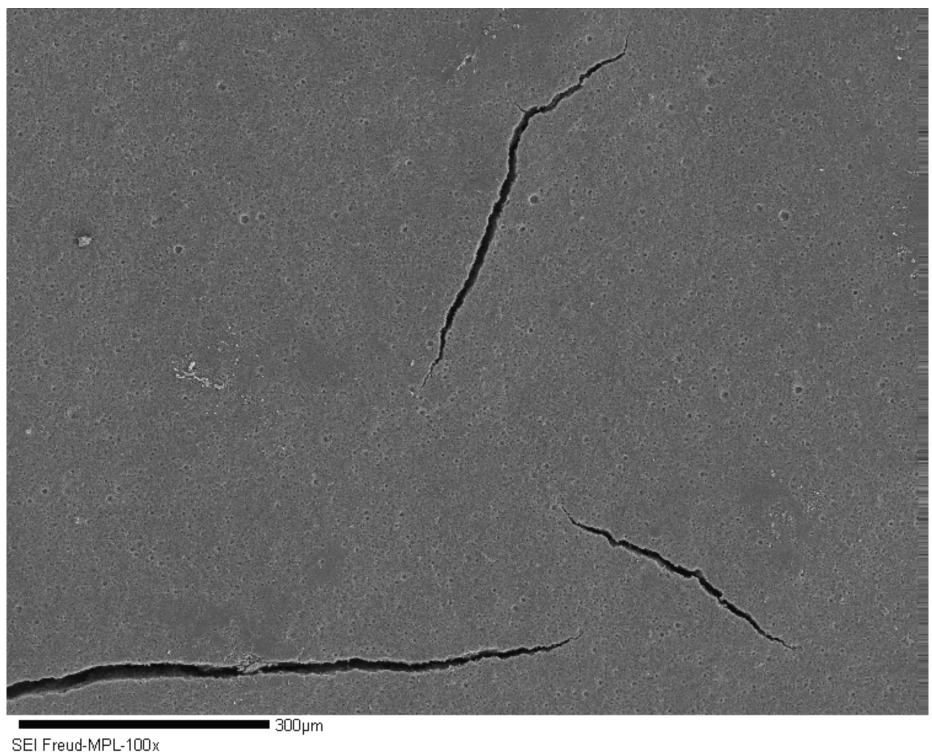

Figure 4.4. SEM image of undamaged MPL on a Freudenberg with MPL at 100x magnification.

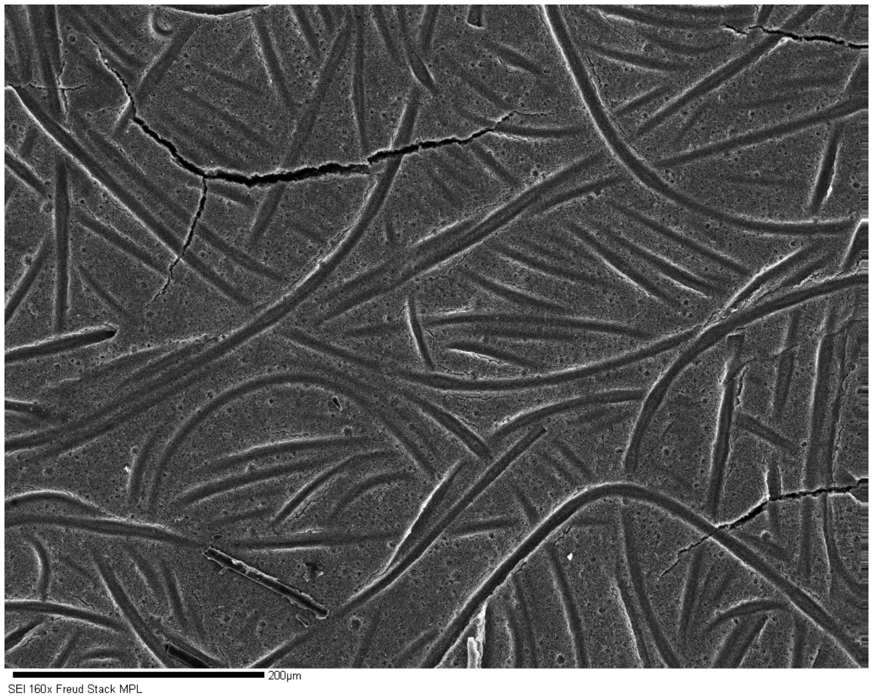

Figure 4.5. 160x magnification SEM image of the damage caused inside the stack of GDLs on the MPL of a Freudenberg GDL.

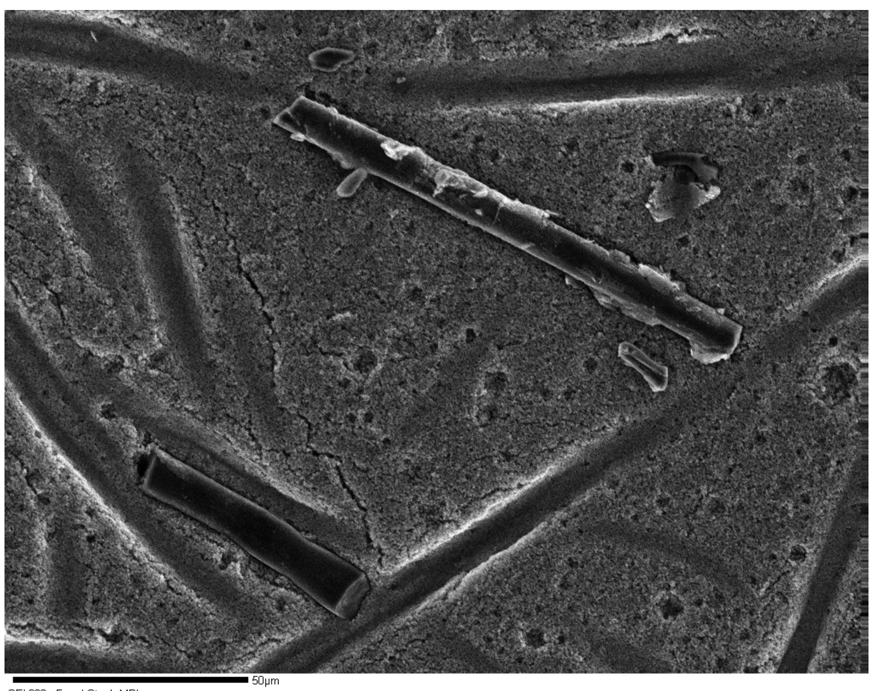

Figure 4.6. 600x SEM image of the damage caused inside the stack of GDLs on the MPL of a Freudenberg GDL.

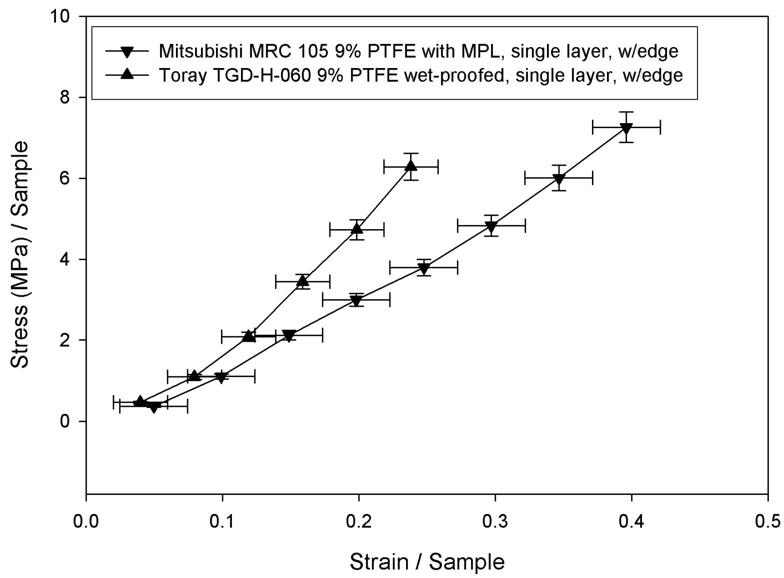

Figure 4.7. Stress-strain curves of Mitsubishi MRC 105 9% PTFE with MPL, and Toray TGD-H-060 9% PTFE wet-proofed, from an incremental compression test.

samples, arranged with the ring pressing into the middle, compressing about half of the sample. A recent paper by Kleemann et al. [14] used a different fixture to eliminate friction and determine the compressive properties of Toray GDL. This fixture used two cylindrical bearings to support the paper while a third bearing displaces the paper in the middle. Their results are shown in Figure 4.8. A significant difference is seen between the data. The journal data has a shallower slope and a significant change in the slope after an amount of strain. General Motors (GM) also provided stress-strain data for the Toray and Freudenberg GDLs [15], and the average stress-strain from these experiments are plotted along with GM's data and the Kleemann data in Figure 4.9.

There are significant differences between all the sets of data. The Freudenberg data from GM shows a steeper slope than the results determined experimentally. The Toray data shows more variance as the data here shows a higher stiffness than either Kleemann et al. [14] or GM, while the Kleemann et al. [14] and GM data share a smiliar slope but have a significant offset in the strain. All of the Toray data reported is from the TGD-H-060 type of GDL. Some of this is likely due to where and how the strain is zeroed in the test. The other major difference is how all the tests are performed. The mount used to compress the GDLs was discussed previously, similarly the Kleemann et al. [14] test method is mentioned above, while General Motors uses a hydraulic press to compress a one inch diameter sample incrementally [16]. The differences between the tests and the results indicates that something,

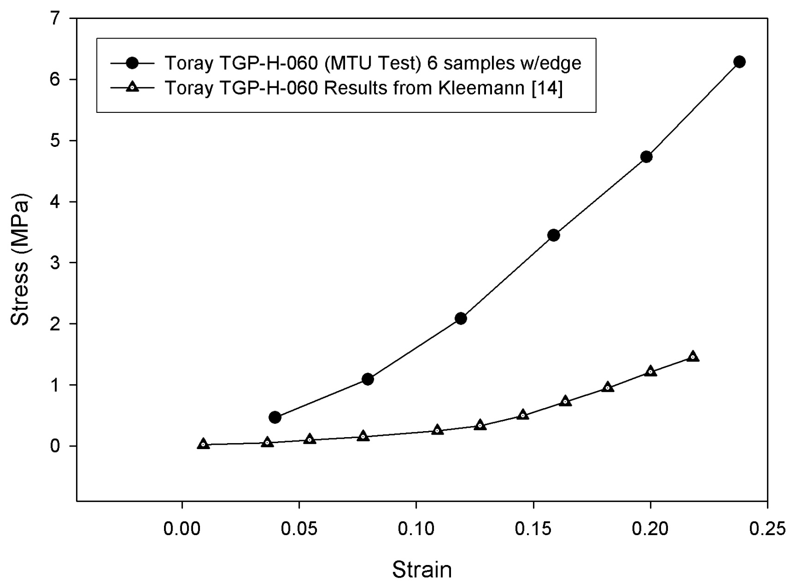

Figure 4.8. Stress-strain curves of Toray TGD-H-060 9% PTFE wet-proofed against Toray TGD-H-060 from Kleemann et al. [14].

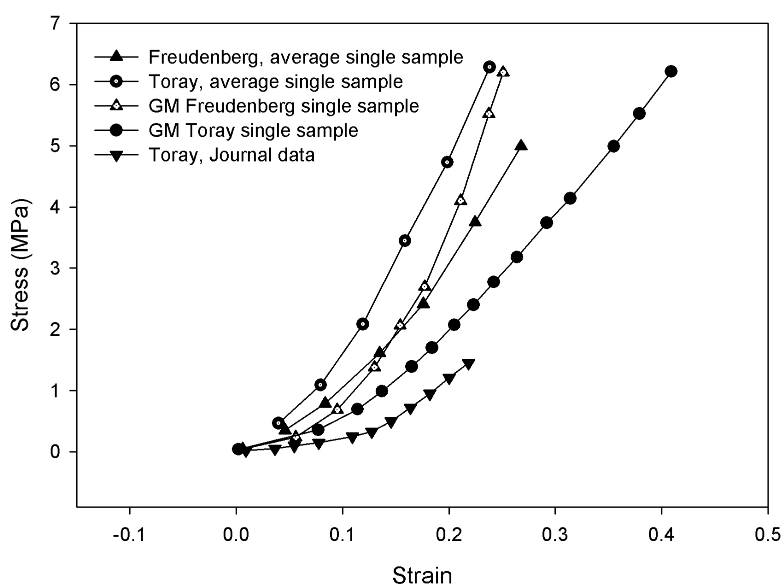

Figure 4.9. Stress-strain curves of Toray TGD-H-060 and Freudenberg GDLs.

possibly friction, is affecting the results between the various tests.

Another important finding in the Kleemann et al. [14] paper is the measurement of the Poisson ratio. A stack of five GDLs were compressed and the lateral and compressive strains measured, which leads to the determination that the Poisson ratio is zero. This value could indicate that friction may not affect the compression much, as with no lateral expansion there would not be a friction force to affect the compression. However the embedding of the fibers in the stack tests presented above could prevent lateral expansion and thus provide a false value for the Poisson ratio.

What this testing has shown is that the method of testing the compressive properties of GDLs must be examined in closer detail. The discrepencies between various methods and the possibility of friction heavily influencing the data further indicate the need for more research into testing methods.

5. CONCLUSIONS

A SEM sample compression mount and measurement fixture was designed, built, and tested and has the ability to compress the GDL, maintain the compression, and allow imaging of the samples while under compression. This imaging can be done along the interfaces between compressed and uncompressed regions, and inside channels by tilting the mount. The mount succeeded in the goal of imaging the damage, and simulating the structure inside a fuel cell. Fibers were seen as cracking near edges and shifting due to increasing the compression. The shifting of the fibers also left behind a remnant that does not conduct as well as the bulk GDL, this could be from breaking the fiber or leaving some of the coating behind. The edges of the compressing ring also appear to cause damage a small distance inwards from the edge.

Due to friction forces that could be present in the compression of a thin sample, the forces calculated during compression may be inaccurate. This friction can dominate the measured force and reduces the usuable data on compression to just the displacement and strain of the GDL. An attempt to limit the friction by stacking multiple samples showed that the stress increased rather than decreased and an embedding of the fibers into the MPL helps explain this. The differences in stress-strain data from different experiment techniques indicates the need to determine the role of friction and the most effective method of determining the true stiffness.

The strain data is useable, and with further testing, the damage observed in the imaging tests can be correlated to the strain. This correlation can then be combined with other studies with regards to other characteristics such as conductivity to determine what damage is useful or harmful to overall performance. This information can then be used to design the GDL to achieve the characteristics desired based on the compression of the fuel cell.

APPENDIX

A. EXPERIMENTAL UNCERTAINTIES OF STRESS-STRAIN DATA

The error involved in the pressure and strain measurements, was calculated using simple propogation of error. The derivation for the strain error is shown below, with the equation for strain given in equation A.1, ϵ is strain, Δx is the displacement of the GDL, and th is the initial thickness of the GDL. Taking the partial derivative of the strain leads to equation A.2. [17] The δ terms are the partial derivative terms.

$$\epsilon = \frac{\Delta x}{th} \tag{A.1}$$

$$\delta\epsilon = \sqrt{\left(\frac{\delta\epsilon}{\delta\Delta x}\delta x\right)^2 + \left(\frac{\delta\epsilon}{\delta th}\delta th\right)^2} \tag{A.2}$$

Using equation A.1, the relationships given in equations A.3 and A.4 are developed and allow substitution into equation A.2, leading to equation A.5.

$$\frac{\delta\epsilon}{\delta\Delta x} = \frac{1}{th} = \epsilon\frac{1}{\Delta x} \tag{A.3}$$

$$\frac{\delta\epsilon}{\delta th} = -\frac{\Delta x}{th^2} = -\epsilon\frac{1}{th} \tag{A.4}$$

$$\delta\epsilon = \sqrt{\left(\epsilon\frac{\delta x}{\Delta x}\right)^2 + \left(\epsilon\frac{\delta th}{th}\right)^2} \tag{A.5}$$

The strain, ϵ, can be divided out of the right hand side, leading to the final error equation, equation A.6. In this relation δx is the known error of the dial indicator, δth is the known error of the micrometer used to measure the initial thickness of the GDL, and $\delta\epsilon$ is the error in the strain measurement.

$$\frac{\delta\epsilon}{\epsilon} = \sqrt{\left(\frac{\delta x}{\Delta x}\right)^2 + \left(\frac{\delta th}{th}\right)^2} \tag{A.6}$$

The derivation for the pressure error is similar to the strain with an additional term, $\frac{\delta A}{A}$, which represents the error in the area measurement. δ A is the error in the area calculation, and A is the area measured. The final error equation is equation

Table A.1. List of errors common to all tests.

Error Variable	Error Value
Test dial indicator resolution δx	$\pm$ 6.35 μm
Micrometer resolution (initial thickness) δth	$\pm$ 1.27 μm
Area measurement accuracy δA	0.3 mm
Spring calibration accuracy δk	0.80 N/mm

Table A.2. Table of spring constants after each calibration.

Spring Number	Original N/mm	3/16/09 N/mm	3/27/09 N/mm	4/13/09 N/mm
1	38.1	35.7	36.4	36.2
2	38.3	36.5	36.3	36.3
3	37.6	35.9	36.0	36.0
4	37.8	36.1	35.9	35.6
5	39.0	36.5	36.6	36.9
6	37.9	35.9	36.0	35.8

A.8, where δP is the error in the pressure calculation, Δx is the displacement of the springs, δx is the error in the dial indicators, δA is the error in determining the area under compression, A is the area under compression, k is the spring constant, and δk is the error in determining the spring constant.

$$P = \frac{F}{A} = \frac{k\delta x}{A} \tag{A.7}$$

$$\frac{\delta P}{P} = \sqrt{\left(\frac{\delta x}{\Delta x}\right)^2 + \left(\frac{\delta k}{k}\right)^2 + \left(\frac{\delta A}{A}\right)^2} \tag{A.8}$$

Table A.2 shows the spring constants measured between compression tests. The large initial change in spring constant is due to compressing the springs to near their solid length, this caused a plastic deformation in the spring, changing the constant. The other tests show some small variations in the spring constants, this is likely due to the uncertainty in the testing apparatus.

B. DATA TABLES

Table B.1. Test Data from Freudenberg GDL, single layer placed with an edge pressing down, six samples used. Compressed area is 15.278 (mm^2)

GDL Displacement (mm)	Spring Displacement (mm)	Force (N)	Strain	Pressure (MPa)	Strain Error (±)	Pressure Error (± MPa)
0.0127	0.287	10.94	0.0439	0.703	0.02193	0.026
0.0254	0.622	23.719	0.0877	1.523	0.02193	0.076
0.0381	1.003	38.241	0.1316	2.456	0.02194	0.145
0.0508	1.427	54.408	0.1754	3.494	0.02194	0.205
0.0635	2.167	82.581	0.2193	5.304	0.02195	0.259
0.0762	3.221	122.758	0.2632	7.884	0.02196	0.330

Table B.2. Test Data from Freudenberg GDL, single layer placed with no edges pressing down, four samples arranged fully under compression ring. Compressed area is 30 (mm^2)

GDL Displacement (mm)	Spring Displacement (mm)	Force (N)	Strain	Pressure (MPa)	Strain Error (±)	Pressure Error (± MPa)
0.0127	0.178	9.632	0.0439	0.32	0.0219	0.014
0.0254	0.371	20.089	0.0877	0.667	0.0219	0.020
0.0381	0.737	39.903	0.1316	1.326	0.0219	0.034
0.0508	1.107	59.992	0.1754	1.993	0.0219	0.050
0.0635	1.654	89.575	0.2193	2.976	0.0219	0.073
0.0762	2.174	117.782	0.2632	3.913	0.022	0.096

Table B.3. Test Data from Freudenberg GDL, 20 samples stacked and placed with no edges pressing down, stacked in four columns arranged fully under compression ring. Compressed area is 30 (mm^2)

GDL Displacement (mm)	Spring Displacement (mm)	Force (N)	Strain	Pressure (MPa)	Strain Error (±)	Pressure Error (± MPa)
0.006	0.012	0.644	0.019	0.022	0.019	0.012
0.013	0.066	3.586	0.038	0.119	0.019	0.012
0.019	0.116	6.298	0.057	0.210	0.019	0.013
0.028	0.181	9.838	0.083	0.328	0.019	0.014
0.034	0.251	13.607	0.102	0.454	0.019	0.016
0.041	0.400	21.744	0.122	0.725	0.019	0.021
0.048	0.513	27.858	0.142	0.929	0.019	0.025
0.054	0.676	36.730	0.161	1.224	0.019	0.032
0.060	0.929	50.429	0.180	1.681	0.019	0.043
0.067	1.213	65.875	0.199	2.196	0.019	0.055
0.074	1.488	80.815	0.221	2.694	0.019	0.067
0.080	1.932	104.903	0.240	3.497	0.019	0.086
0.087	2.669	144.897	0.261	4.830	0.019	0.118

Table B.4. Test Data from Freudenberg GDL, 20 samples stacked and placed with no edges pressing down, stacked in four columns arranged fully under compression ring and recompressed. Compressed area is 30 (mm^2)

GDL Displacement (mm)	Spring Displacement (mm)	Force (N)	Strain	Pressure (MPa)	Strain Error (±)	Pressure Error (± MPa)
0.020	0.357	19.399	0.081	0.647	0.026	0.019
0.031	1.034	56.129	0.124	1.871	0.026	0.047
0.038	1.734	94.146	0.156	3.138	0.026	0.077

Table B.5. Test Data from Freudenberg GDL, 20 samples stacked and placed with an edge pressing down, stacked in four columns arranged half under compression ring and recompressed. Compressed area is 15.85 (mm^2)

GDL Displacement (mm)	Spring Displacement (mm)	Force (N)	Strain	Pressure (MPa)	Strain Error (±)	Pressure Error (± MPa)
0.006	0.058	3.126	0.026	0.208	0.026	0.028
0.013	0.125	6.804	0.052	0.454	0.026	0.040
0.019	0.257	13.929	0.078	0.929	0.026	0.072
0.026	0.478	25.927	0.104	1.728	0.026	0.129
0.032	0.759	41.189	0.131	2.746	0.026	0.203
0.039	1.079	58.565	0.157	3.904	0.026	0.288
0.045	1.597	86.699	0.184	5.780	0.026	0.425
0.052	2.094	113.683	0.212	7.579	0.026	0.557

Table B.6. Test Data from Freudenberg GDL, 20 samples stacked and placed with an edge pressing down, stacked in four columns arranged half under compression ring and recompressed again. Compressed area is 15.85 (mm^2)

GDL Displacement (mm)	Spring Displacement (mm)	Force (N)	Strain	Pressure (MPa)	Strain Error (±)	Pressure Error (± MPa)
0.008	0.019	1.011	0.034	0.064	0.026	0.022
0.013	0.168	9.102	0.053	0.574	0.026	0.028
0.020	.342	18.572	0.085	1.172	0.026	0.042
0.026	0.507	27.536	0.107	1.737	0.026	0.057
0.032	0.817	44.361	0.134	2.799	0.026	0.088
0.039	1.353	73.460	0.161	4.635	0.026	0.143
0.045	1.987	107.891	0.187	6.807	0.026	0.209

Table B.7. Test Data from Freudenberg GDL, four single samples compressed fully under ring. Compressed area is 30 (mm^2)

GDL Displacement (mm)	Spring Displacement (mm)	Force (N)	Strain	Pressure (MPa)	Strain Error (±)	Pressure Error (± MPa)
0.016	0.098	5.532	0.048	0.178	0.019	0.017
0.029	0.286	15.538	0.086	0.518	0.019	0.040
0.041	0.560	30.386	0.121	1.013	0.019	0.075
0.055	1.048	56.911	0.164	1.897	0.019	0.140
0.064	1.347	73.138	0.192	2.438	0.019	0.179
0.078	1.791	97.226	0.232	3.241	0.019	0.238
0.091	2.255	122.418	0.273	4.081	0.019	0.300

Table B.8. Test Data from Freudenberg GDL, four single samples re-compressed fully under ring. Compressed area is 30 (mm^2)

GDL Displacement (mm)	Spring Displacement (mm)	Force (N)	Strain	Pressure (MPa)	Strain Error (±)	Pressure Error (± MPa)
0.016	0.121	6.574	0.048	0.219	0.019	0.020
0.025	0.248	13.469	0.073	0.449	0.019	0.035
0.038	0.443	24.042	0.114	0.801	0.019	0.060
0.052	0.901	48.912	0.154	1.630	0.019	0.120
0.065	1.317	71.483	0.194	2.383	0.019	0.175
0.076	1.919	104.168	0.227	3.472	0.019	0.255

Table B.9. Test Data from Mitsubishi MRC 105 9% PTFE with MPL GDL, six single samples compressed while about half under the ring. Compressed area is 14.4 (mm^2)

GDL Displacement (mm)	Spring Displacement (mm)	Force (N)	Strain	Pressure (MPa)	Strain Error (±)	Pressure Error (± MPa)
0.013	0.112	4.255	0.050	0.296	0.025	0.028
0.025	0.353	13.443	0.099	0.934	0.025	0.061
0.038	0.691	26.307	0.149	1.827	0.025	0.113
0.051	0.980	37.332	0.198	2.593	0.025	0.158
0.064	1.242	47.294	0.248	3.284	0.025	0.200
0.076	1.585	60.350	0.297	4.191	0.025	0.254
0.089	1.976	75.245	0.347	5.225	0.025	0.315
0.102	2.395	91.203	0.396	6.334	0.025	0.381

Table B.10. Test Data from Toray TGD-H-060 9% PTFE wet-proofed GDL, six single samples compressed while about half under the ring. Compressed area is 14.62 (mm^2)

GDL Displacement (mm)	Spring Displacement (mm)	Force (N)	Strain	Pressure (MPa)	Strain Error (±)	Pressure Error (± MPa)
0.013	0.178	6.777	0.040	0.464	0.020	0.029
0.025	0.419	15.974	0.079	1.093	0.020	0.060
0.038	0.800	30.496	0.119	2.086	0.020	0.111
0.051	1.321	50.342	0.159	3.443	0.020	0.181
0.064	1.814	69.124	0.198	4.728	0.020	0.248
0.076	2.410	91.874	0.238	6.284	0.020	0.330

C. STANDARD OPERATING PROCEDURE

C.1 Preparing GDL Samples

1. Choose the GDL material for testing
2. Wearing powder free latex gloves, carefully slide the diffusion media out of the protective container and use the hole punch to create the desired number of samples. (usually 4 or 6)
3. Using a pair of tweezers carefully transfer the punched samples onto the base of the SEM mount, being careful to ensure the MPL side is facing the direction needed. (usually MPL side down)
4. Depending on how much of the samples are to be compressed they should be located either towards the outer edge for more/all of the sample to be comrpessed and towards the center for less of the sample and consequently higher pressures. Figure C.1

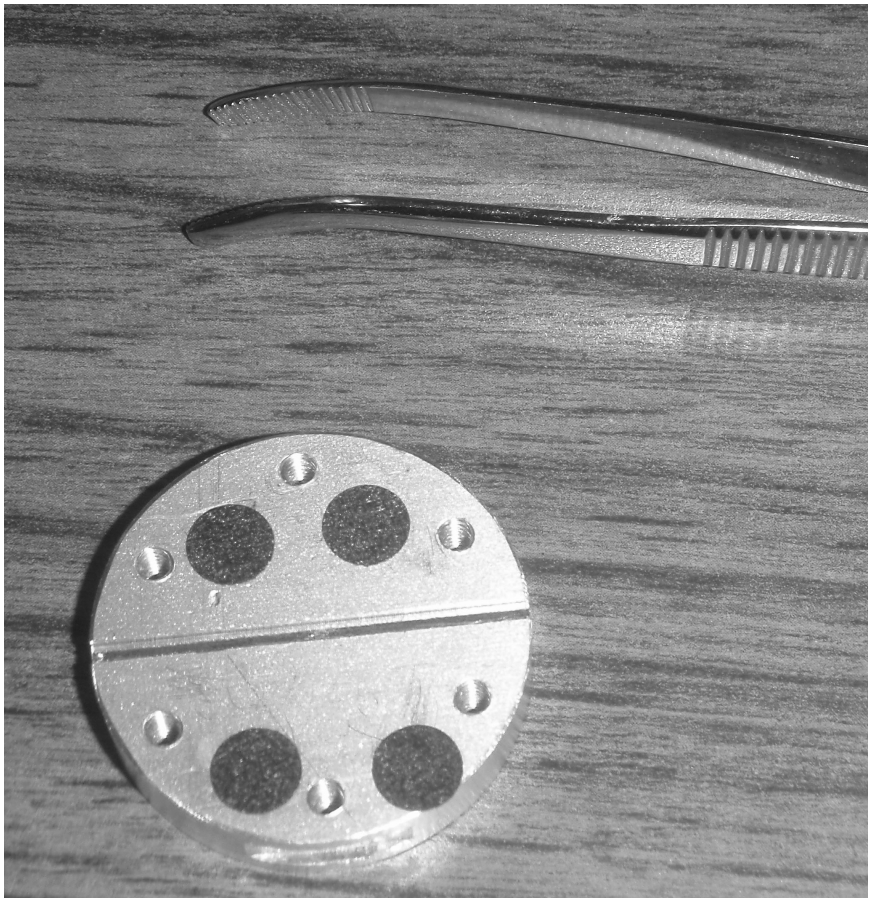

Figure C.1. Base with GDL samples placed, note lower right sample is closer to edge and would be fully covered by ring

C.2 Adding Compressing Rings

1. Prepare the rings by placing the springs into the notches in the middle ring, making sure to record the location of each spring. Figure C.2

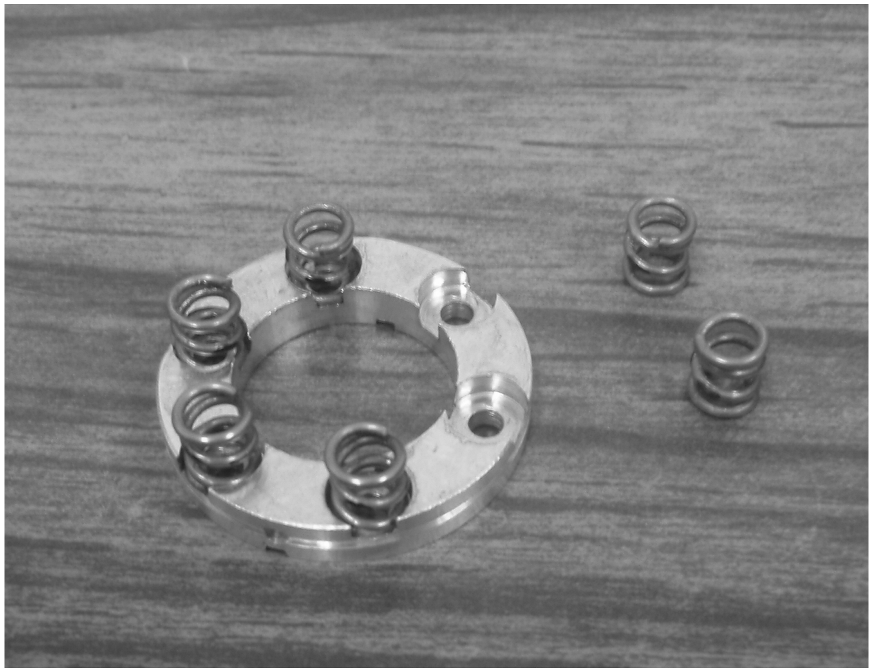

Figure C.2. Placement of springs into middle ring

2. Add the top ring and place the screws through the whole assembly. Figure C.3

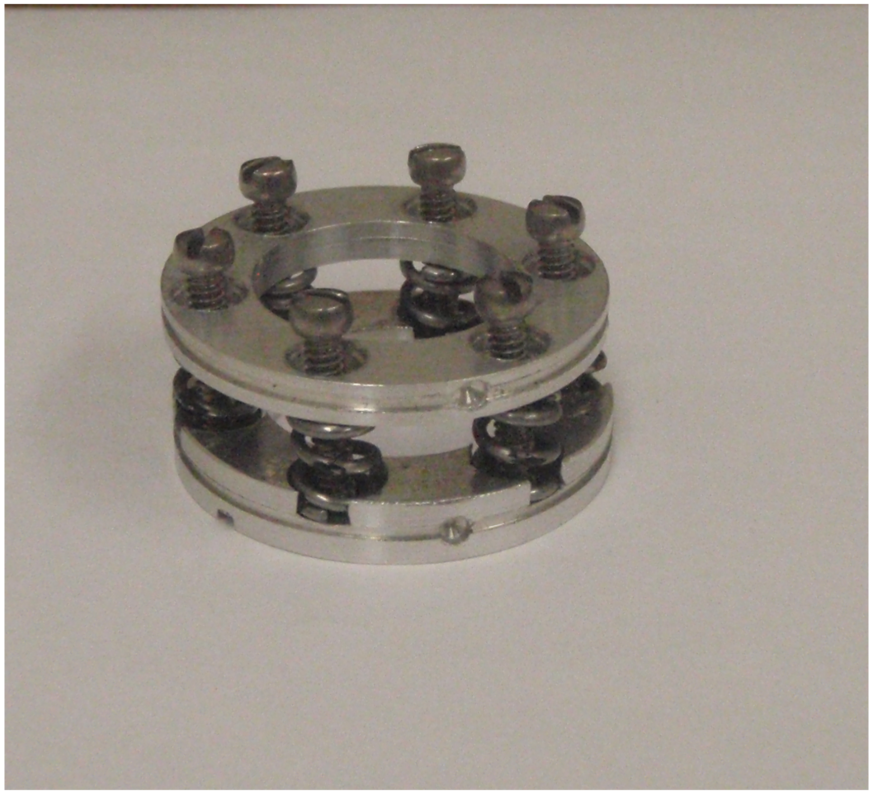

Figure C.3. Complete ring assembly, containing middle ring, springs, top ring, and screws running through both rings.

3. Place this assembly on top of the base with the GDL samples already in place.

4. Being careful not to apply extra pressure to the rings, tighten the screws until you just barely feel resistance to turning the screws. This should hold the whole assembly together with no movement but have no force being applied to the samples yet. See figure C.4

C.3 Setting up the Test Fixture

1. Place the shim stock into the mount holder, figure C.5, and then slide the SEM mount in, matching the notches on the mount with the slot on the holder. When pushing the mount in, apply pressure only to the base to prevent unknown forces being applied to the GDLs. The mount does not need to be inserted all the way to the back, only to where the fixture is secure inside the holder, figure C.6

(a) (b) (c)

Figure C.4. Total SEM mount before testing; (a) Mount with no screws tightened, (b) Mount with some screws just tightened, and (c) Mount with all screws just tightened and ready for testing

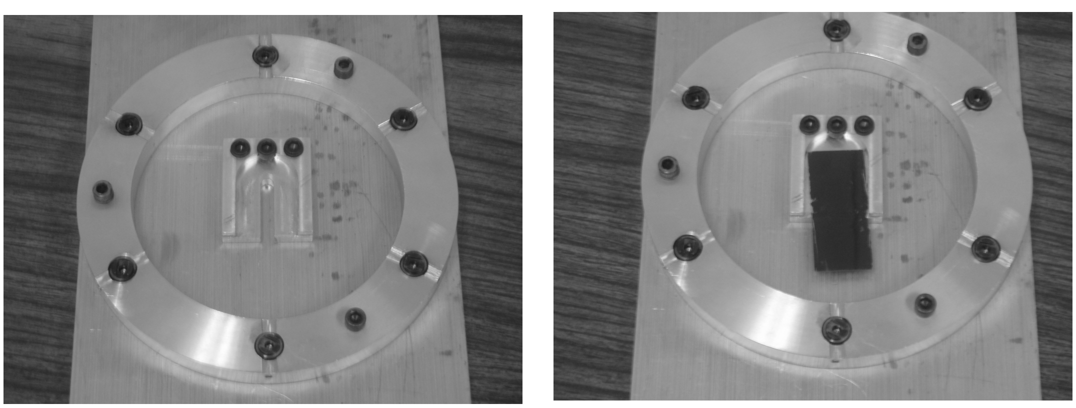

Side View Top View

Figure C.5. Base fixture with before use (left) and with shim stock placed (right)

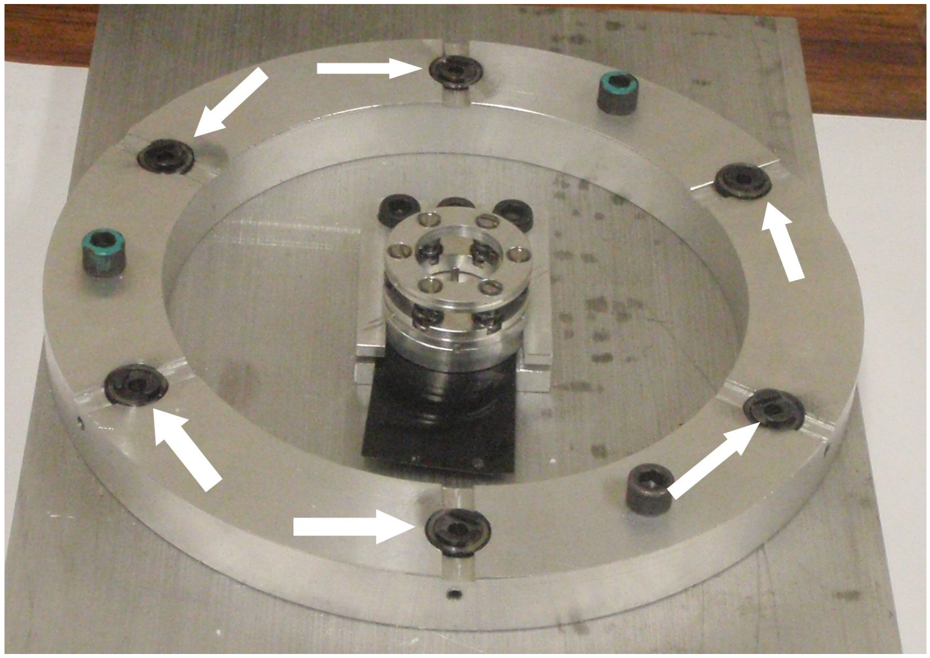

Figure C.6. Holder with SEM mount inserted into slots.

2. There are six (6) dovetail holders located around the ring of the fixture, see arrows in figure C.6, and held in place by set screws. These holders have been positioned so that the test dial indicators can be slid into the holder and are able to twist. When twisted clockwise the holder will tighten on the indicators, holding them stationary.

3. Insert the dial indicators and twist to tighten as indicated in figure C.7, positioning the tip onto the groove around each ring. The dial indicators should alternate which ring they are positioned on, with three measuring the top ring and three measuring the middle ring. The position marked "A" on figure C.8 needs to be placed on the top ring, otherwise it is possible for the indicator to stick on the screws.

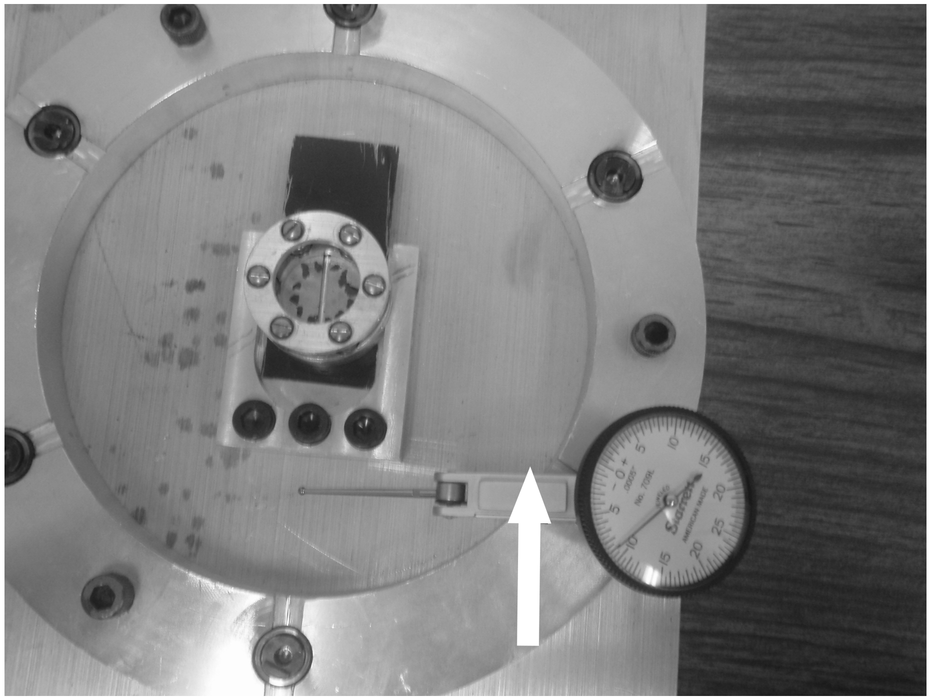

Figure C.7. Dial Indicator inserted and direction to twist indicated.

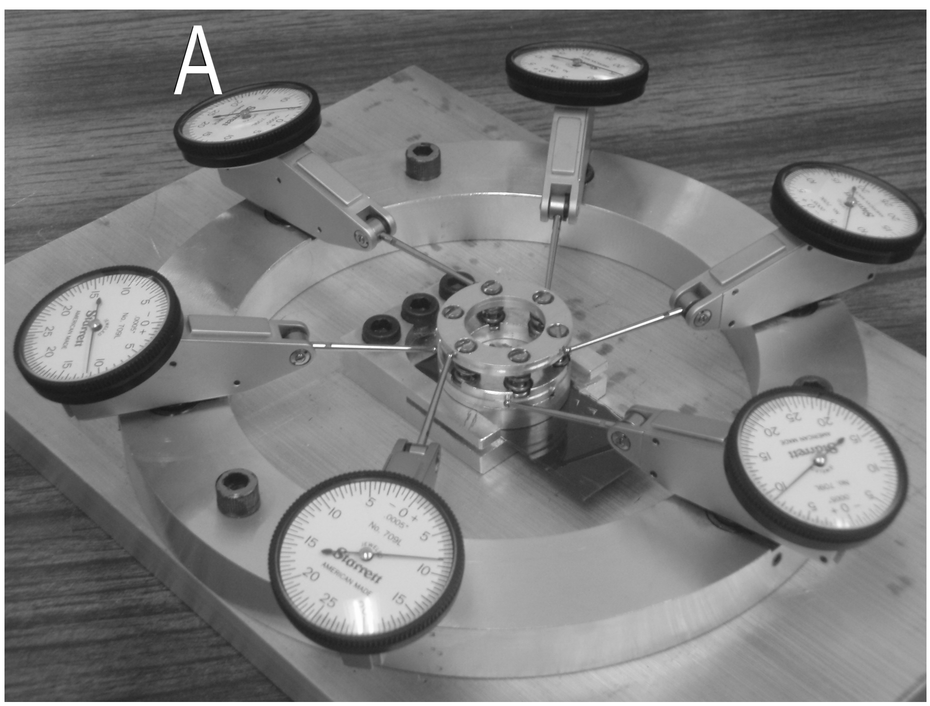

Figure C.8. Mount with all indicators positioned around, note the alternating of which ring is measured.

4. Note: when placing the indicators be sure to adjust the tips so that the indicators measuring the middle ring are already past their neutral measuring point and that the top ring indicators are very close to their upper limit of measurment. This is due to the indicators switching which direction the dial turns at the neutral point. To adjust the tips just apply firm pressure to move them farther up or down as needed.

5. When the indicators are positioned, turn the dial faces to zero all the readings, being sure to only turn these faces clockwise, as shown in figure C.9. This prevents accidently loosening the dovetail holders.

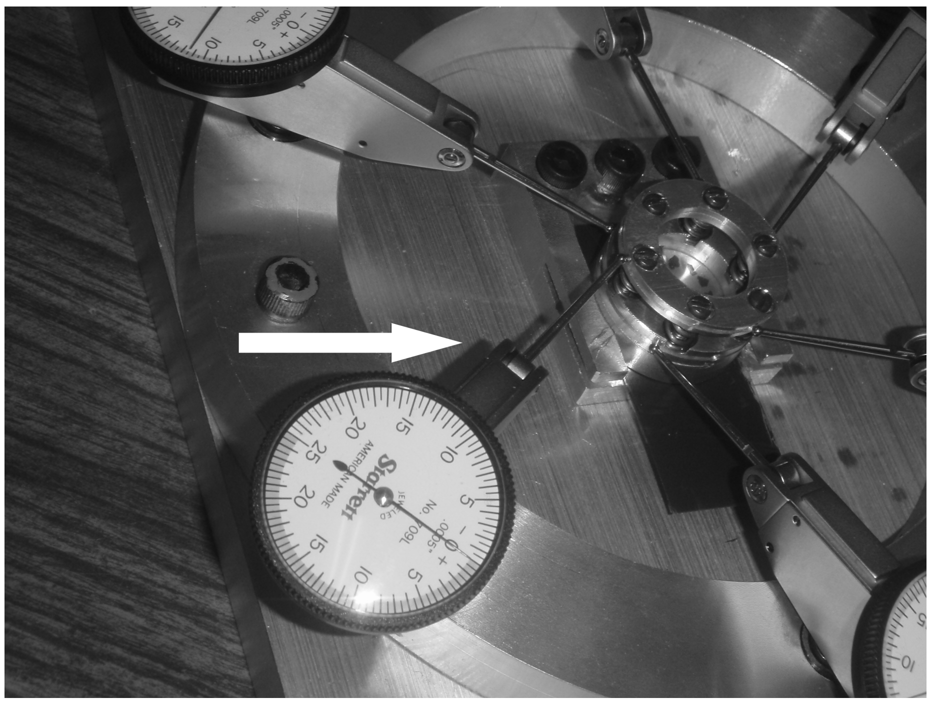

Figure C.9. Grasping the black edge of the dial, twist in the indicated direction to zero.

C.4 Applying Compression

1. Using a flathead screwdriver begin tightening the screws one at a time in an alternating pattern; begin at one screw and tighten the next on the other side of the mount, thus compressing fairly evenly. The compression should be in small increments, no larger then five thousandths of an inch before tightening the remaining screws to re-level the rings. Once level compression can be continued.

2. Once the target compression is reached, the displacements should be recorded. If imaging is desired the mount can be removed as described below, if not

continue compression as before.

3. Note: To prevent the dials reversing direction the dials should be reset at known displacements and re-zeroed. To re-zero twist the indicator counter-clockwise to remove the tip from the ring, and adjust the tip to again be farther from the neutral point, then retighten the indicator and place the tip back on the ring.

4. To remove the mount, first twist all the dials counter-clockwise so they are no longer touching the mount and are out of the way. Then slide the shim back out, this should allow the mount to be easily slid out.

C.5 Relieving Compression

1. To remove the compressing rings completely, the dial indicators should be twisted so they are no longer in contact, this prevents the displacement from accidentally maxing out the indicators. Then the screws should be un-tightened in the opposite pattern as before. Again small increments should be used to prevent overly stressing any one side of the mount.

D. IMAGE LIBRARY OF MITSUBISHI MRC 105 9% PTFE WITH MPL

D.1 Incremental Compression Imaging Results, Six Single Samples w/Edge

This run of tests was an incrementally increasing load, this test began on February 19, 2009. The accelerating voltage was 10 keV. An SGL baseline GDL was chosen and the displacement of the GDL was incrementally increased starting at 0 and increasing in increments of 12.7 μm. This increment is the smallest which can be accurately measured with the dial indicators. The tests were performed all the way to a total displacement of 108 μm on the GDL. All images taken looking into the channel pressing down were taken with a tilt on the stand of 32.4 degrees, as measured by the SEM gauge.

D.1.1 12.7 μm Compression

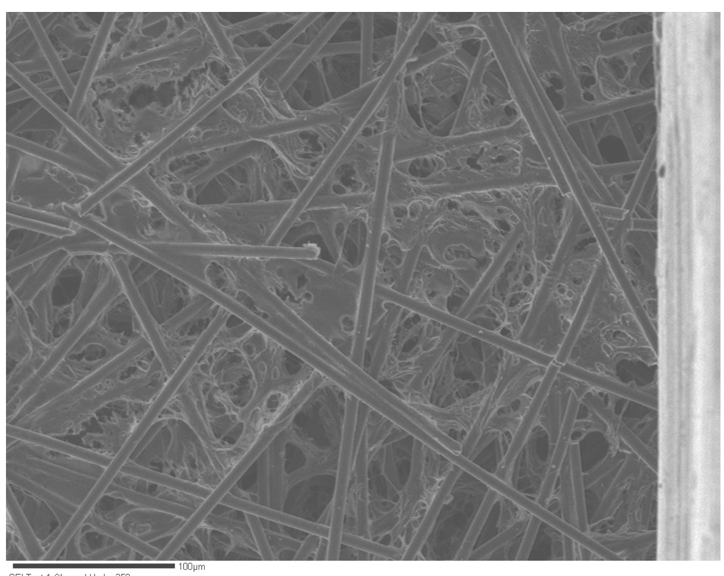

Figure D.1. This sample has a channel running underneath the GDL. This image was taken at 250x. Some damage can be seen in the area with several fibers snapped already.

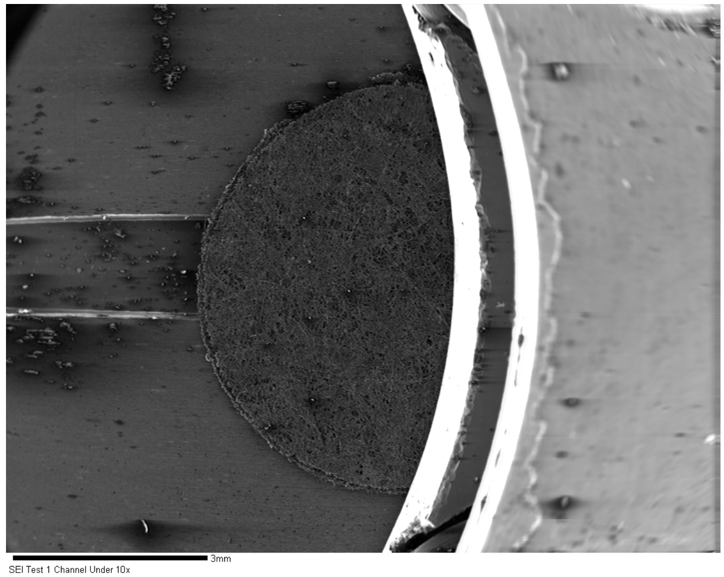

Figure D.2. This image is taken at 10x and is the same as the previous figure. The purpose of this image is to calculate what area is under compression and determine the pressure from this information.

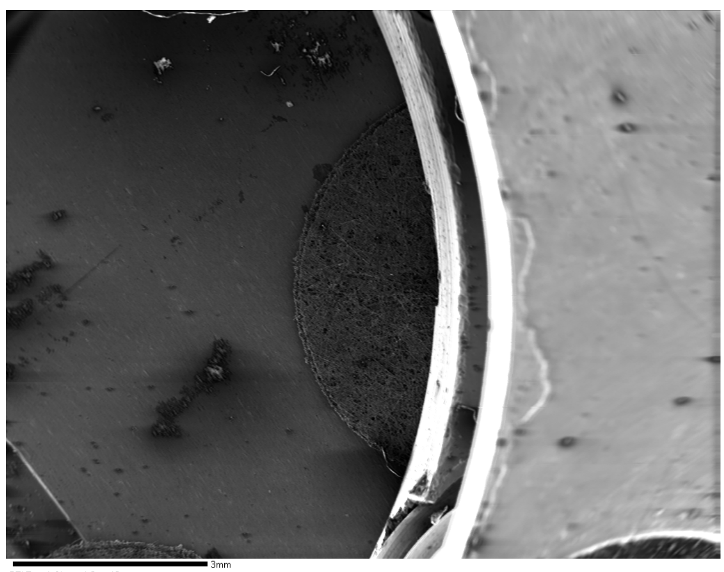

Figure D.3. This image is taken at 10x as well. This sample has a channel above the sample pressing down onto it. This channel is difficult to see in this image.

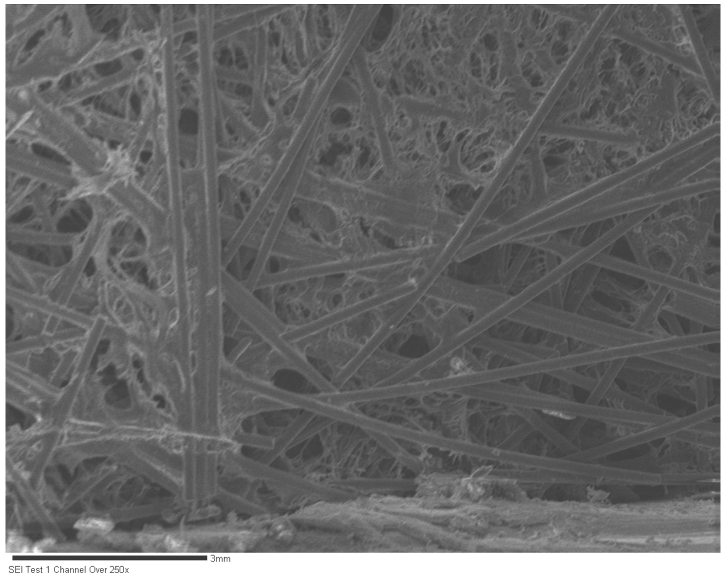

Figure D.4. This image is taken at 250x and is looking at the inside of the channel. The major damage appears to be the large fiber group on the left that is snapped at the wall as well as the fiber running along the bottom which is bent along the wall.

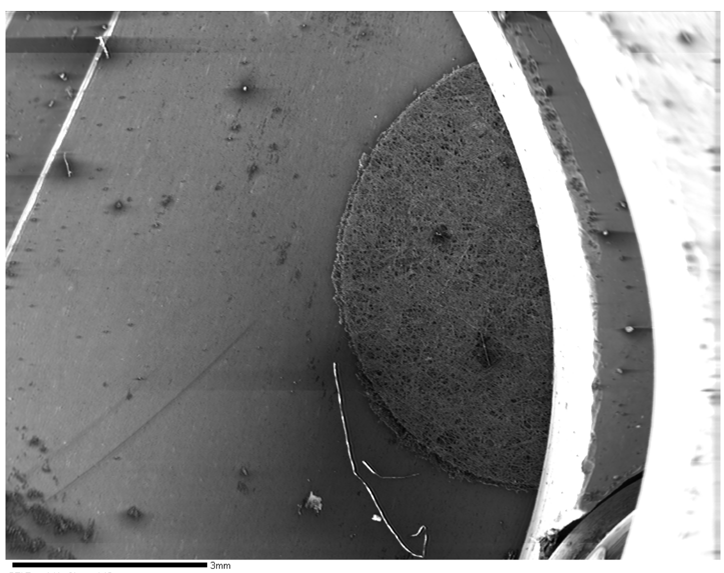

Figure D.5. This image is taken at 10x and has no channel above or below the sample. This image is also to determine the area and pressure on the sample.

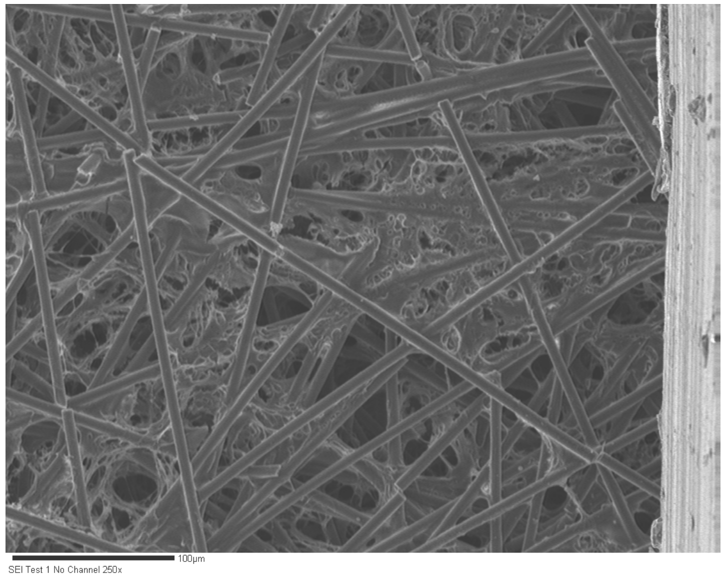

Figure D.6. This image is taken at 250x and is the area with no channels. Not as much damage near the wall is observed, but there are a few broken fibers close to it, as well as the broken fibers crossing each other in the upper left of the image.

D.1.2 25.4 μm Compression

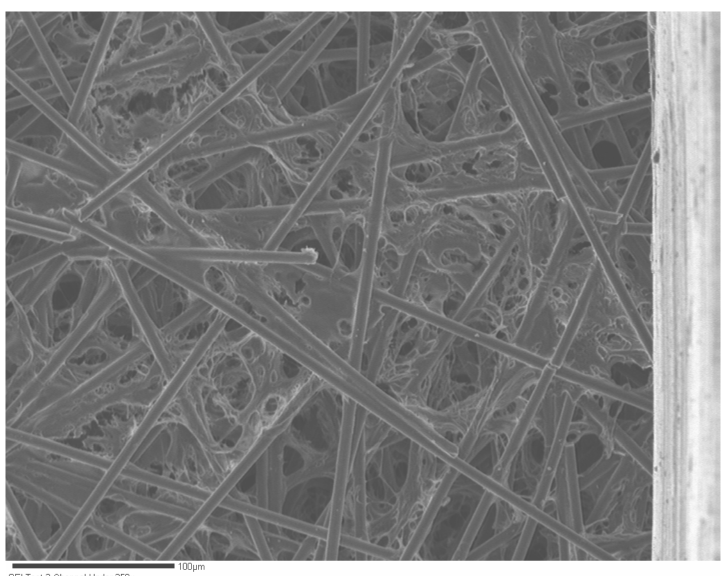

Figure D.7. This image is at 250x magnification and shows the GDL with a channel underneath it. No discernible difference is seen between this figure and Figure D.1.

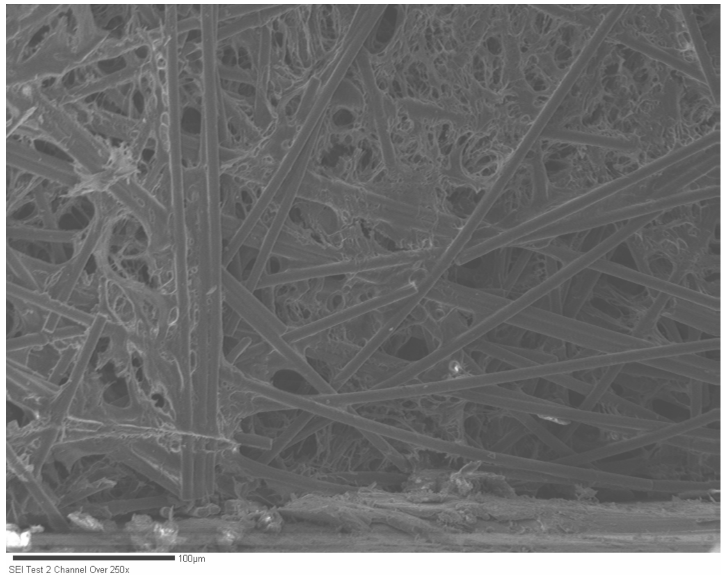

Figure D.8. This GDL has the channel above pressing down, thsi image is looking into that channel and is at 250x magnification. There are no major differences between this and figure D.4 but along the bottom left an already broken fiber has shifted downwards, perhaps being pulled by the compression. Also the ends of the fibers sticking straight up appear slightly shifted, but this may be due to slight diffences in rotation.

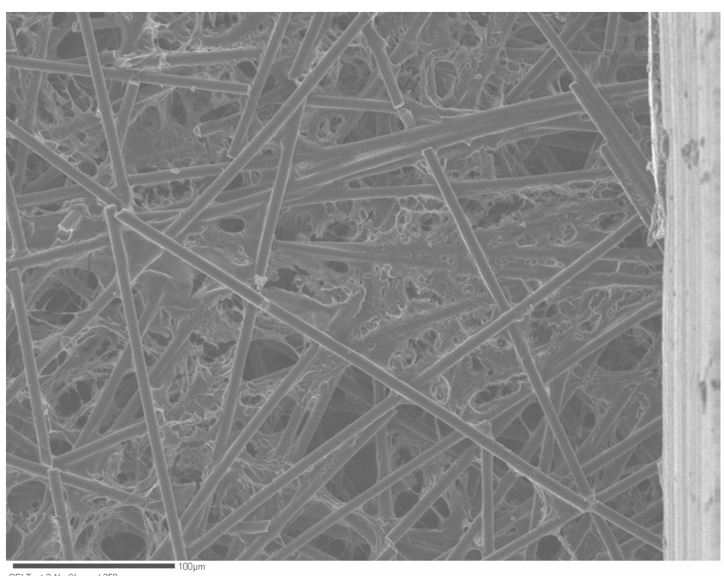

Figure D.9. This image shows the sample with no channel on either side and is taken at 250x magnification. No differences are noticed between this and figure D.6.

D.1.3 38.1 μm Compression

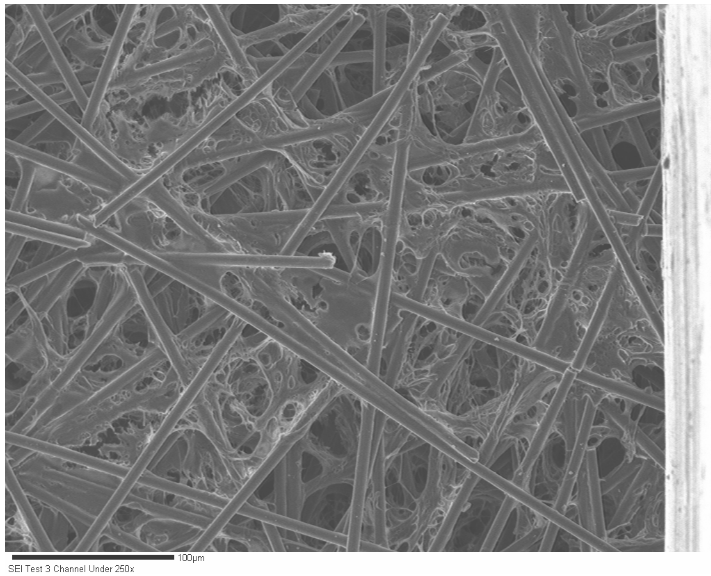

Figure D.10. This image shows the GDL with a channel underneath and is at 250x magnification. No major differences are apparant. It is possible that this image shows a very small shift of the GDL towards the wall, as several features appear closer than in figure D.7.

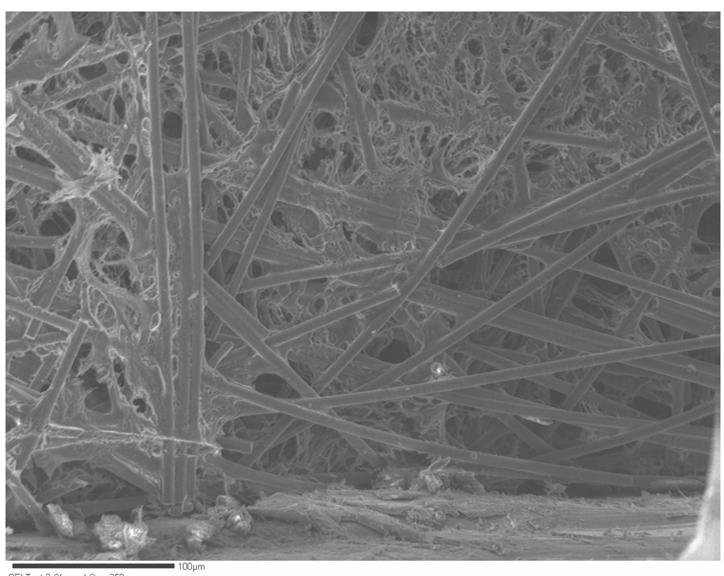

Figure D.11. This image is looking into the channel pressing down and is at 250x magnification. No new damage appears to have occured.

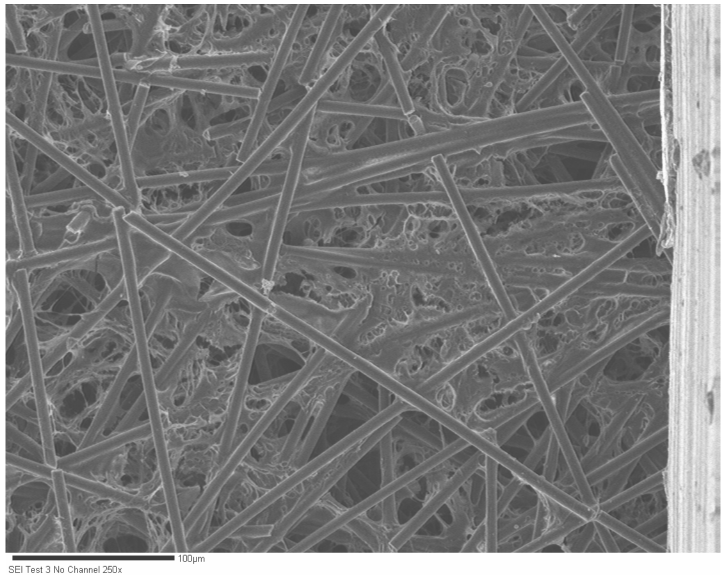

Figure D.12. This image shows the sample with no channels and is at 250x magnification. No new damage is noticed from this increase.

D.1.4 50.8 µm Compression

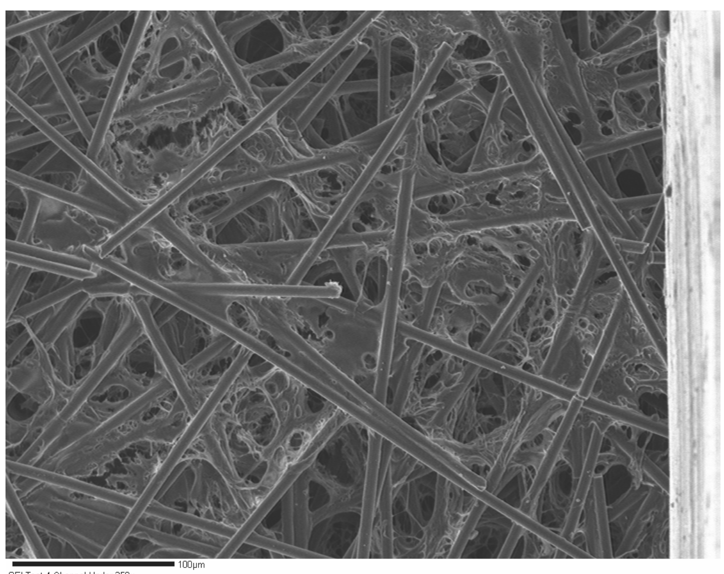

Figure D.13. This image shows the sample with a channel underneath. It is taken at 250x magnification. Again no new damage is shown, but another slight shift towards the ring is noticed. Perhaps this indicates the GDL is being drawn in due to the channel running underneath, since this isn't noticed in the other two samples.

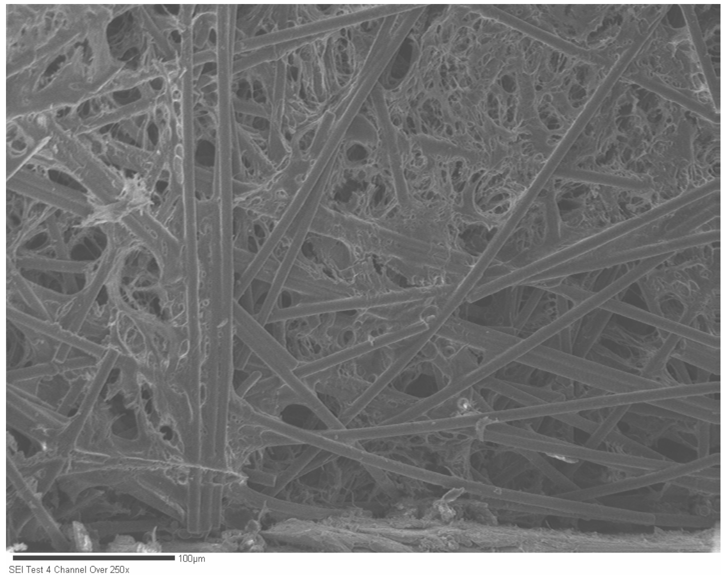

Figure D.14. This image is looking into the channel pressing down and is at 250x magnification. No major changes, the bottom left appears to have had a fiber shift slightly, and the fiber running along the bottom and ending about a third of the way across may be shifting up slightly. Both of these are very slight changes however.

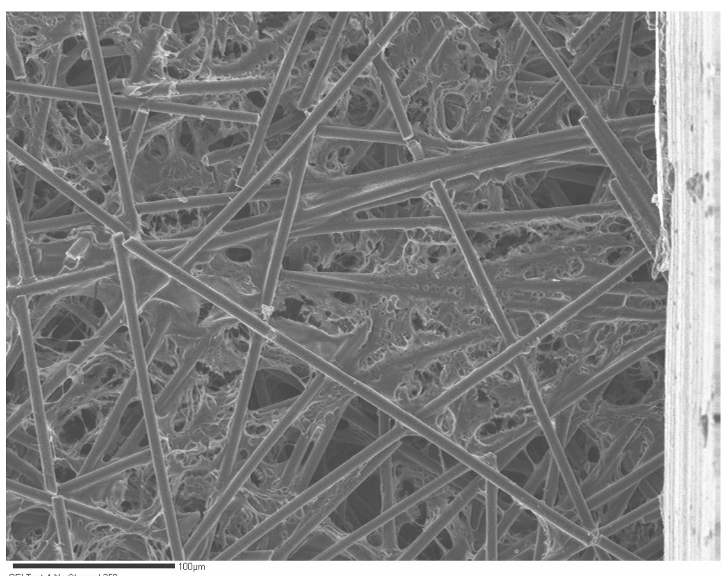

Figure D.15. This image shows the GDL with no channels pressing on it. Again no new damage or shifting of the GDL is observed.

D.1.5 63.5 μm Compression

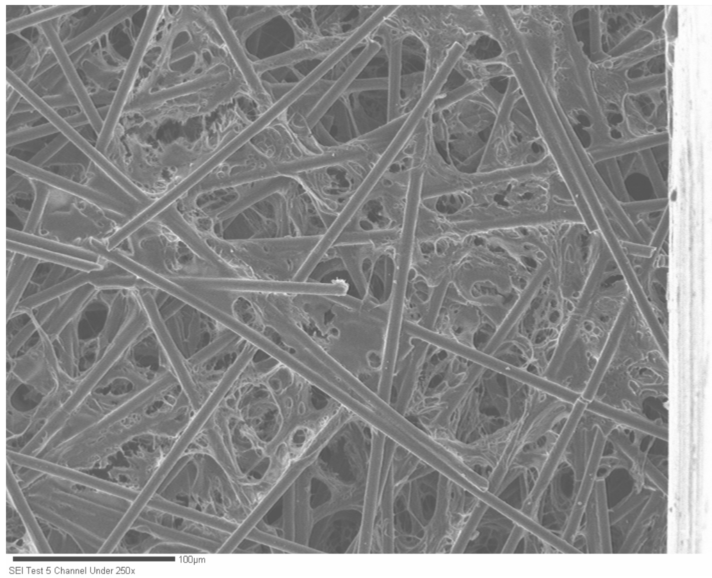

Figure D.16. This image is the sample with a channel underneath. This image is taken at 250x magnification. Again little damage is observed but the fibers continue to shift or be pulled towards the wall.

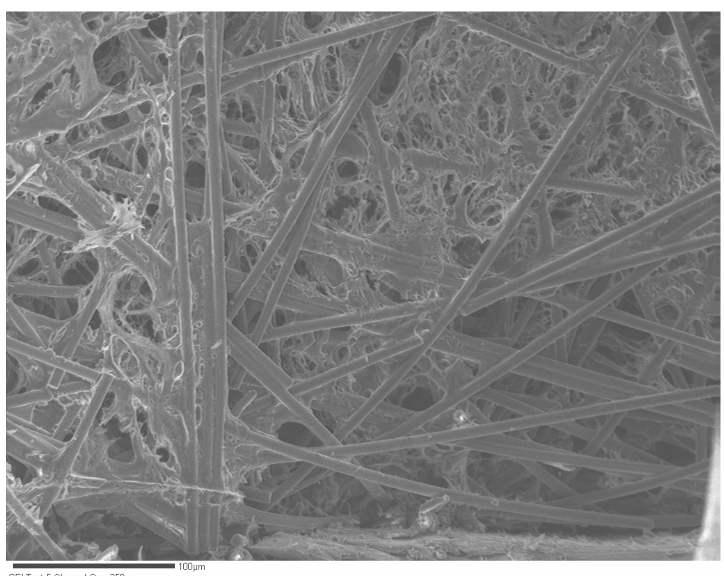

Figure D.17. This image is looking into the channel pressing down and is taken at 250x magnification. No new damage is noticed and no shifts are observed.

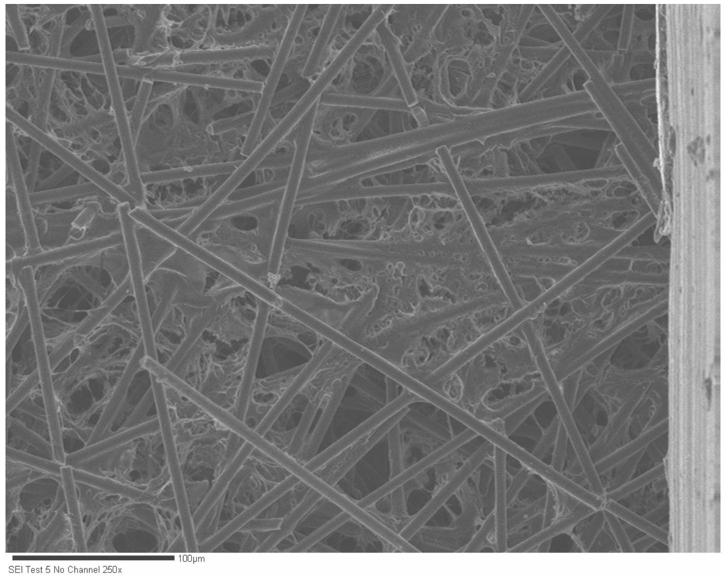

Figure D.18. This image is taken of the sample with no channels pressing on it. This image is taken at 250x magnification. The obvious difference is that there is a new fiber which has appeared in the bottom half intersecting the bottom edge almost at the centerpoint. No other changes are noticed though.

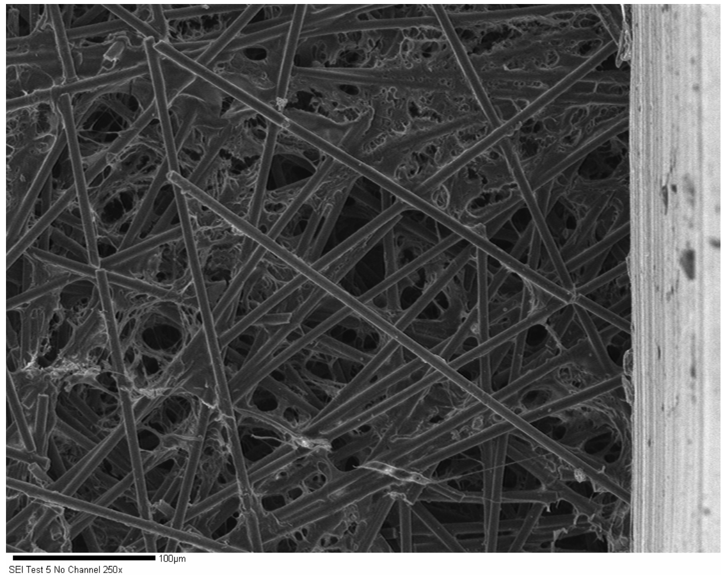

Figure D.19. This image is of the same sample as figure D.18 but the focus is shifted downwards to image the location the new fiber originated from. This image is also taken at 250x magnification. The fibers traveling horizontally should show what location this lines up with. The origin appears to be the higher charged areas running along the bottom half of the image. This charging appears to be common when fibers break and change positions after the manufacturing process. What causes this charging is unknown though.

D.1.6 76.2 μm Compression

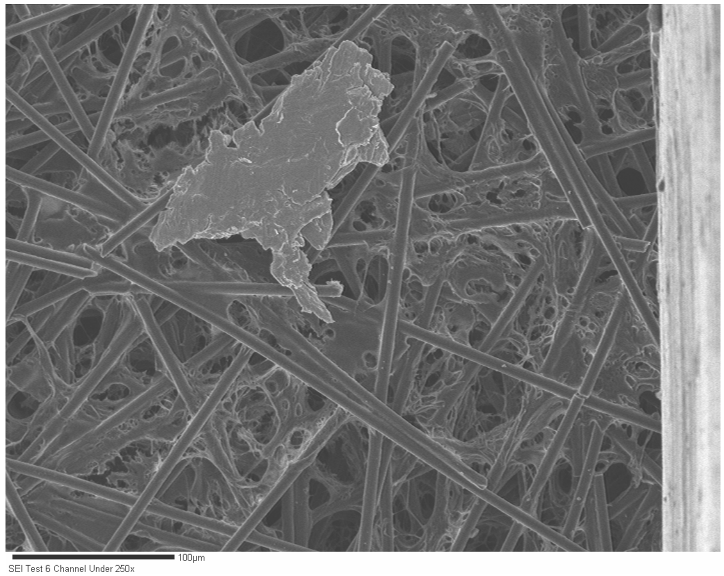

Figure D.20. This image shows the sample with a channel running under it. This image is taken at 250x magnification. The large clump in the upper middle appears to be a piece of dust. This dust is gone by the next run and doesn't appear to cover any damage, based on the images taken in further tests. Again no damage is seen but the material continues getting pulled into the wall.

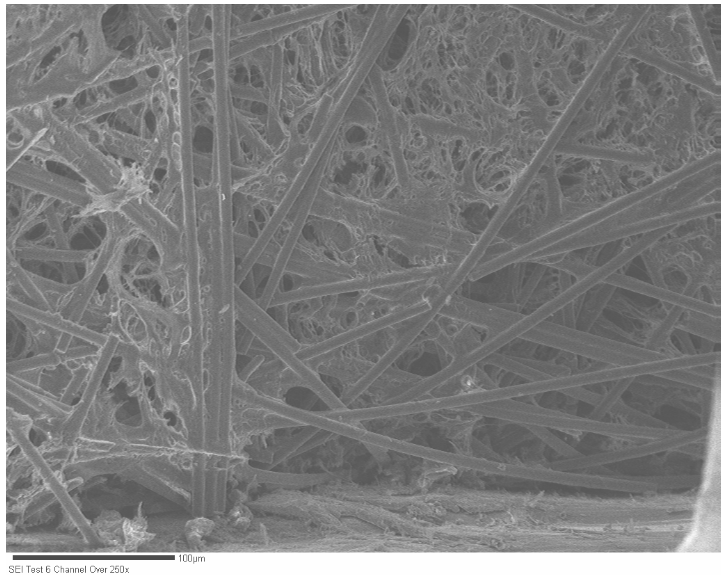

Figure D.21. This image is taken at 250x magnification and shows the sample with a channel running under it. No further damage was noticed between this image and figure D.17.

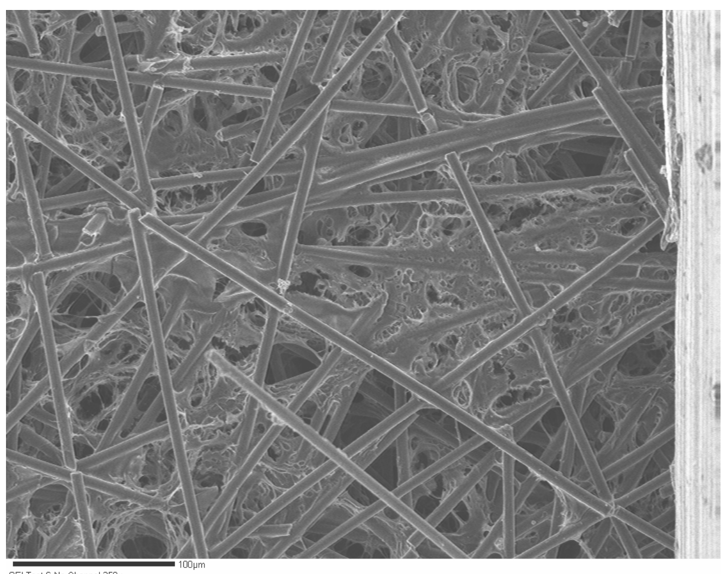

Figure D.22. This image shows the sample with no channels at 250x magnification. The only difference noticed is that the new fiber which appeared in the last run has further shifted moving closer to the long fiber that runs across the entire image.

D.1.7 88.9 μm Compression

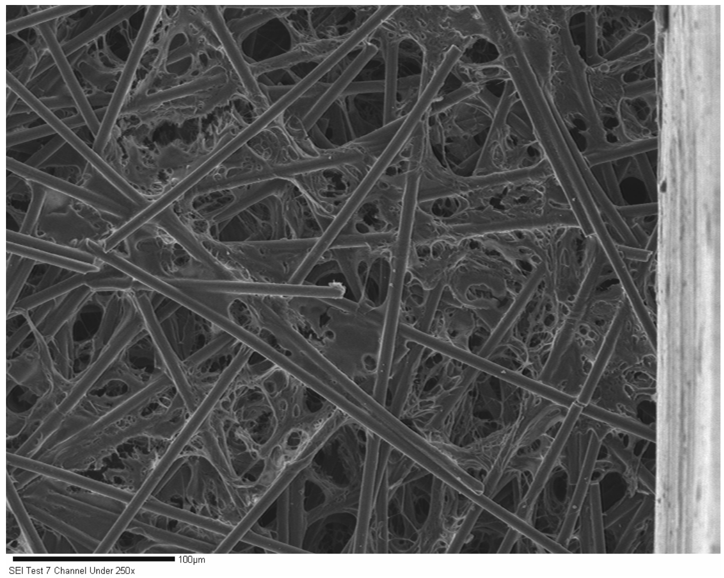

Figure D.23. This image shows the sample with a channel underneath at 250x magnification. As was mentioned previously the piece of dust has disappeared, it landing right on the spot being imaged appears to have been bad luck. No fibers are broken but the GDL has again shifted towards the compressing ring.

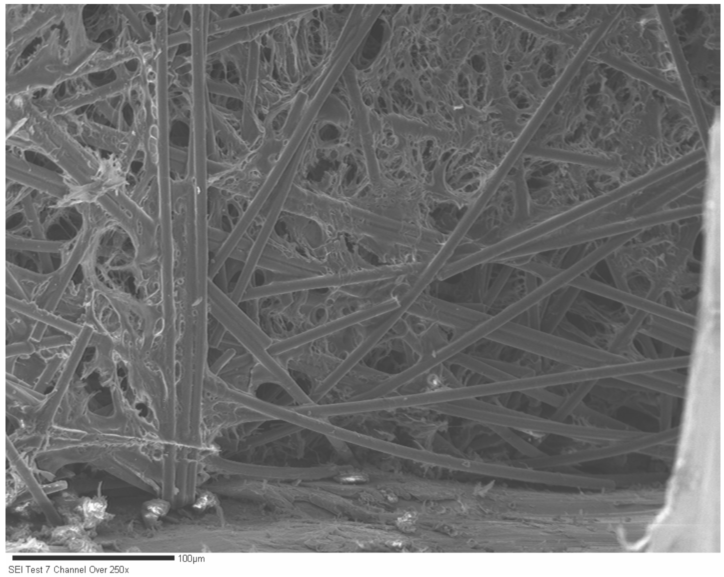

Figure D.24. This image shows the sample with a channel pressing down onto it. This image is taken at 250x magnification. The only difference noticed is that along the wall, about halfway across a fiber runs to the left and is significantly more visible than in previous images. It appears the ring has compressed far enough to force this fiber outwards.

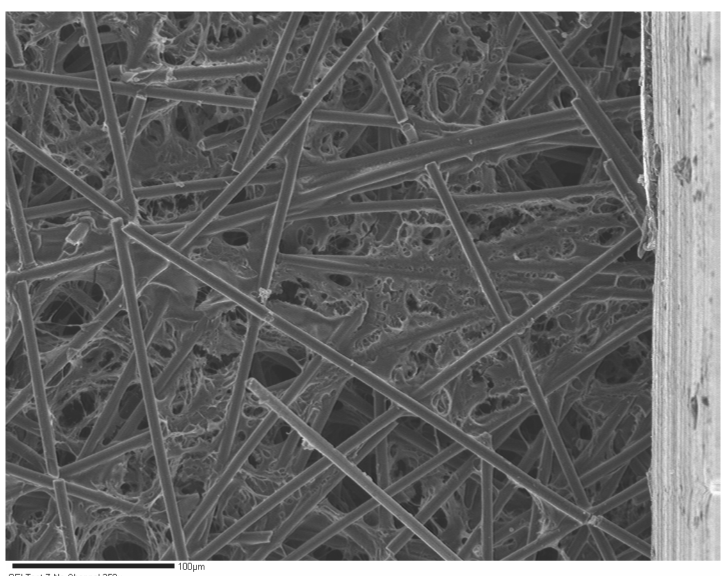

Figure D.25. This image shows the sample with no channels, it is imaged at 250x magnification. No changes occured except that the new fiber has again shifted, this time appearing to retract straight back along its path. This makes it appear shorter than in the previous images.

D.1.8 101.6 μm Compression

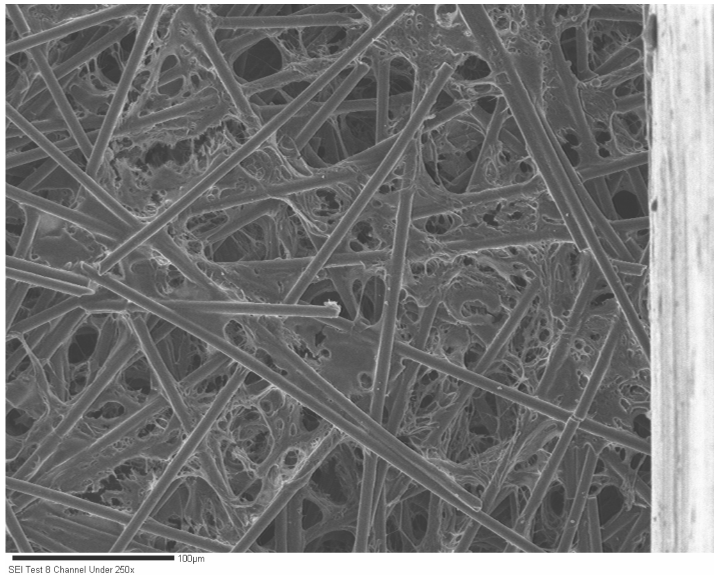

Figure D.26. This image shows the GDL with a channel underneath. It is imaged at 250x magnification. No new damage is observed. In addition this is the first test where the sample does not appear to have moved towards the ring.

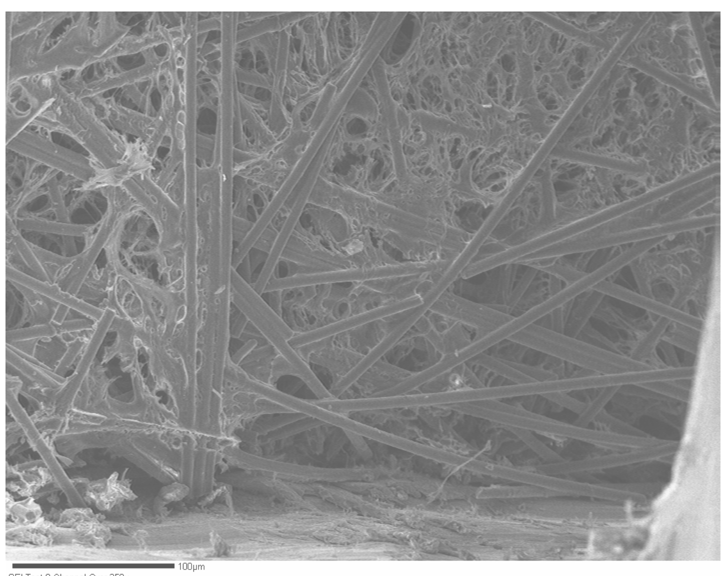

Figure D.27. This image shows the sample with a channel pressing down onto it. This was imaged at 250x magnification. In the bottom right a fiber is now sticking up that was in the background previously. This appears to be the only significant change.

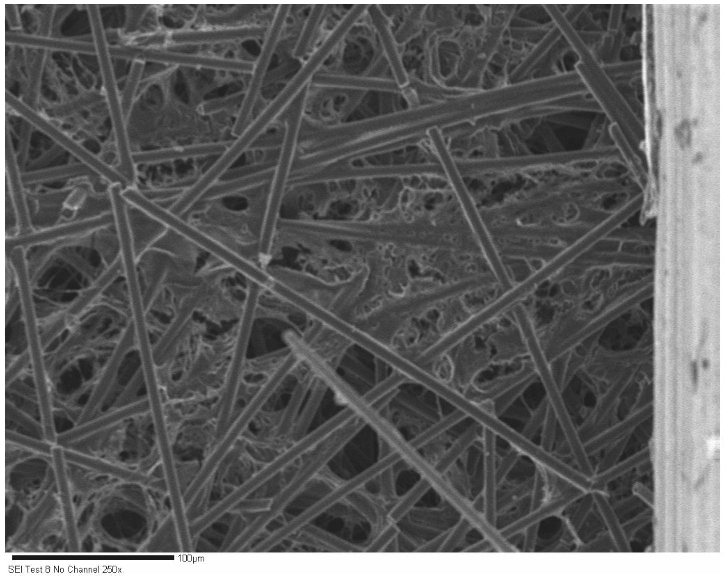

Figure D.28. This image shows the sample with no channels at 250x magnification. This image was mistakenly recorded, and was subsequently re-focused and re-imaged. This can be seen in the next figure.

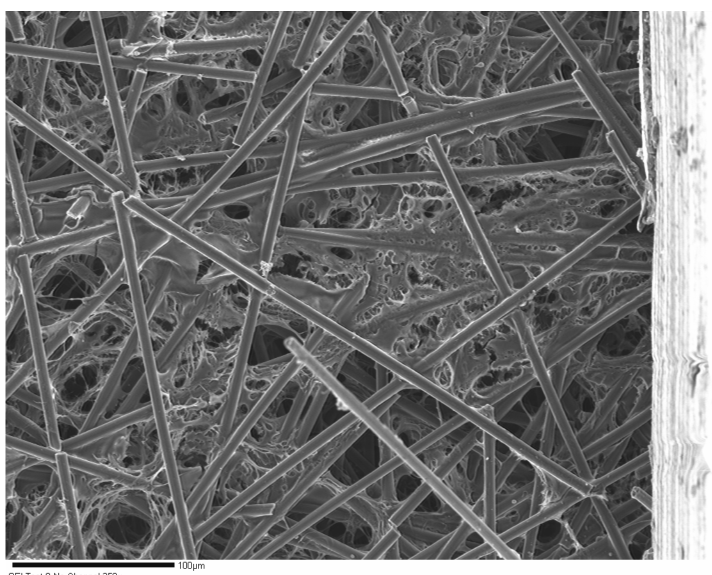

Figure D.29. This shows the sample with no channels at 250x magnification as before. The new fiber has again moved pulling back and rotating upwards a little more. Also in the bottom right corner the fiber that has been broken in all the images has now been signifcantly moved.

D.1.9 Force and Compressing Ring Removed

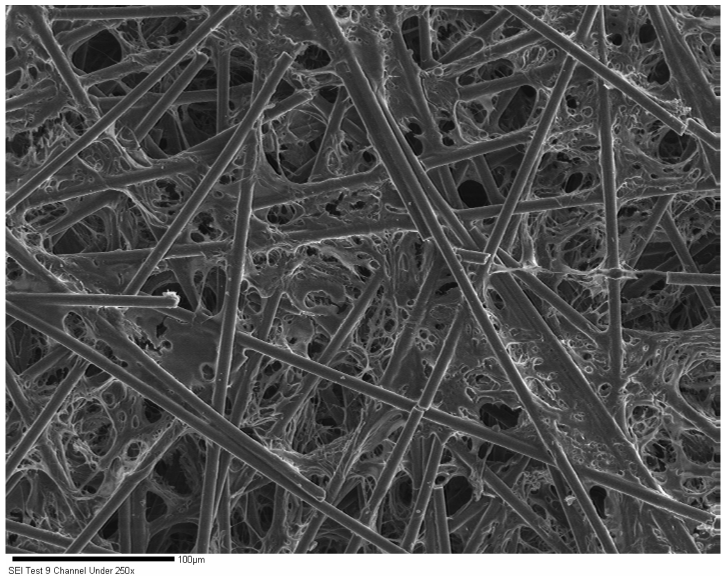

Figure D.30. This shows the sample which had the channel underneath at 250x magnification with the compressing ring removed. The sample shows some damage where the ring was but surprisingly less than anticipated. There appears to be a missing piece of fiber in the center, right side, and a few fibers are broken or cracked but these defects all appear approximately 100 micrometers inside of the ring's edge.

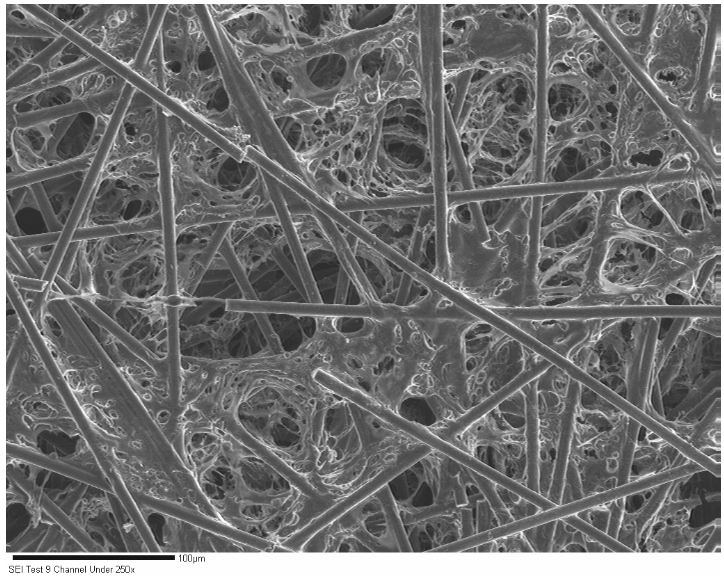

Figure D.31. This image moves farther in on the same sample as previous and is also at 250x magnification. Again not much damage is seen overall, part of this is because this area is located over the channel, which means that the force has nothing to press this portion against.

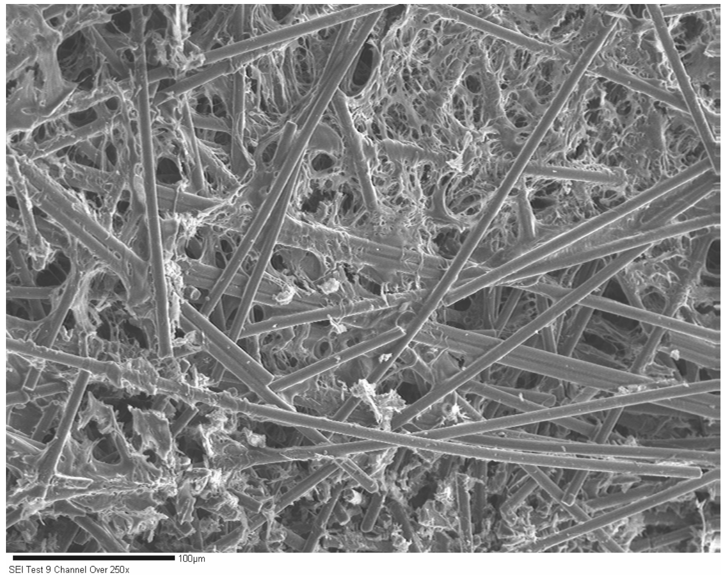

Figure D.32. This image shows the area which had the channel pressing down onto it at 250x. This image also was tilted to match the previous images. This image shows significant changes from the previous images. Several fibers which ran vertically along the left half are now gone or small portions of what they were. Several fibers along the bottom have shifted or disappeared. Significant damage is seen where the ring was pressing along the bottom.

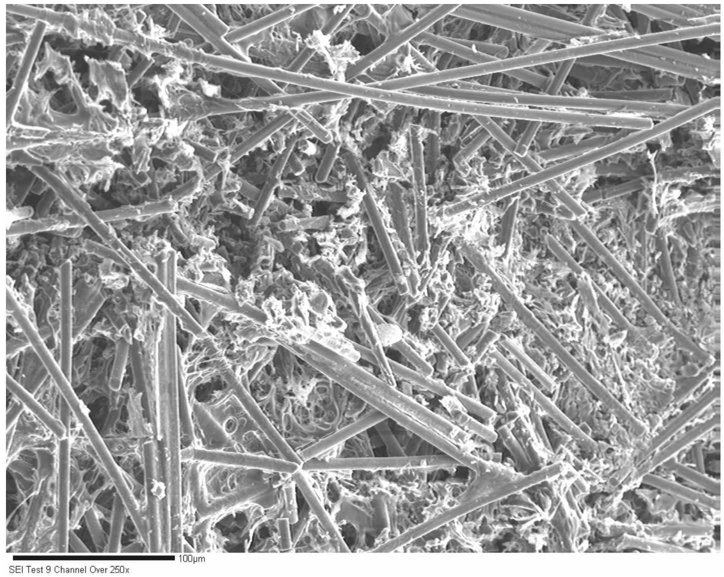

Figure D.33. This image is also of the sample with a channel pressing down at 250x magnification. This image is further down from the previous image. As can be seen the compressed area has significant damage with most of the fibers being broken pieces rather than long continous ones. The binder in the area has a very pressed look to it. The damage is a little more noticeable near the edge where the fibers are shattered as opposed to further in where the fibers are cracked and pressed together.

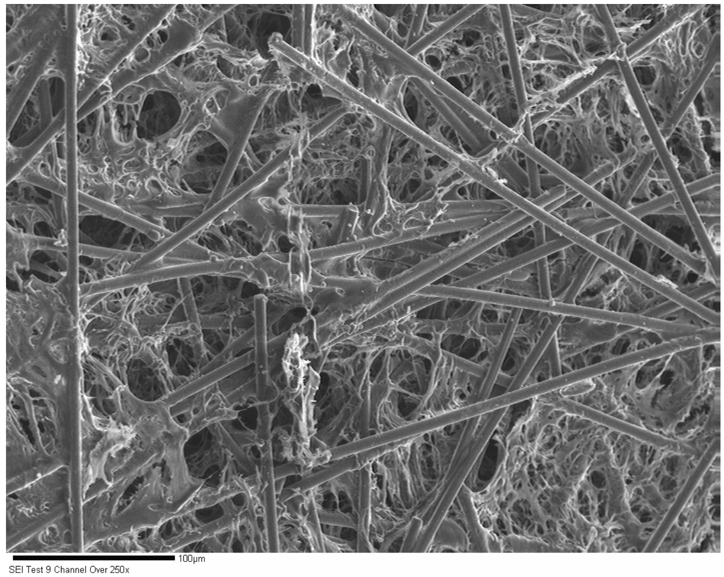

Figure D.34. This image is still focused on the sample with a channel pressing down and is at 250x magnification. This location is directly above the area of figure D.32. The purpose was to attempt to find the missing fibers, which was unsuccessful. It appears that those fibers being removed left some damage behind but overall little damage is observed in this image.

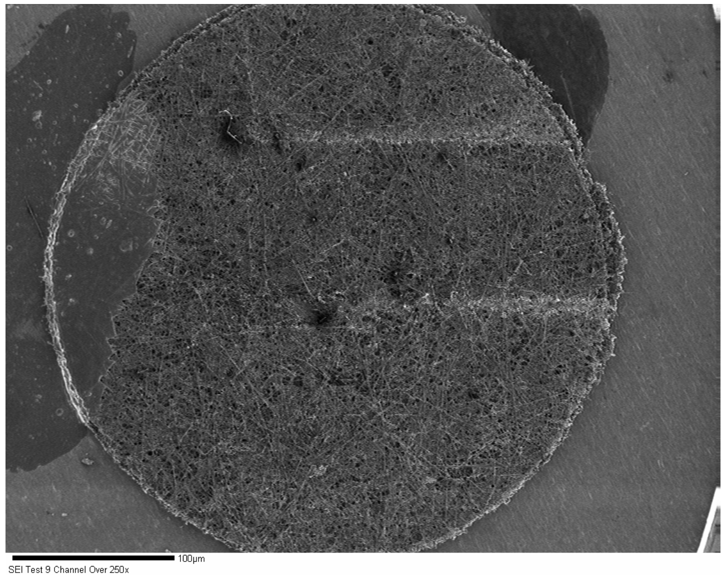

Figure D.35. This image is a 14x magnification view of the GDL with a channel pressing down onto it. The area which was compressed is fairly clear on this image. The darker area along the center and left side are the uncompressed areas and the lighter areas along the top and bottom are the areas under compression. The bottom half is less distinct for an unknown reason. Also a few dark spots appear on this image. This is caused by particles which charge, this charge becomes so bright that the surrounding area appears dark or black due to the contrast. The area imaged at 250x was alond the lower of the walls, which would be almost centered in this image.

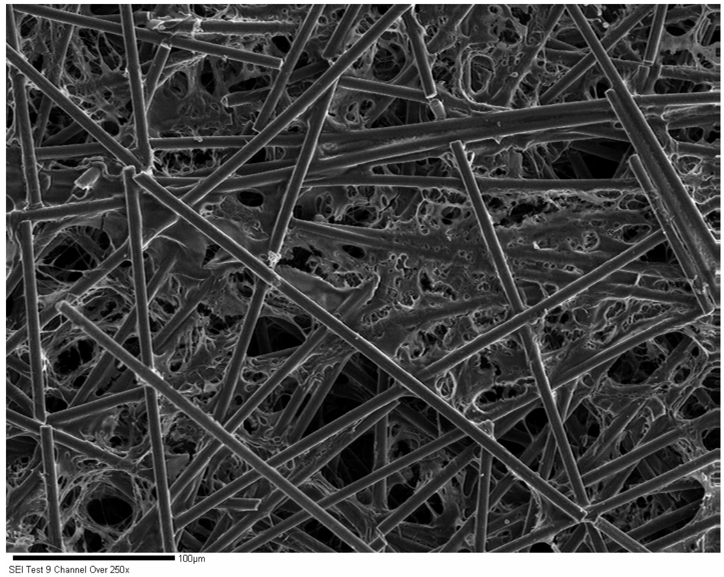

Figure D.36. This image shows the sample with no channels at 250x magnification. This image shows the area previously imaged, as is seen the new fiber has shifted significantly back towards the bottom of the image. The right side doesn't show much damage but only a small amount of where the ring was is visible.

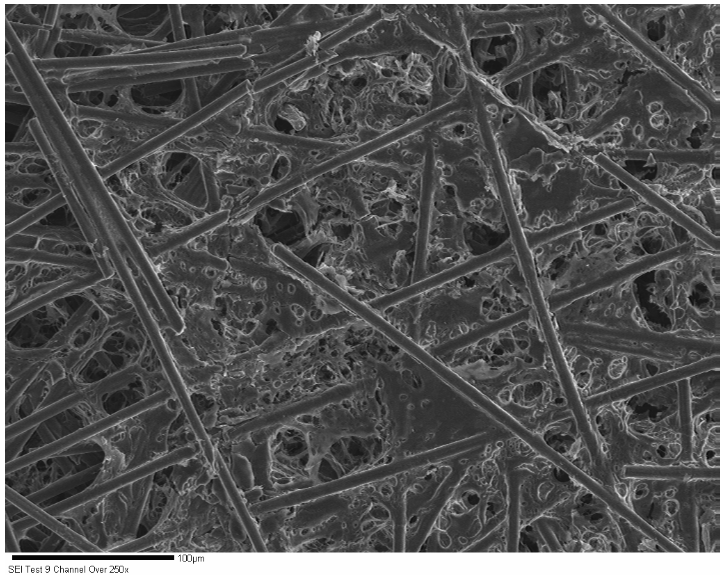

Figure D.37. This image is the sample with no channels at 250x magnification. The location is directly to the right of the previous image. As can be seen there is a vertical line of damage almost a third of the from the left side. The rest of the damage appears to be the pressing together of the material as was seen before. There is less damage observed here as opposed to figure D.33, this may be due to the lack of a channel in this location.

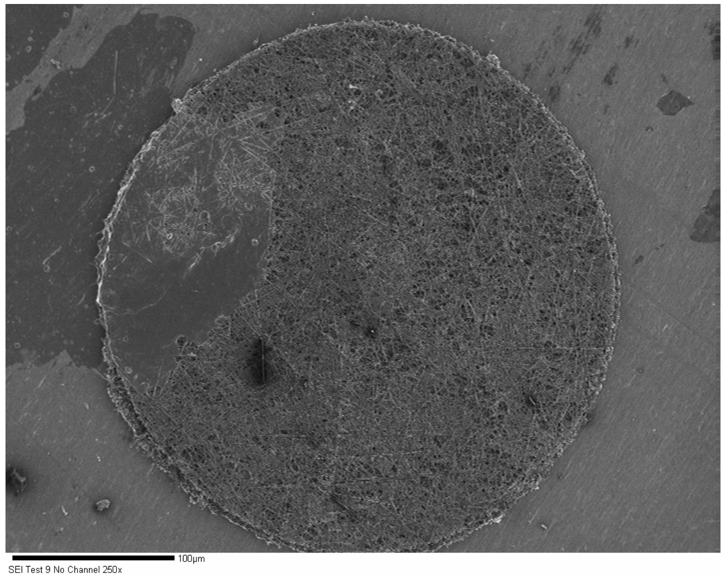

Figure D.38. This image shows the GDL with no channels at 13x magnification. The damage line can be seen running down the middle of the sample, with the left side being uncompressed and the right bearing the compression. Again a few particles are visible which affect the image in isolated areas.

E. IMAGE LIBRARY OF FREUDENBERG WITH MPL

E.1 Incremental Compression Imaging Results, Six Single Samples w/Edge

This run of tests was an incrementally increasing load. The accelerating voltage was 10 keV. The Freudenberg GDL was chosen and the displacement of the GDL was incrementally increased starting at 0 and increasing in increments of 12.7 μm. This increment is the smallest which can be accurately measured with the dial indicators. The GDL was compressed all the way to a total displacement of 76.2 μm. All images taken looking into the channel pressing down were taken with a tilt on the stand of 32.4 degrees, as measured by the tilt indicator on the SEM.

This GDL material shows significant differences in structure compared to the baseline material. The fibers appear to be much denser and more flexible than the baseline. Also the images appear to be easier to focus which would indicate that the material conducts better than the baseline material.

E.1.1 No Compression, No Rings

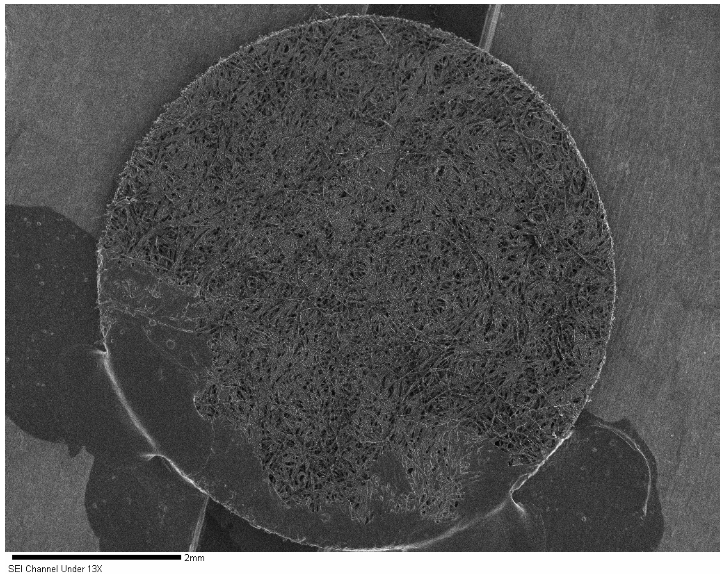

Figure E.1. This image is the sample with a channel running under it at 13x magnification. This image is mainly to see the area and for comparing to the image after compression has been applied.

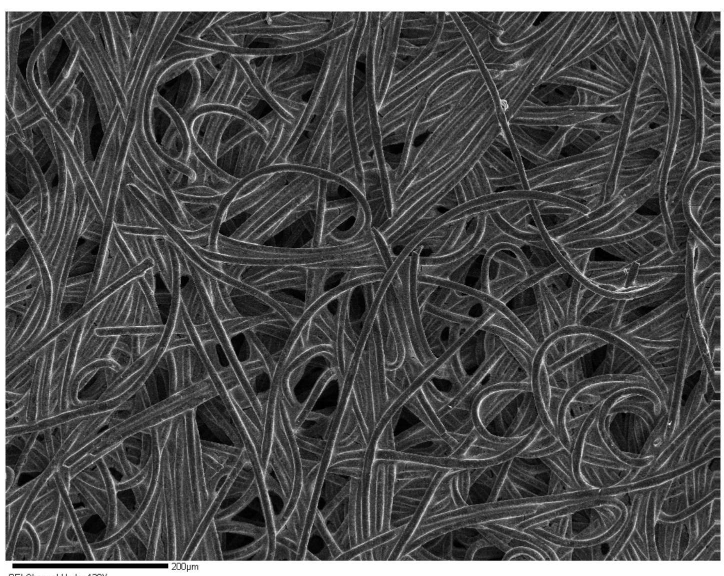

Figure E.2. This image is the same sample at 120x. The magnification was kept low because it was a guess at what area would be compressed, also as will be seen this image should have been rotated 90 degrees clockwise to match the later images.

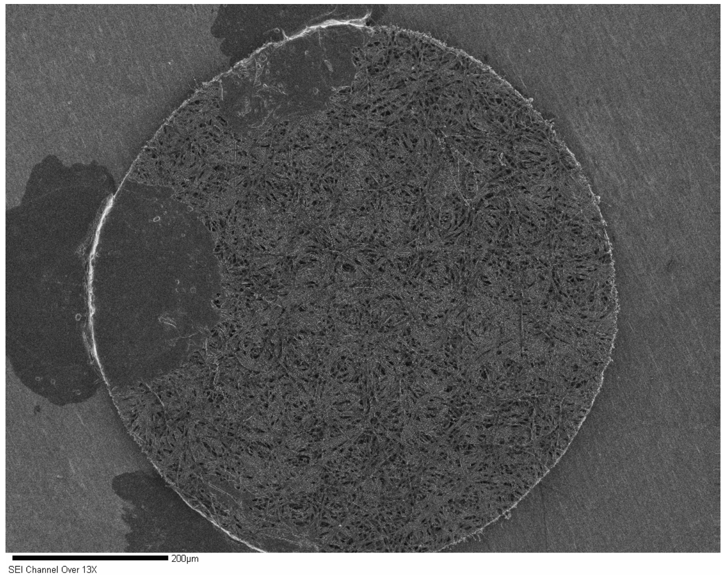

Figure E.3. This image is the sample that will have a channel pressing down onto it. This image is at 13x magnification.

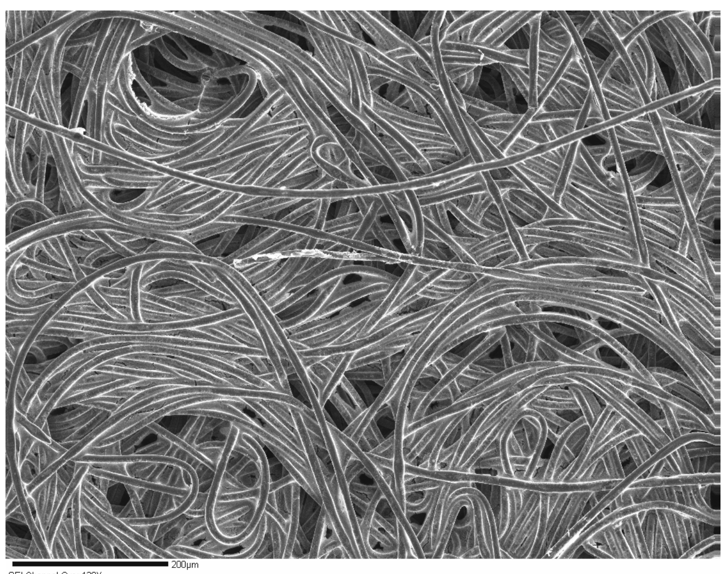

Figure E.4. This image is the area that is expected to be compressed and imaged on the same sample as figure E.3. This image is at 120x magnification. It is rotated the correct direction but is not tilted the as the later images were.

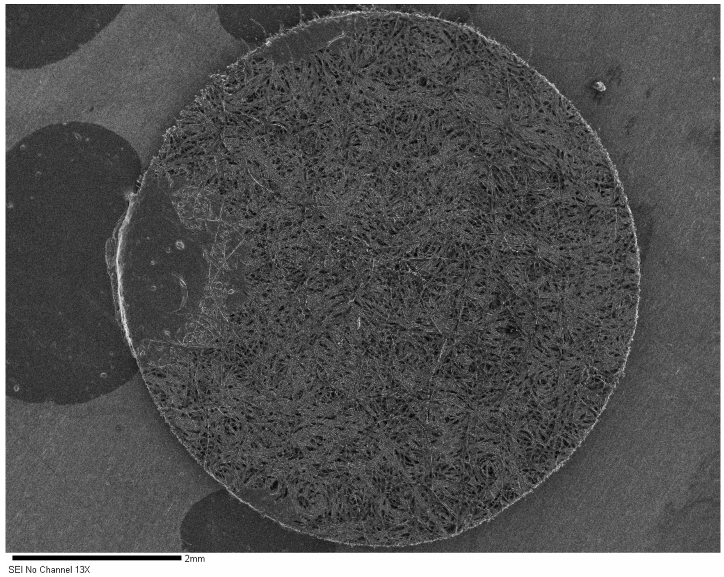

Figure E.5. This image is the sample that will have no channels pressing on it. This image is taken at 13x magnification. It is rotated to match the later images.

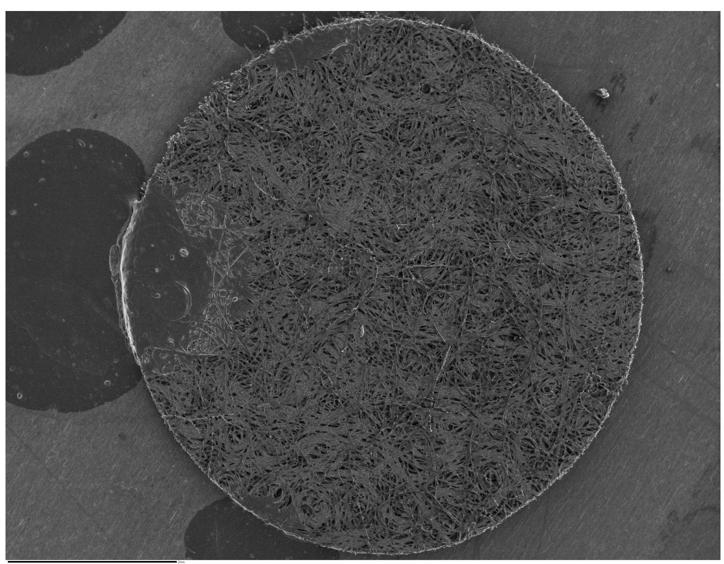

Figure E.6. This is the same image and magnification as figure E.5, but with the difference that this image was taken with 3x as many pixels. The reason was to see the feasability of running one long test and zooming into the image afterwards to find the correct areas.

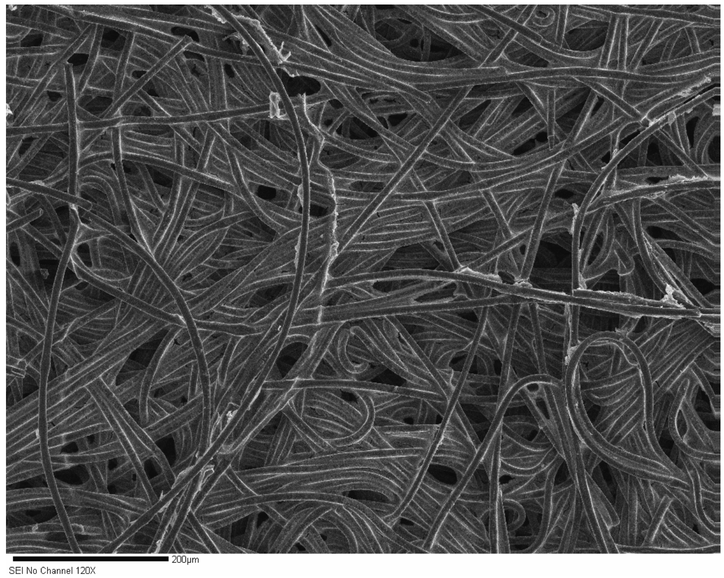

Figure E.7. This image is the sample with no channels at 120x magnification. As is seen a fiber has already moved before the tests, but this allows for easy finding of this area for future imaging.

E.1.2 No Compression, with Rings On

This section has images where the rings were set up and tightened enough to hold in place but not apply any additional force to the samples. The samples were then imaged to allow for comparisons with the no-ring images as well as seeing what damage is caused by future tests.

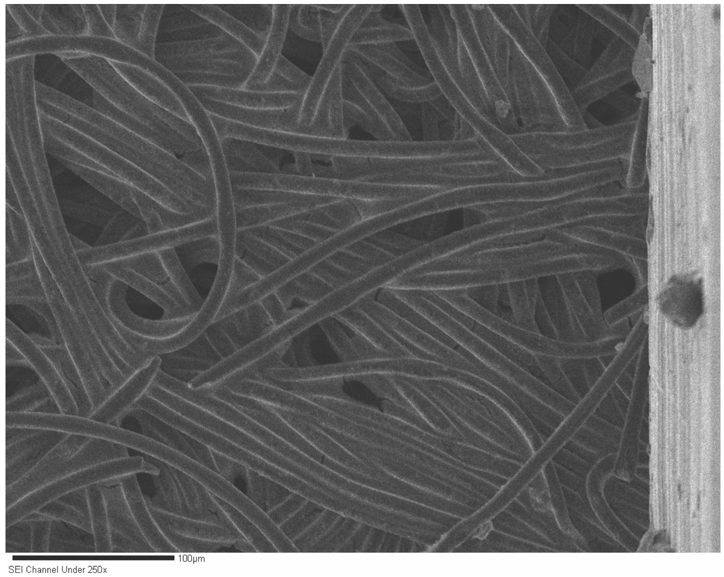

Figure E.8. This image is the sample with a channel running under it at 250x magnification. The ring falls right at the edge of the previous image, figure E.2. It is close but no damage is seen.

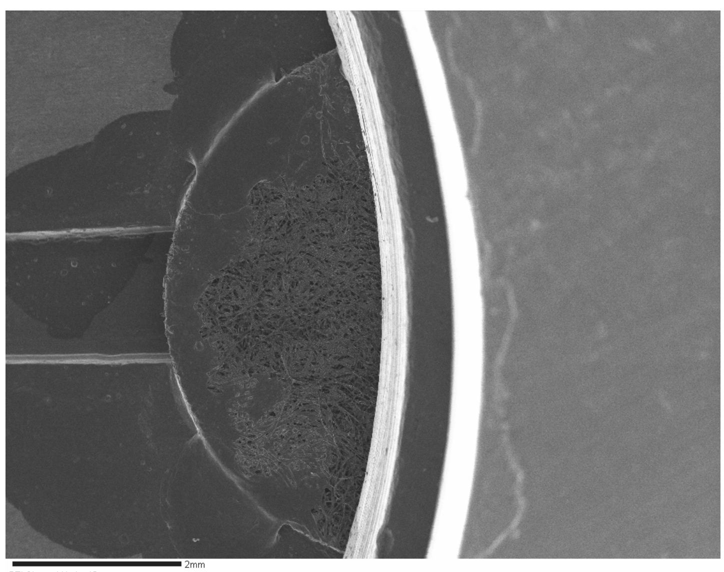

Figure E.9. This image is the same sample at 13x. Too much carbon paint was used on this sample.

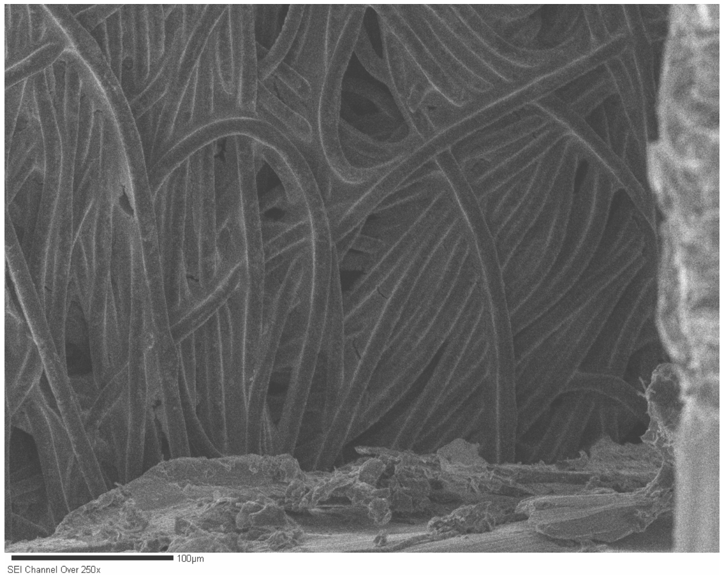

Figure E.10. This image is the sample with a channel pressing down onto it. This image is at 250x magnification. The area imaged doesn't line up with figure E.4 at all, and this is because the center of the sample was imaged rather then more towards where the channel edge would be. Much of the debris along the bottom edge is remnants that were cleaned off afterwards.

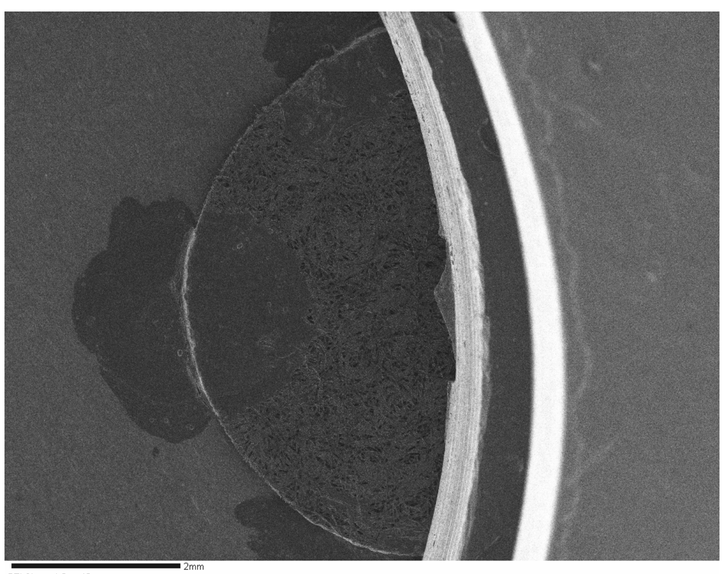

Figure E.11. This image is the sample with a channel pressing down onto it. This image is at 13x magnification. The discoloration in the middle is a burr which does not affect the compression, and only affects the imaging at low magnification.

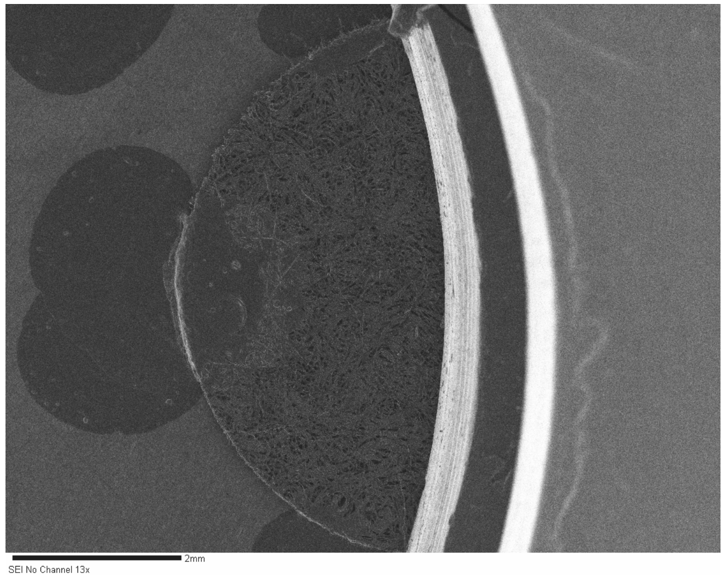

Figure E.12. This image is the sample that will have no channels pressing on it. This image is taken at 13x magnification.

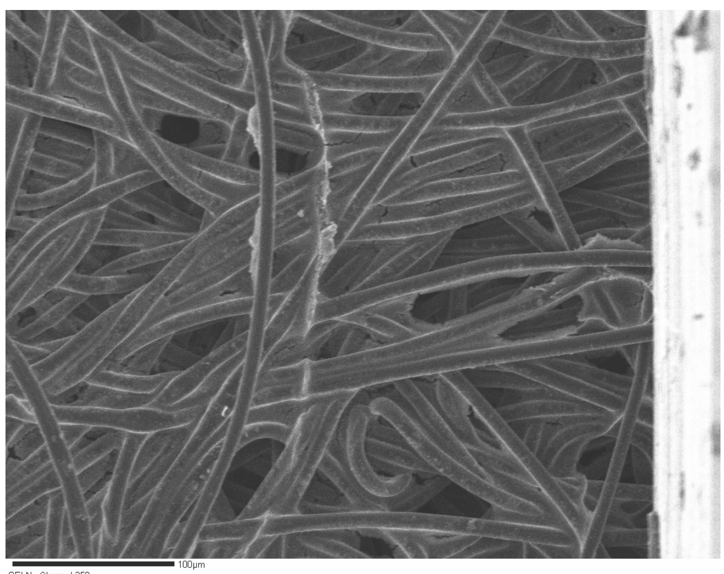

Figure E.13. This image is the sample with no channels at 250x magnification. This image matches very well with figure E.7 and comparing them is very easy. No damage is noted or changes seen though.

E.1.3 12.7 μm Compression

For this set of tests, the rings were removed, cleaned, and reset before running this test, to remove the debris visible in Figure E.10.

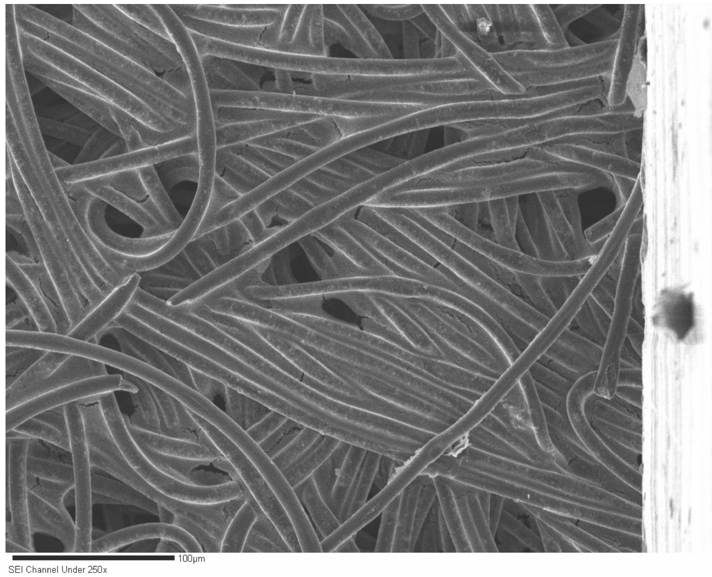

Figure E.14. This is the sample with a channel running under it, and is imaged at 250x magnification. The image is slightly shifted from figure E.10 due to the rings being reset in place. No new damage is observed though.

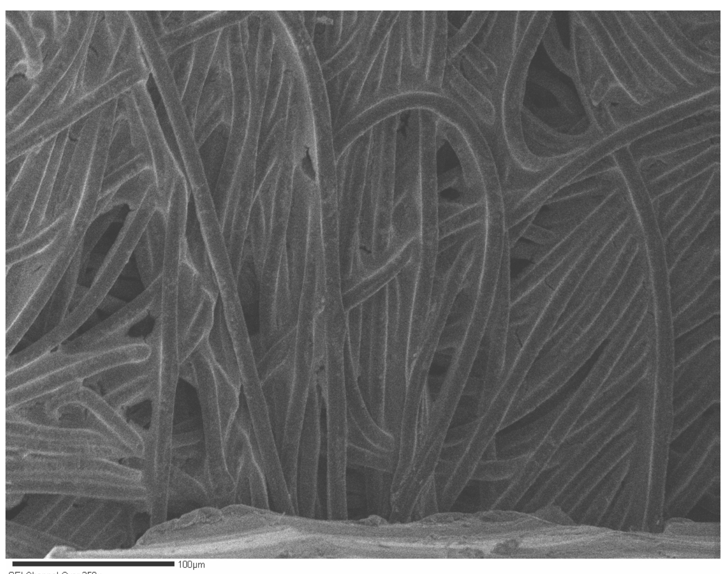

Figure E.15. This image is the sample with a channel pressing down on it, and is imaged at 250x magnification. The bottom edge is much cleaner compared to previous images. No new damage is observed however.

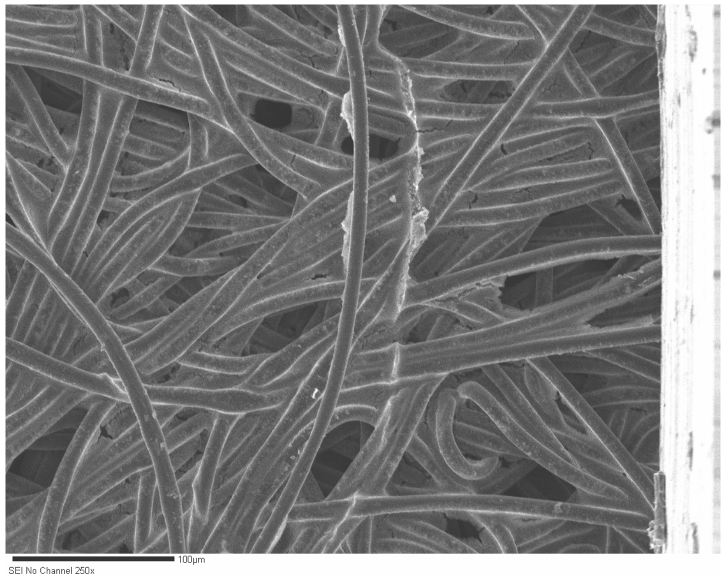

Figure E.16. This image is the sample with no channels and is taken at 250x magnification. It is slightly shifted as well, and is believed to be due to reseting the compressing rings.

E.1.4 25.4 μm Compression

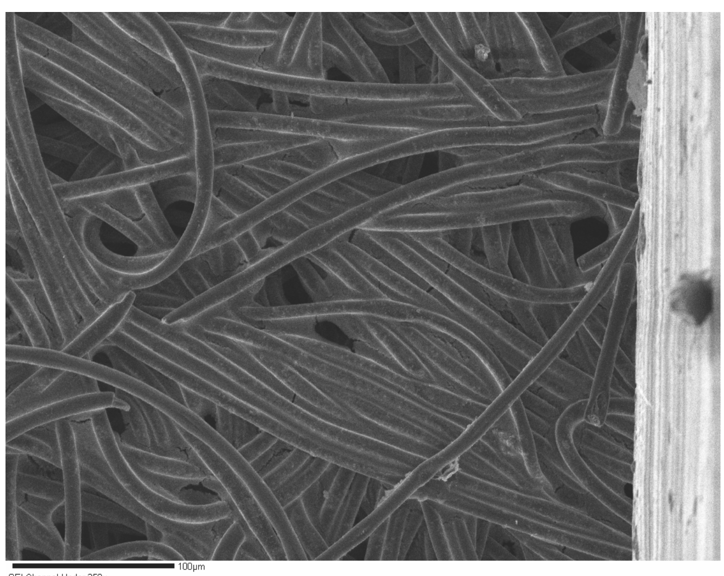

Figure E.17. This is the sample with a channel running under it, and is imaged at 250x magnification. No major differences are apparant in this image. No shifting of the sample towards the wall is seen as compared to the baseline GDL sample.

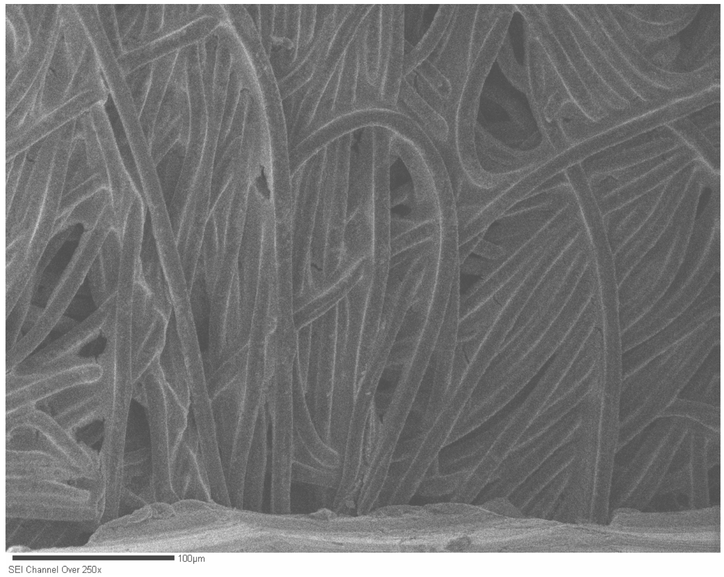

Figure E.18. This image is the sample with a channel pressing down on it, and is imaged at 250x magnification. The only difference is maybe the middle fibers heading vertically from the bottom. They appear slightly shifted or separated compared to the previous image.

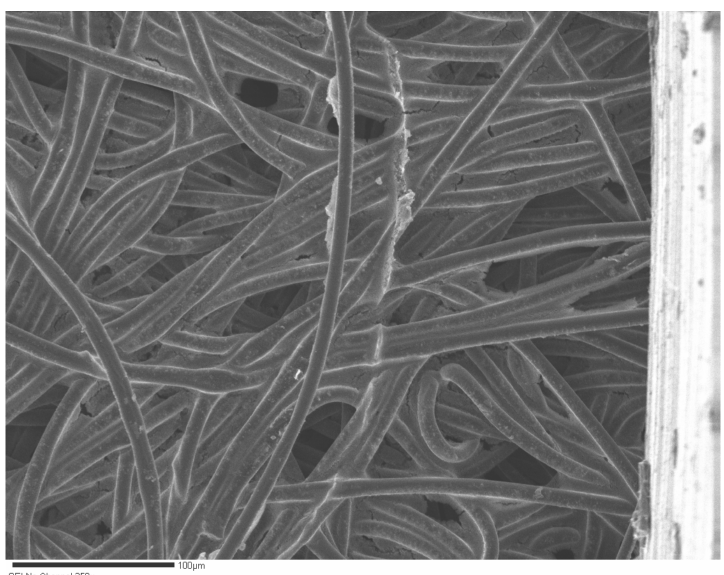

Figure E.19. This image is the sample with no channels and is taken at 250x magnification. No major differences are observed from this test. It does appear the sample may have shifted a little away from the walls, as if being forced away.

E.1.5 38.1 μm Compression

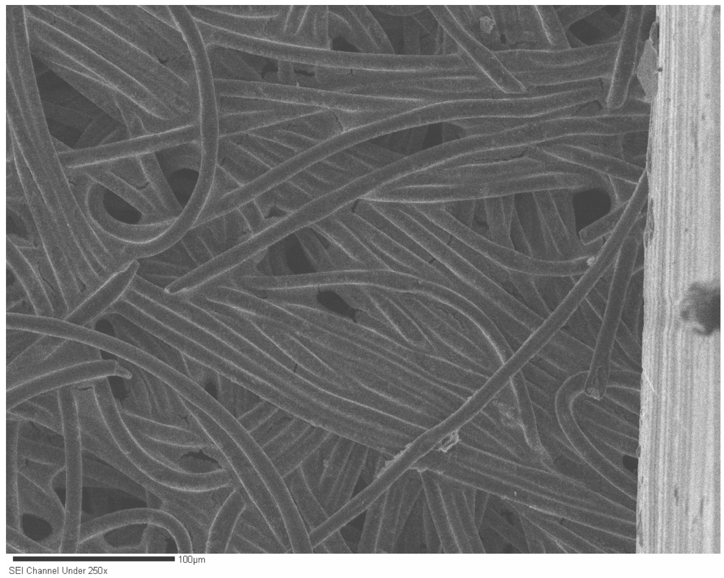

Figure E.20. This is the sample with a channel running under it, and is imaged at 250x magnification. A shifting of the sample away from the wall is seen, which seems to go opposite the results from the baseline material.

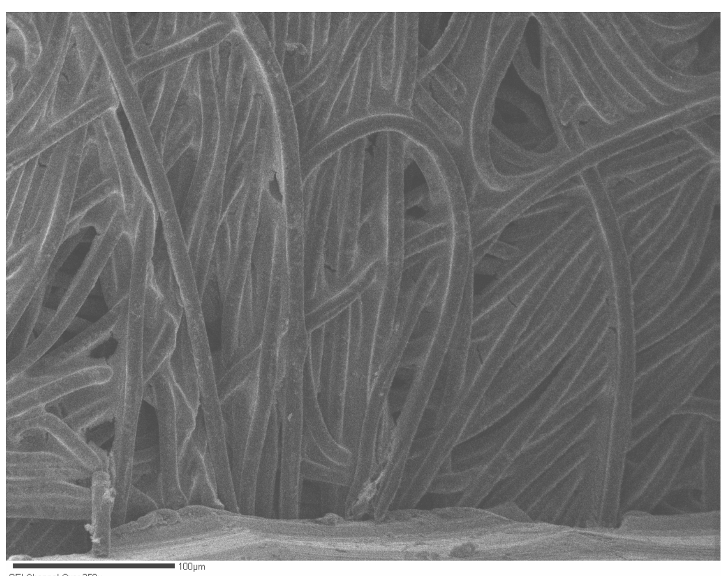

Figure E.21. This image is the sample with a channel pressing down on it, and is imaged at 250x magnification. Near the bottom left a piece of fiber is now seen, although where this piece originated is not readily apparant. Also the fibers near the middle appear to be higher on the plate pressing down, showing the downward displacement of the ring.

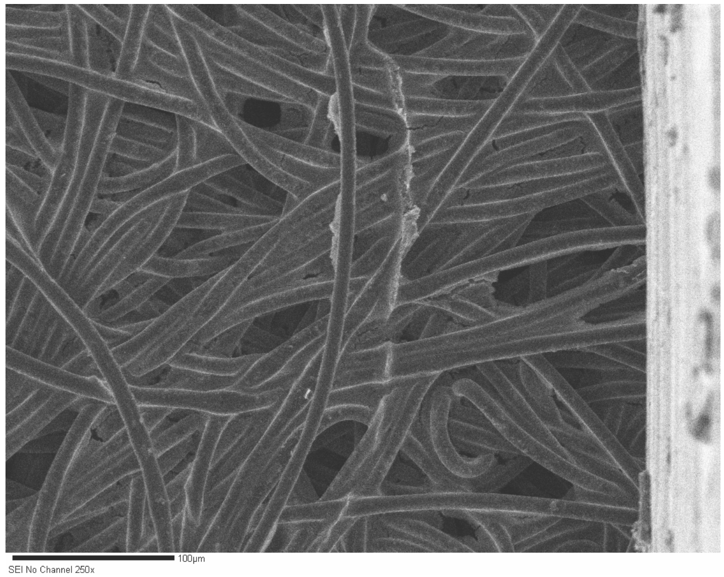

Figure E.22. This image is the sample with no channels and is taken at 250x magnification. Unlike the previous image now the sample appears to have shifted towards the edge, reversing the direction of the last shift. Also a little right of the center of the image the binder appears to have begun pulling apart.

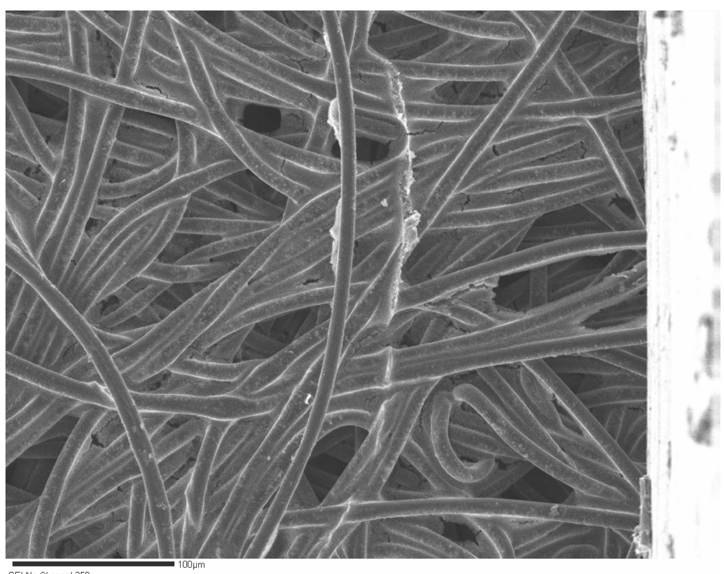

Figure E.23. This image is the sample with no channels and is taken at 250x magnification. This image is the same as the last, but the condenser lens was reduced to clean the image up.

E.1.6 50.8 μm Compression

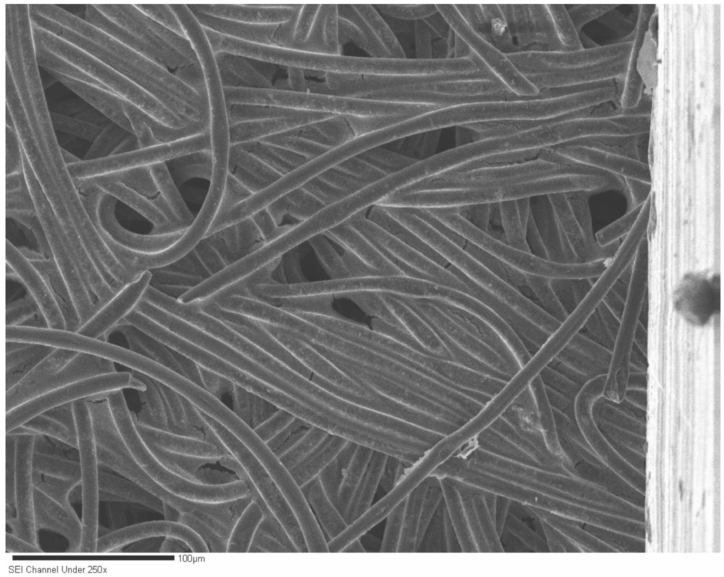

Figure E.24. This is the sample with a channel running under it, and is imaged at 250x magnification. The shifting observed in the last test, has now reversed and the material is shifting towards the wall. No other damage is noted.

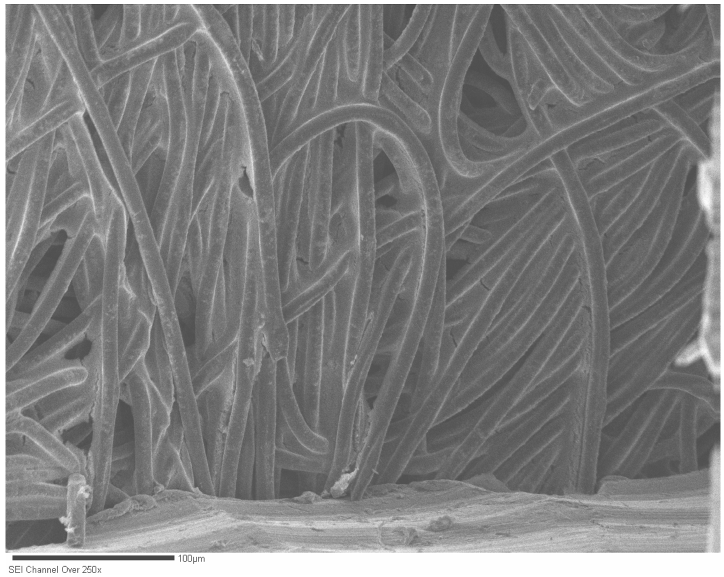

Figure E.25. This image is the sample with a channel pressing down on it, and is imaged at 250x magnification. Several things have occured in this image. The whole material appears to have shifted downwards towards the bottom edge. The fragment in the bottom left corner appears to have tilted further, perhaps due to the shifting. The fiber about a third of the way across from left to right and a little over half way down has snapped.

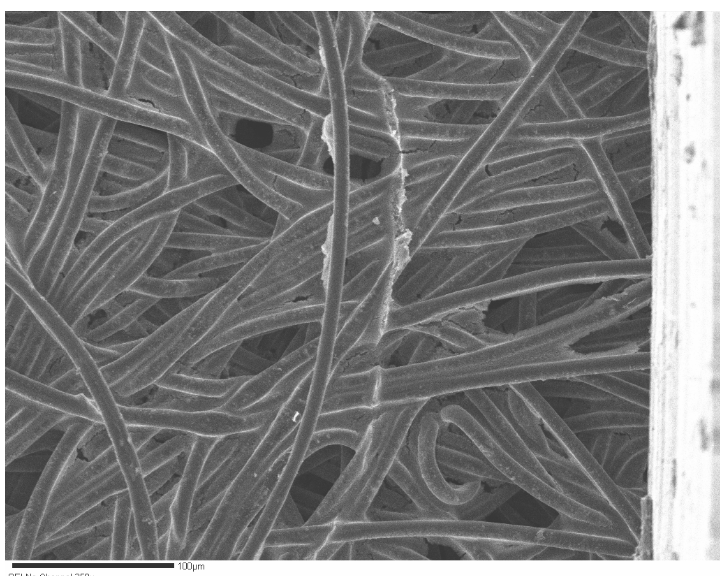

Figure E.26. This image is the sample with no channels and is taken at 250x magnification. Again the shifting has reversed direction and has now moved away from the wall. No other damage is noted.

E.1.7 63.5 μm Compression

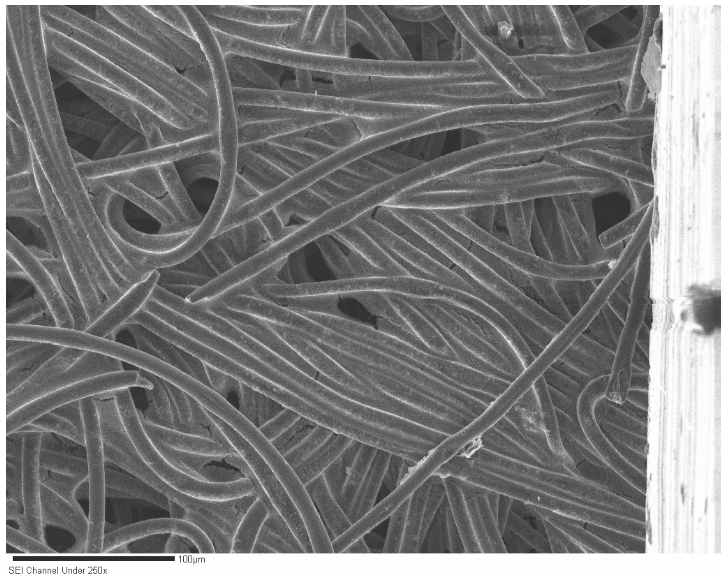

Figure E.27. This is the sample with a channel running under it, and is imaged at 250x magnification. No shifting is noticed in this image, and no other damage is observed either. A small artifact on the imaging is noticed near the middle right, but it does not appear to have obscured any features and does not appear in future images.

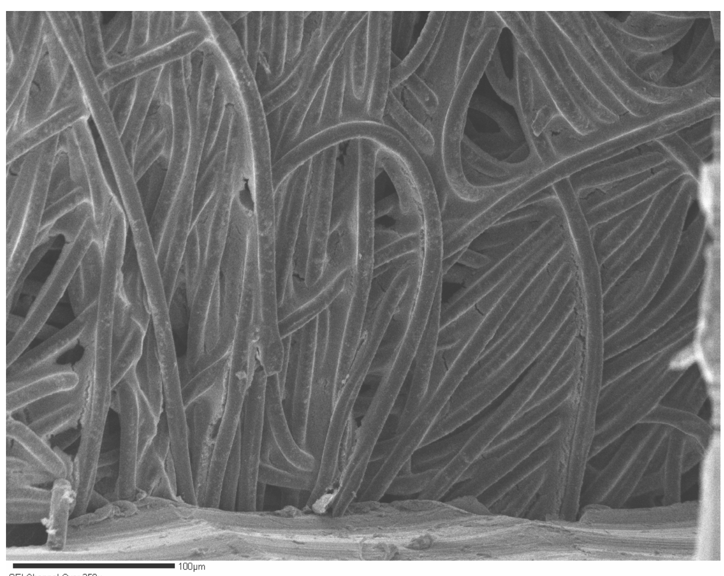

Figure E.28. This image is the sample with a channel pressing down on it, and is imaged at 250x magnification. No shifting is noticed in this image, and no other damage is observed either.

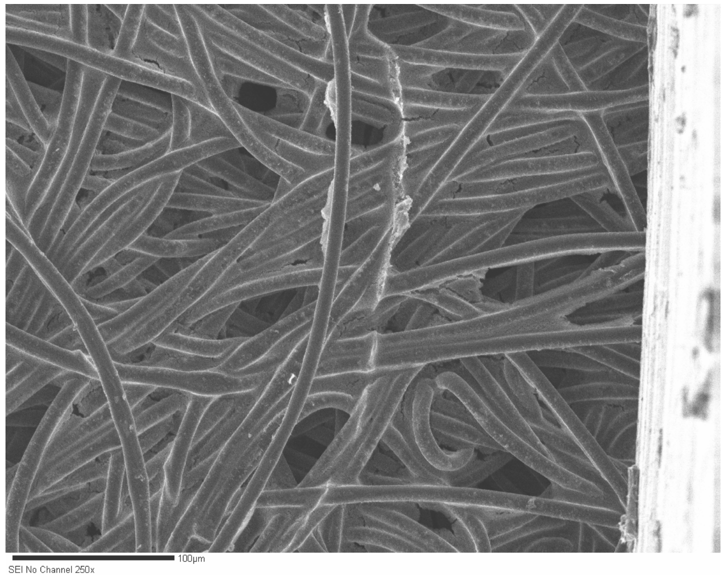

Figure E.29. This image is the sample with no channels and is taken at 250x magnification. No new damage is observed, there does appear to be a very slight shift towards the wall, but it is a very slight shift.

E.1.8 76.2 μm Compression

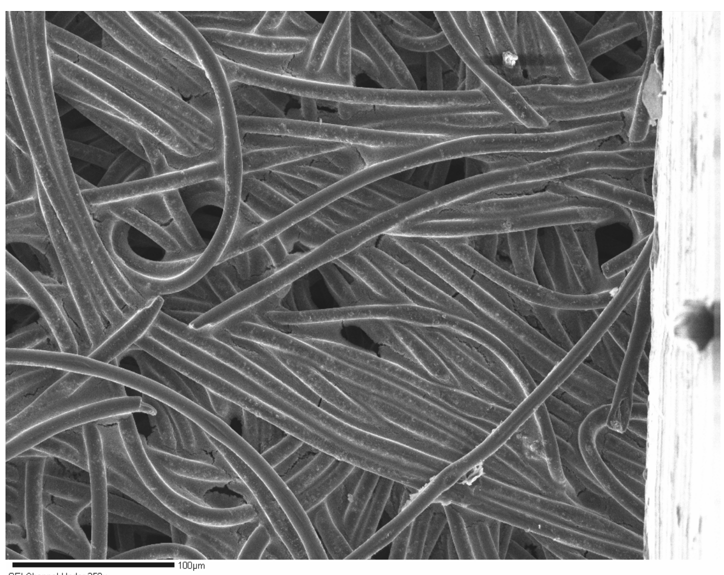

Figure E.30. This is the sample with a channel running under it, and is imaged at 250x magnification. A very slight shift towards the wall is observed, but no further damage is noted.

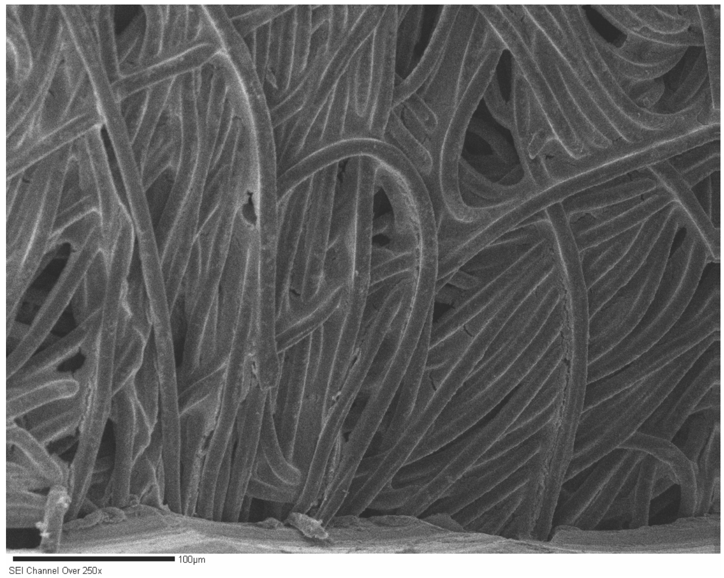

Figure E.31. This image is the sample with a channel pressing down on it, and is imaged at 250x magnification. No significant differences were observed in this image.

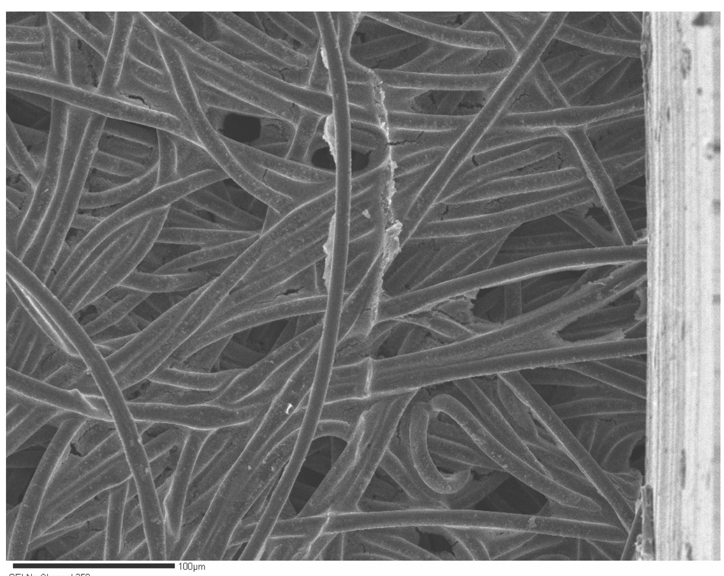

Figure E.32. This image is the sample with no channels and is taken at 250x magnification. The material appears to have shifted away from the wall this time. In the bottom right the hole in the binder along the wall appears it may have ripped larger than it was originally, as the amount of binder in figure E.29 appears to be more than is left now.

E.1.9 Compression Force and Ring Removed

This series of tests could not be continued any further due to the springs almost reaching their solid length. This indicates the force to compress this material is significantly higher than required for the baseline material.

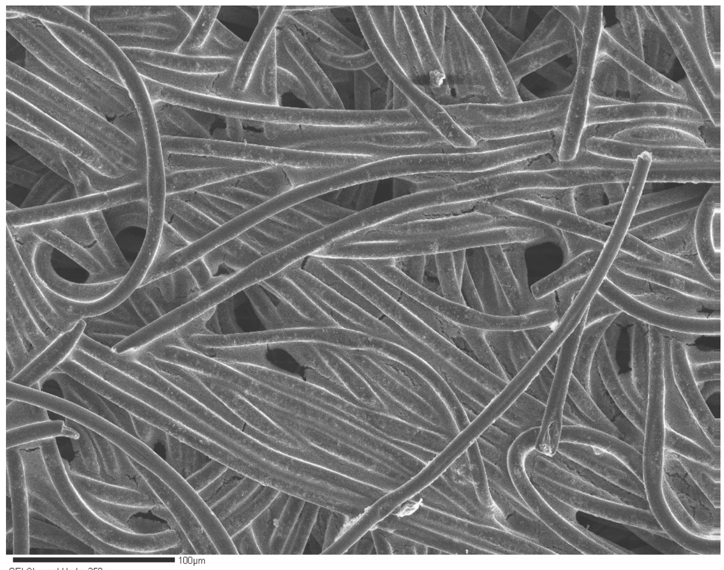

Figure E.33. This image is the sample with a channel underneath imaged at 250x magnification. There is very little residual damage remaining from the tests, and this is expected somewhat due to the channel underneath relieving some of the stress applied.

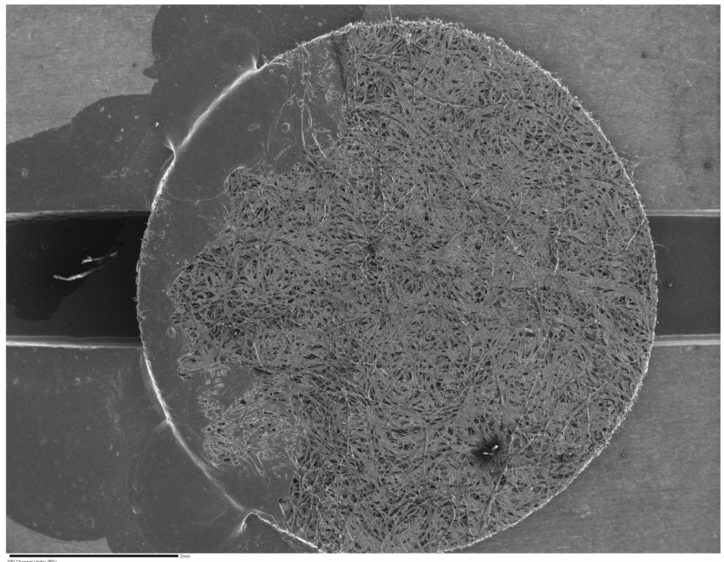

Figure E.34. This image is the sample imaged at 13x magnification. Unlike the baseline material there is not an obvious line denoting the compressed area and the uncompressed area on the sample. The bright spots surrounded by darkness are again dust or other particles that charge and affect the contrast.

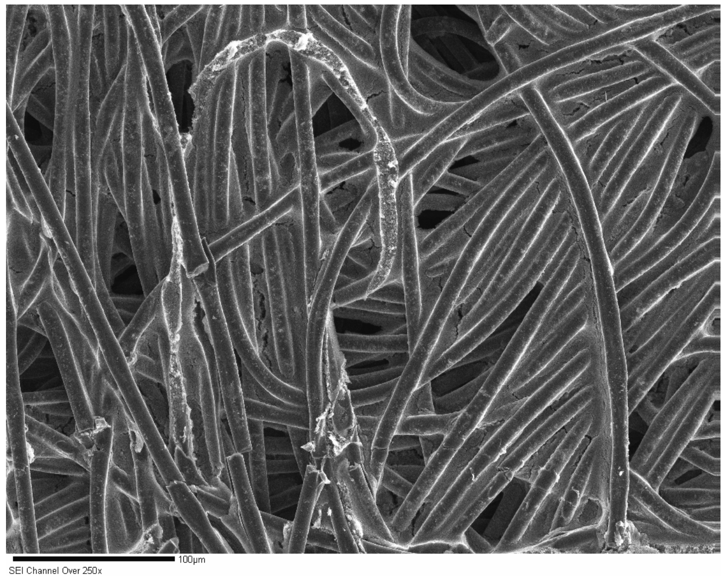

Figure E.35. This image is the sample that had a channel pressing down on it, and is imaged at 250x magnification. A lot of damage is observed in this image. A large piece of fiber appears to have been ripped out and a charging ghost left behind. Along the bottom where the ring was a lot of cracked fibers can be observed. This sample was not tilted like the other images so some shifting of features is expected.

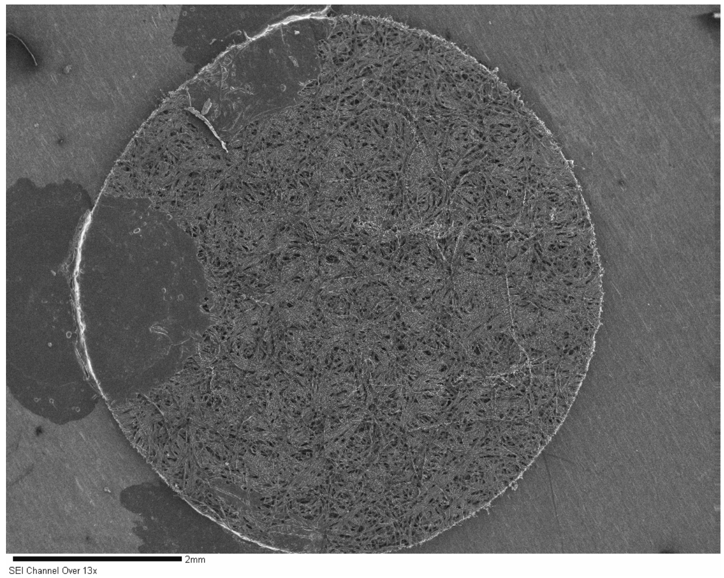

Figure E.36. This image shows the same sample at 13x magnification. Some portions of a damage line can be observed in this image, but it is still not as distinct as the baseline material had for these lines. It is interesting that the top edge of the channel left more of a imprint then the bottom edge.

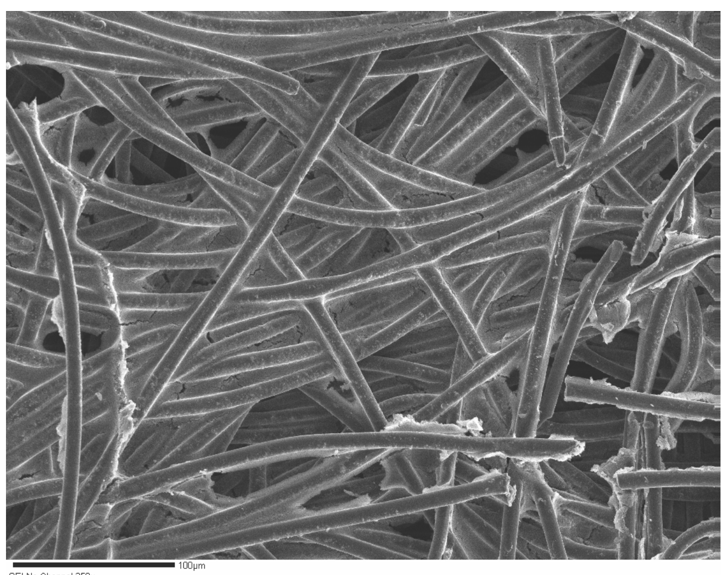

Figure E.37. This image shows the sample with no channels on it at 250x magnification. A significant amount of damage is observed as would be expected. A lot of the broken fibers appear to start approximately 100 microns inside from where the edge of the ring was. The cause of this is unknown.

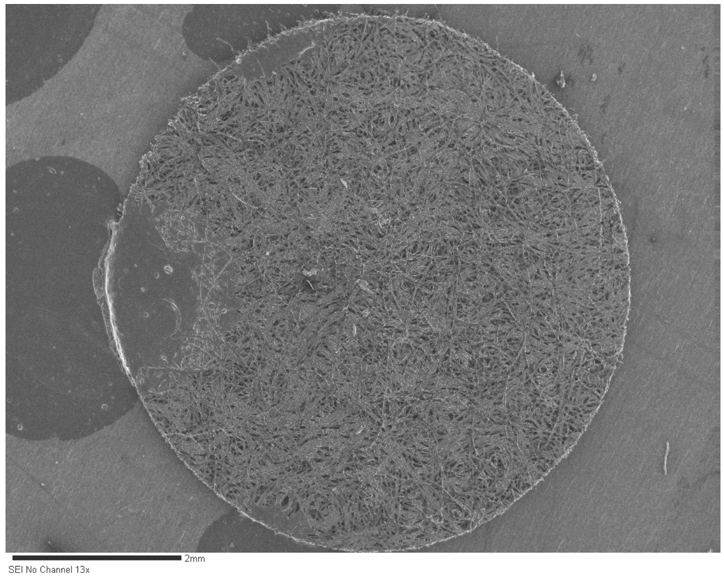

Figure E.38. This is the same sample at 13x magnification. Again very little of a damage line is observable at this magnification, in contrast with the baseline results.

F. IMAGE LIBRARY OF TORAY TGD-H-060 9% PTFE WET-PROOFED GDL

F.1 Incremental Compression Imaging Results, Six Single Samples w/Edge

This run of tests was an incrementally increasing load. The accelerating voltage was 10 keV. The Toray TGD-H-060 9% PTFE wet-proofed GDL was chosen and the displacement of the GDL was incrementally increased starting at zero and increasing in increments of 12.7 μm. This increment is the smallest which can be accurately measured with the dial indicators. The GDL was compressed all the way to a total displacement of 76.2 μm. All images taken looking into the channel pressing down were taken with a tilt on the stand of 32.4 degrees, as measured by the SEM gauge.

F.1.1 No Compression, No Rings

The samples were placed on the base, and the positioning was estimated by holding the ring over the samples. The GDL was then painted to the base and imaged. The imaging was taken over a larger area at high resolution to find the location under compression and compare to the compressed images.

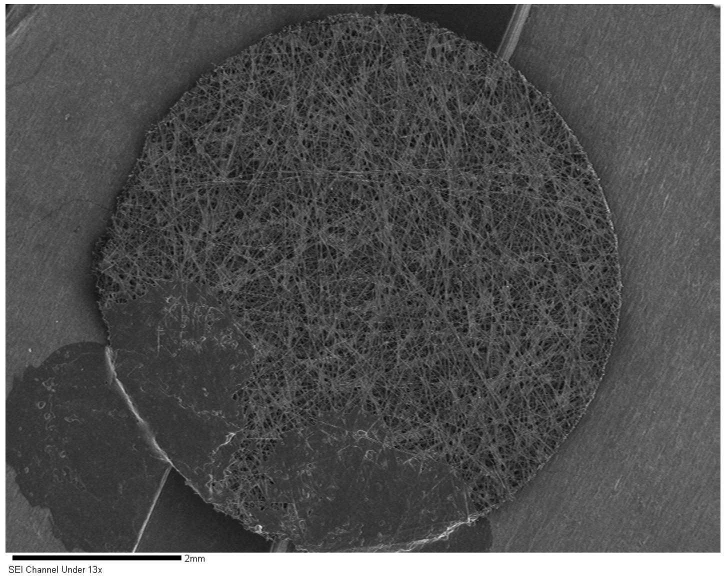

Figure F.1. This image is the sample with a channel running under it at 13x magnification. This image is mainly to calculate the area and for comparing to the image after compression has been applied.

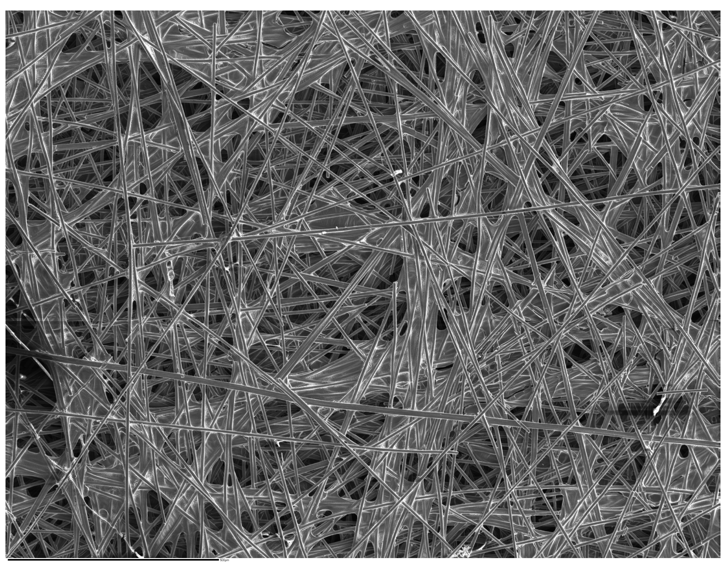

Figure F.2. This image is the sample with a channel running under it at 65x magnification. The image is captured at 3072 pixels, and is in the general area where the compression ring will lie. This will allow for the image to be magnified later on the exact area so comparisons between the original state and the compressed state can be seen.

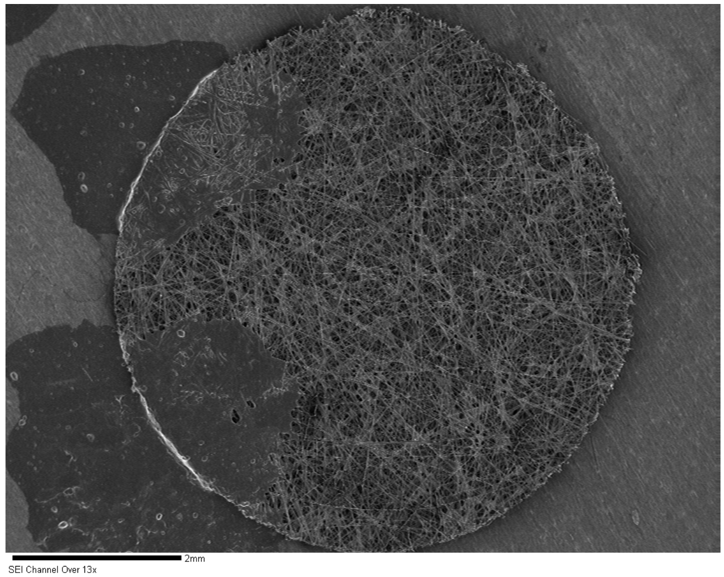

Figure F.3. This image is the sample with a channel running above it at 13x magnification. This image is mainly to calculate the area and for comparing to the image after compression has been applied.

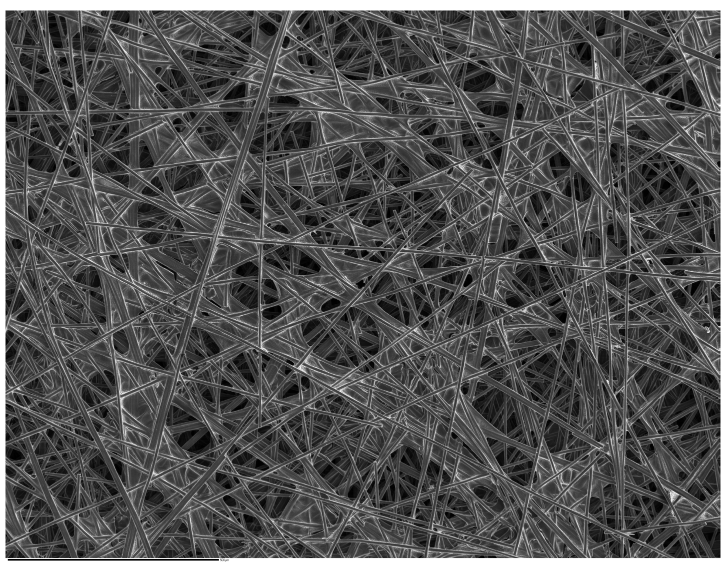

Figure F.4. This image is the sample with a channel running above it at 65x magnification. The image is captured at 3072 pixels, and is in the general area where the compression ring will lie. This will allow for the image to be magnified later on the exact area so comparisons between the original state and the compressed state can be seen.

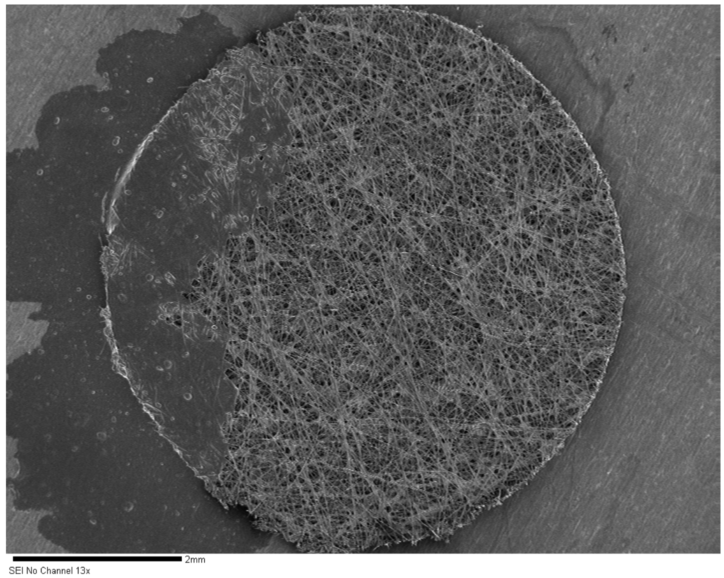

Figure F.5. This image is the sample with no channel affecting it at 13x magnification. This image is mainly to calculate the area and for comparing to the image after compression has been applied.

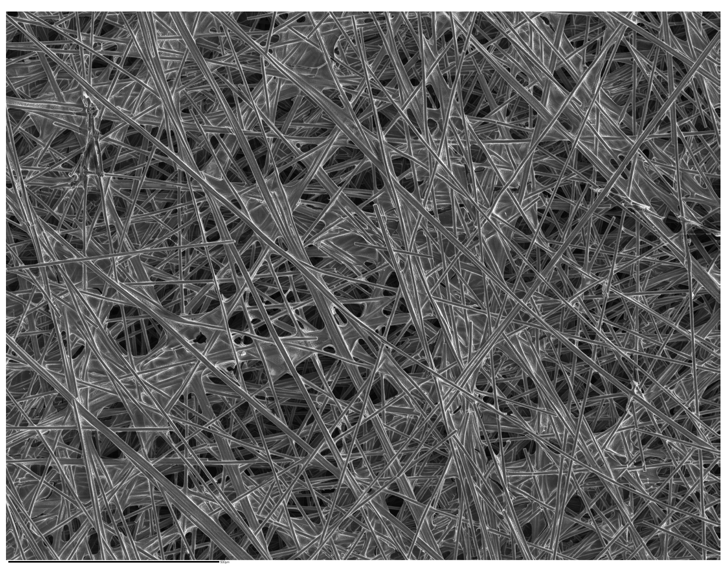

Figure F.6. This image is the sample with no channel affecting it at 65x magnification. The image is captured at 3072 pixels, and is in the general area where the compression ring will lie. This will allow for the image to be magnified later on the exact area so comparisons between the original state and the compressed state can be seen.

F.1.2 No Compression, Rings in Place with no Force Applied

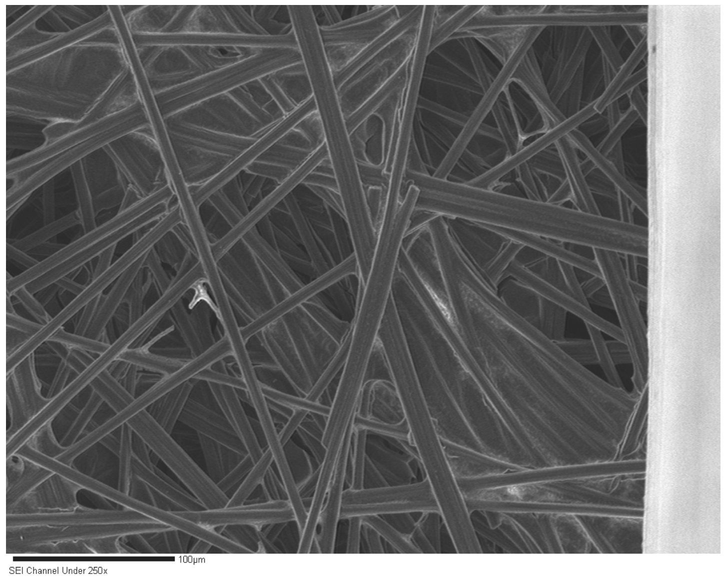

Figure F.7. This image is the sample with a channel running under it at 250x magnification. No damage was observed from the placement of the compressing ring.

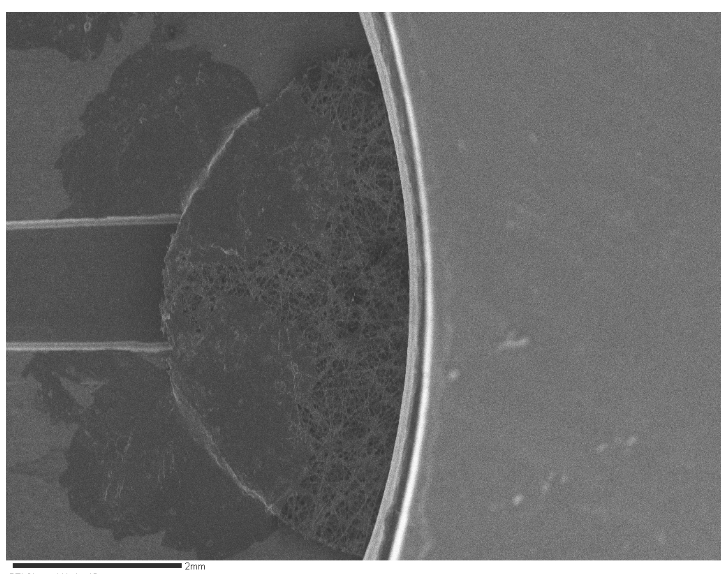

Figure F.8. This image is the sample with a channel running under it at 13x magnification. This image is mainly to calculate the area and for comparing to the image after compression has been applied.

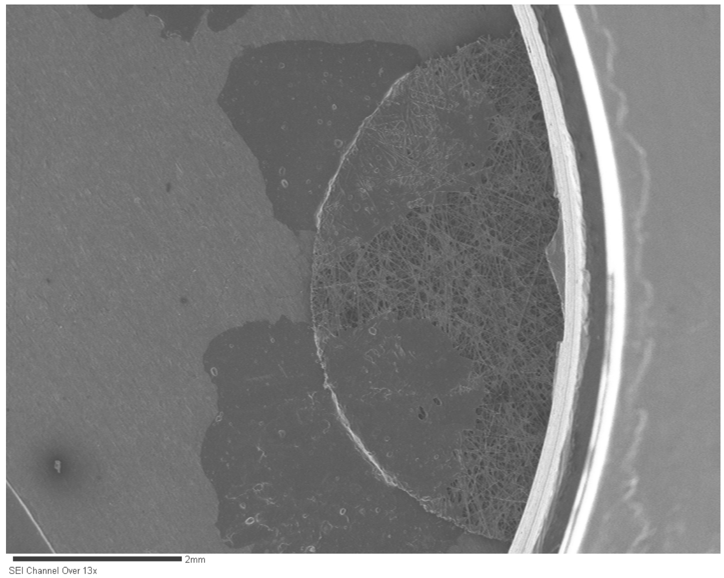

Figure F.9. This image is the sample with a channel running above it at 13x magnification. This image is mainly to calculate the area and for comparing to the image after compression has been applied.

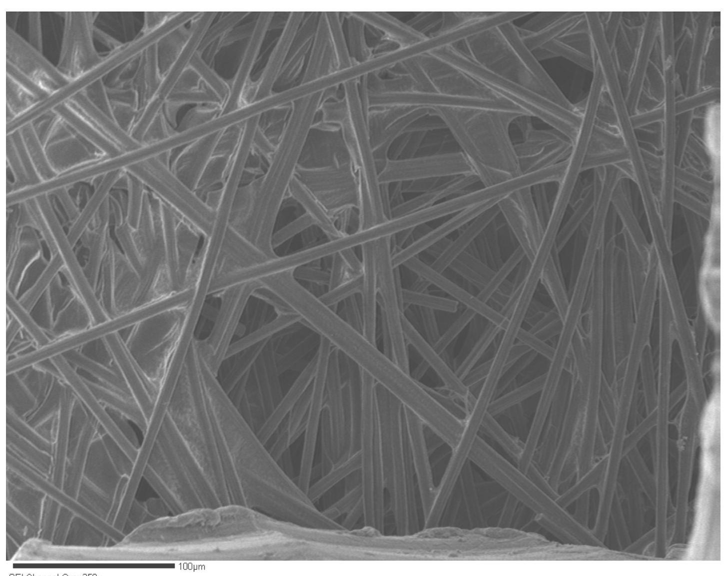

Figure F.10. This image is the sample with a channel running above it at 250x magnification. No damage observed from placement of comprssing ring.

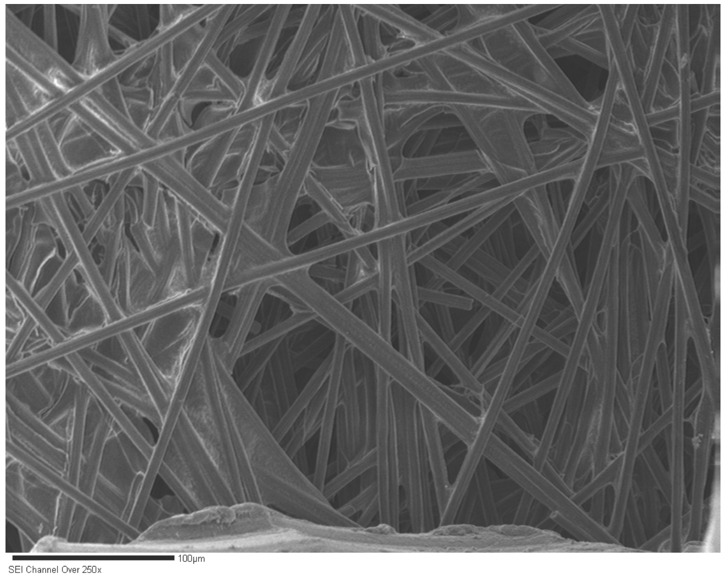

Figure F.11. This image is the sample with a channel running above it at 250x magnification. This is the same image as Figure F.10, the image was recaptured to better focus and adjust the brightness.

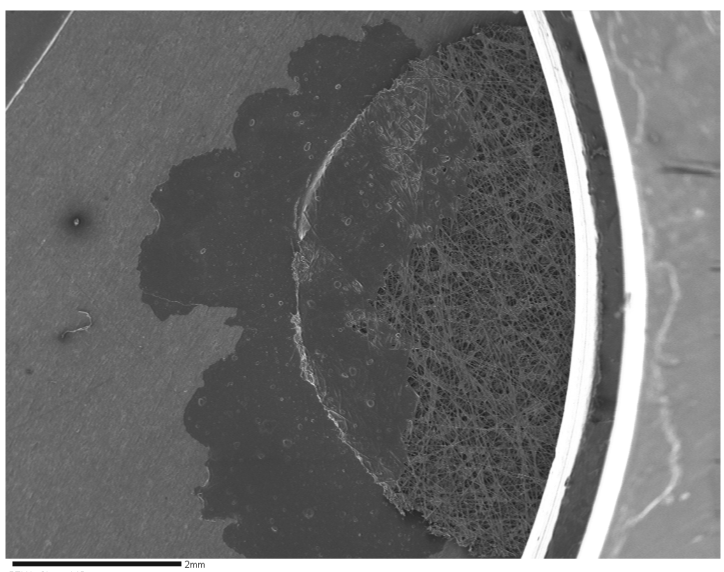

Figure F.12. This image is the sample with no channel affecting it at 13x magnification. This image is mainly to calculate the area and for comparing to the image after compression has been applied.

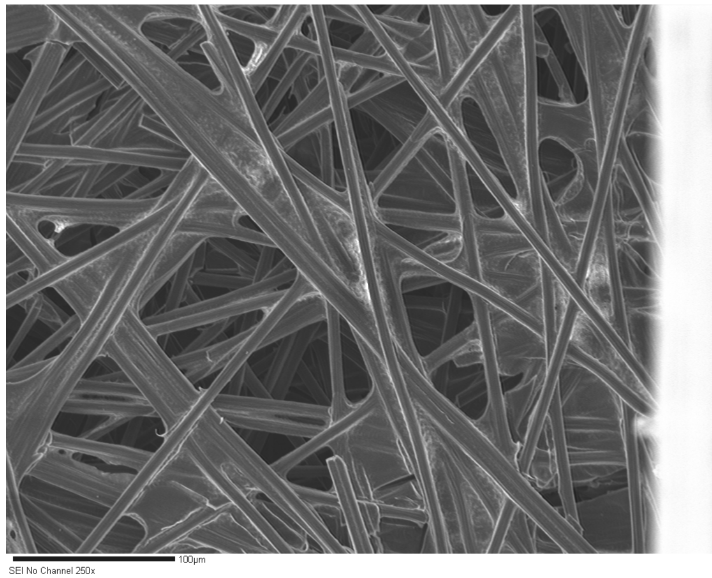

Figure F.13. This image is the sample with no channel affecting it at 250x magnification. This image was too close to the ring and was blurry in that area, it was re-imaged in Figure F.14.

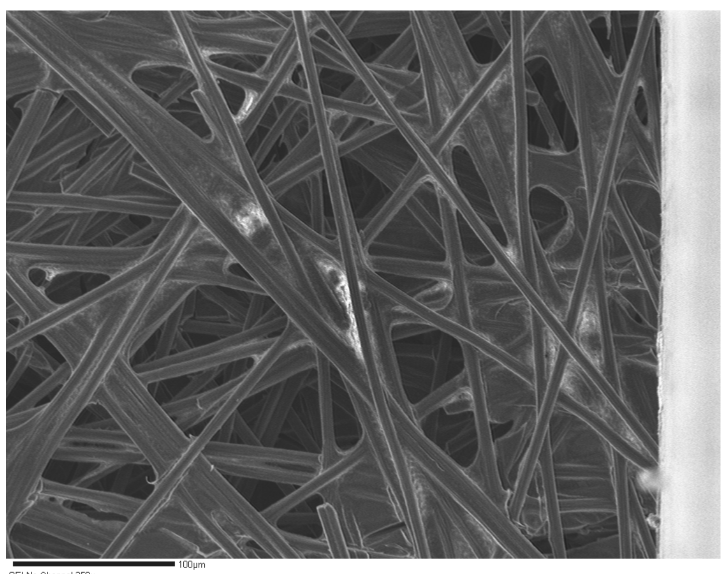

Figure F.14. This image is the sample with no channel affecting it at 250x magnification. This is re-imaged and shows no damage from the ring.

F.1.3 12.7 μm Compression

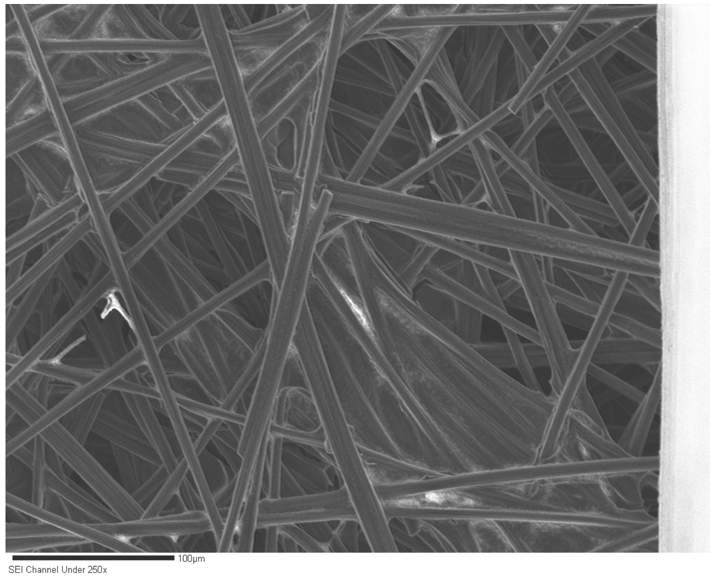

Figure F.15. This image is the sample with a channel running under at 250x magnification. No damage is noted, but a shift of the sample towards the left is seen, however this may be due to correcting the tilt inside the SEM.

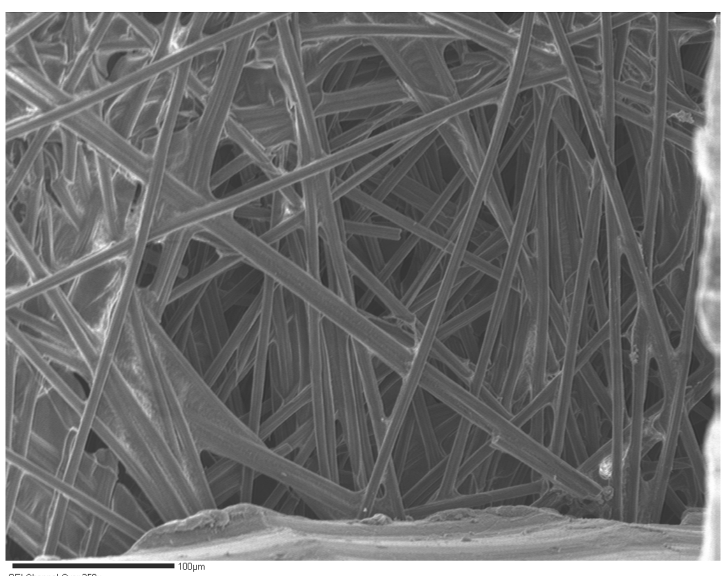

Figure F.16. This image is the sample with a channel above the sample at 250x magnification. The sample is shifted as well, moving towards the top of the image. This may be due to tilting on the sample as well as general shifting of the GDL caused by compressing the GDL.

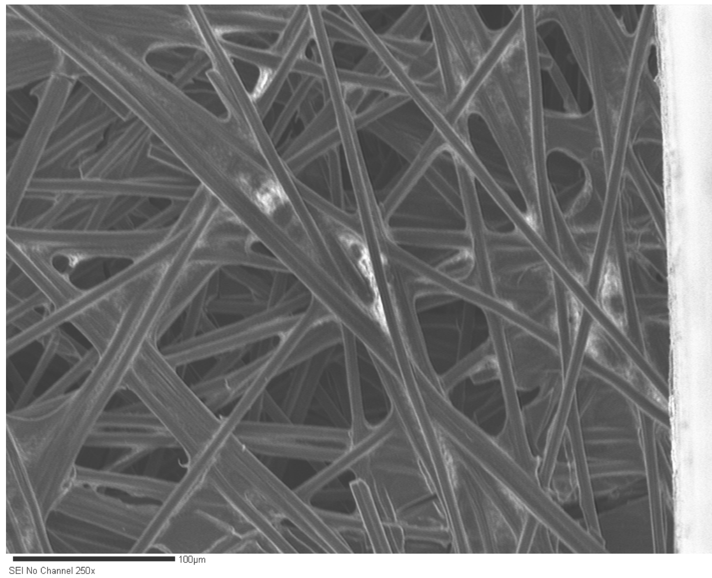

Figure F.17. This image is the sample with no channel affecting the sample at 250x magnification. Again a slight shift to the left is seen when the compression is added.

F.1.4 25.4 μmCompression

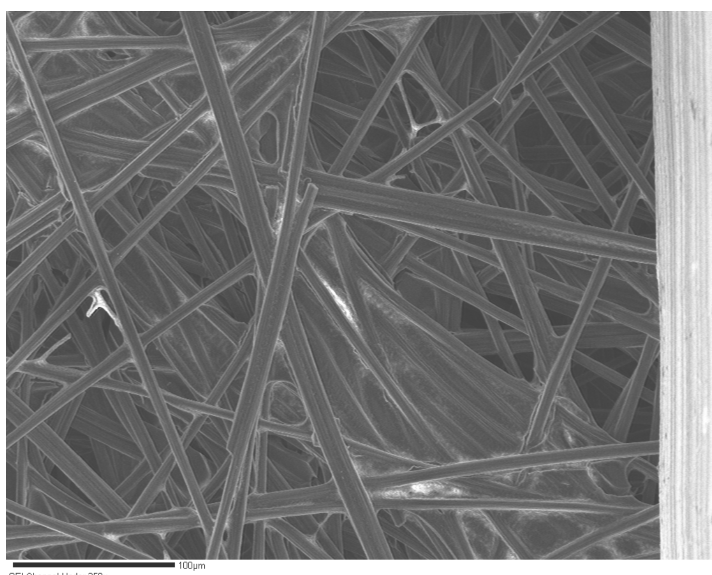

Figure F.18. This image is the sample with a channel running under at 250x magnification. No additional damage is observed, and a small shift is seen, but is reversed so may be due to correcting for the tilt.

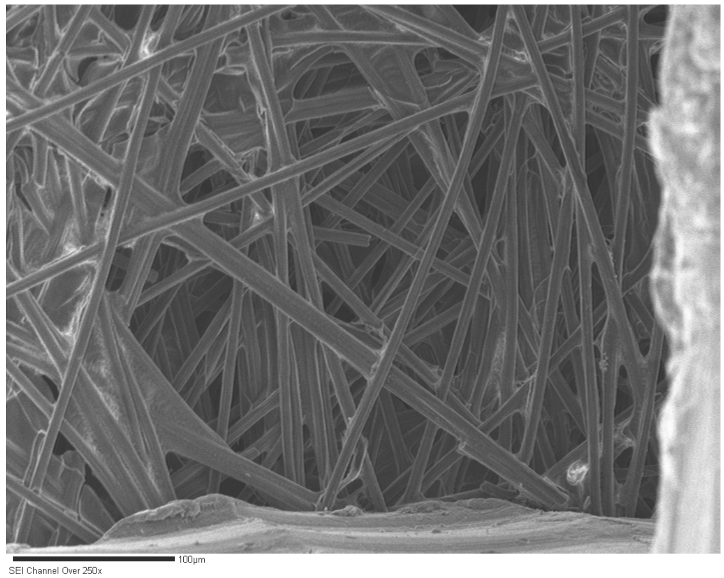

Figure F.19. This image is the sample with a channel above the sample at 250x magnification. No damage and a small shift is seen after the compression.

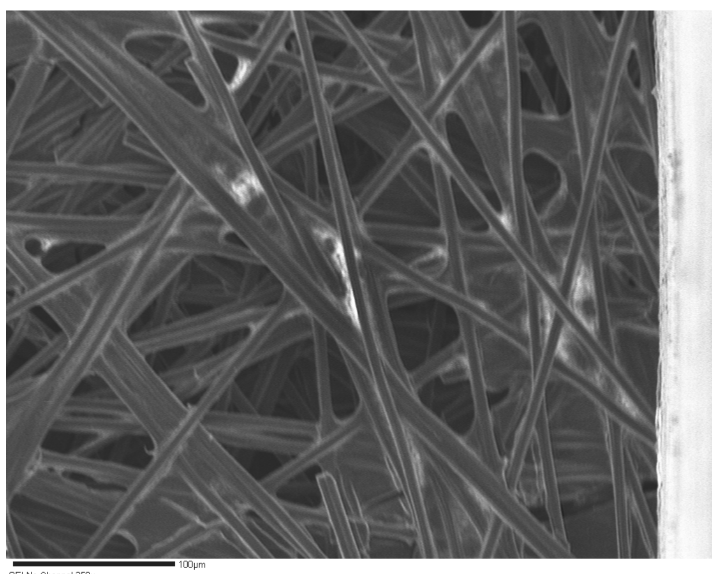

Figure F.20. This image is the sample with no channel affecting the sample at 250x magnification.

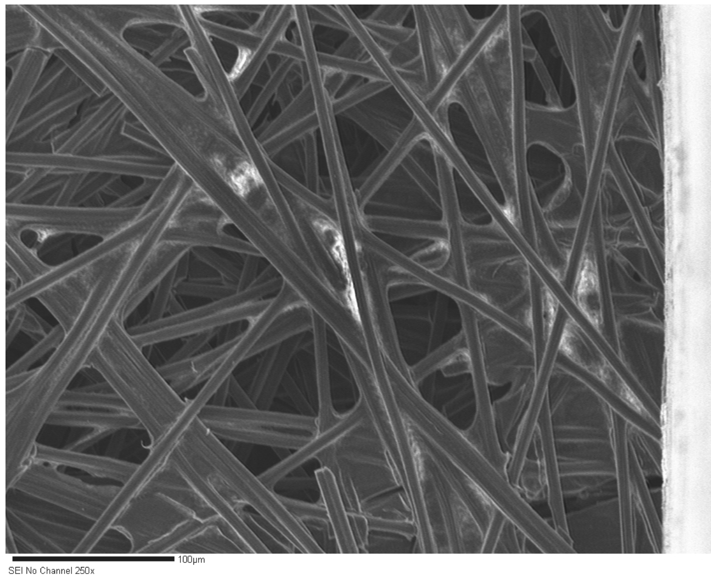

Figure F.21. This image is the sample with no channel affecting the sample at 250x magnification, and is a re-focused image of the same area as Figure F.20. No damage is observed from the compression.

F.1.5 38.1 μm Compression

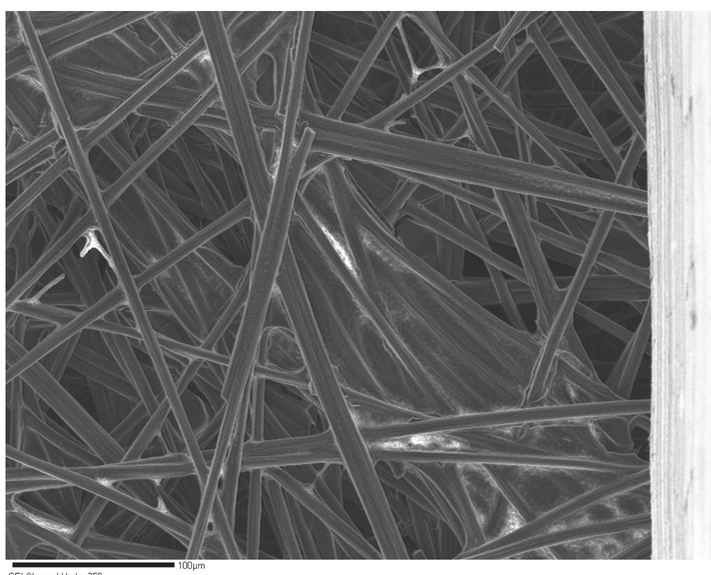

Figure F.22. This image is the sample with a channel running under at 250x magnification. No obvious damage is seen, some minor tearing between the fibers and connective materials may be occuring near the middle of the image.

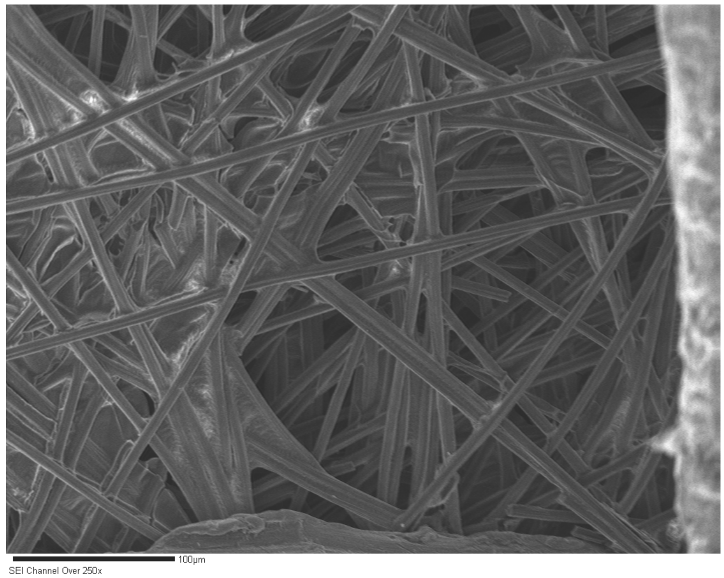

Figure F.23. This image is the sample with a channel above the sample at 250x magnification. Near the bottom right of the image, a fiber can be seen as broken and shifted compared to Figure F.19. Also the fibers along the right appear bent at more of an angle and some tearing appears to be occuring near the upper left corner.

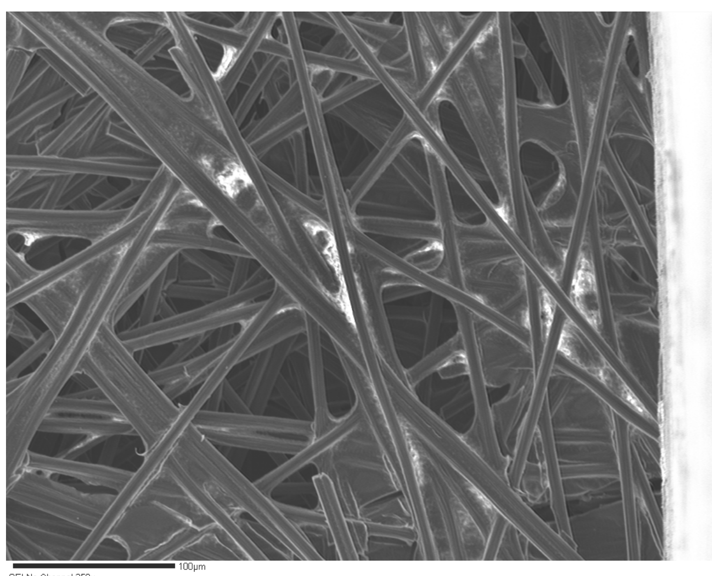

Figure F.24. This image is the sample with no channel affecting the sample at 250x magnification. No damage or shifting is observed in this image.

F.1.6 50.8 μm Compression

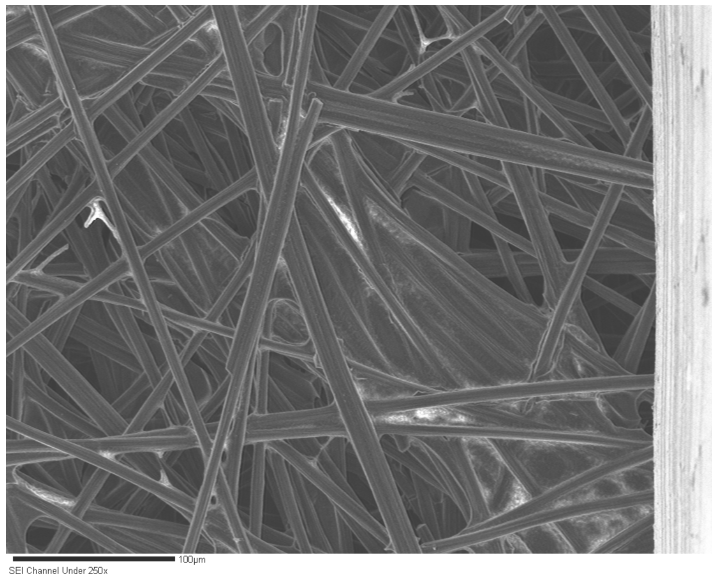

Figure F.25. This image is the sample with a channel running under at 250x magnification. No damage or shifting is observed in this image.

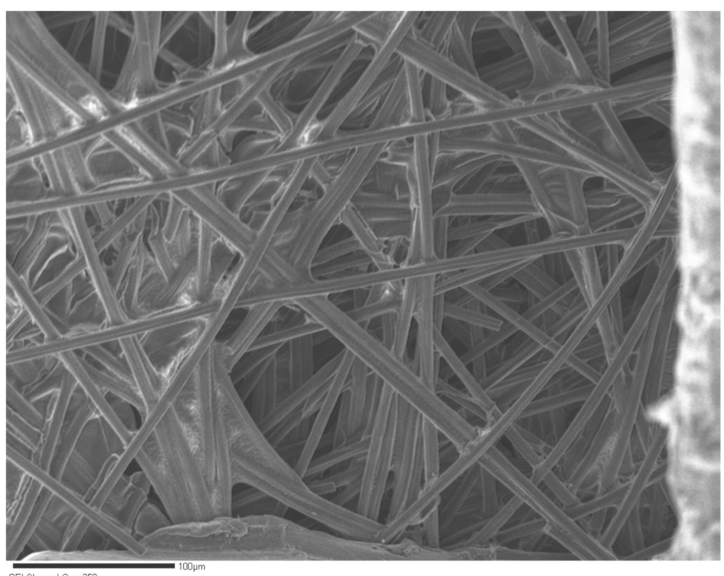

Figure F.26. This image is the sample with a channel above the sample at 250x magnification. The fiber in the bottom left is now raised and is clearly seen against the ring edge. The snapped fibers in the bottom right are no longer visible, and the binding material near the bottom left appears to have separated somewhat.

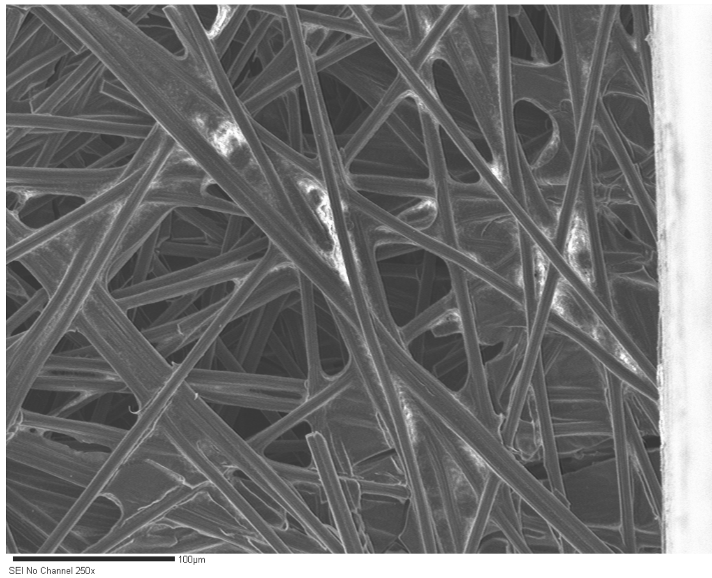

Figure F.27. This image is the sample with no channel affecting the sample at 250x magnification. No damage or shifting is observed in this image.

F.1.7 63.5 μm Compression

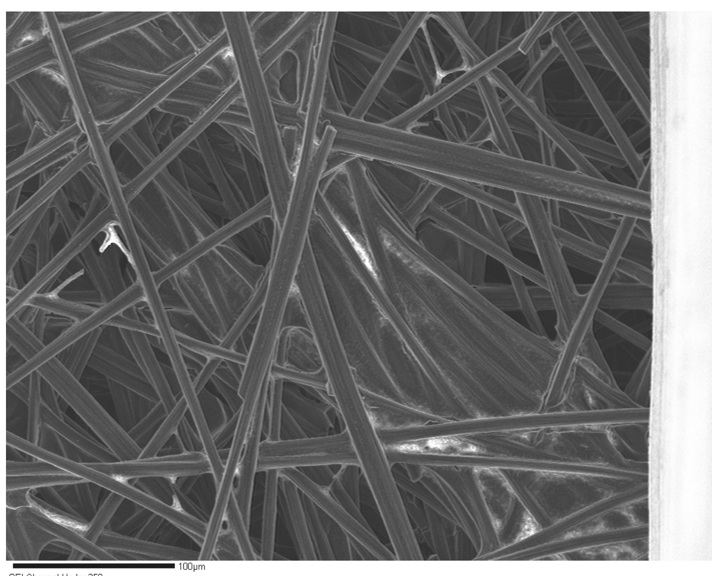

Figure F.28. This image is the sample with a channel running under at 250x magnification. A small amount of minor tearing appears near the upper middle and left middle, but is very minor. A small shift to the right is seen near the edges again.

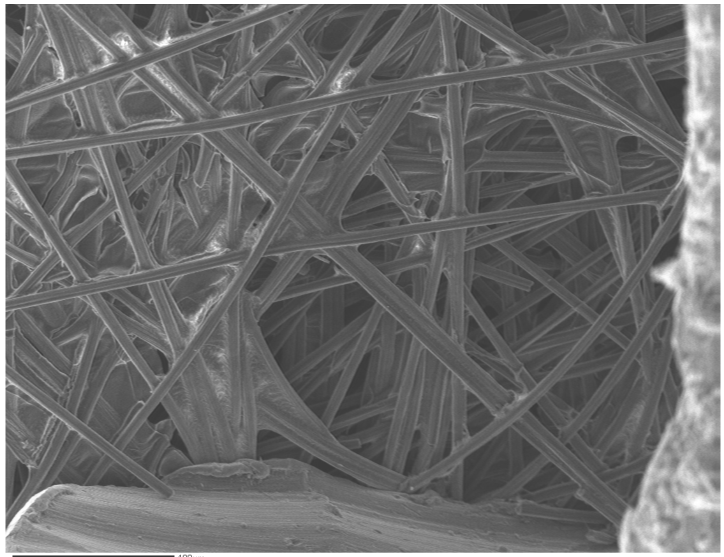

Figure F.29. This image is the sample with a channel above the sample at 250x magnification. The fiber in the bottom left is still raised, and a new fiber along the bottom right is visible against the ring edge.

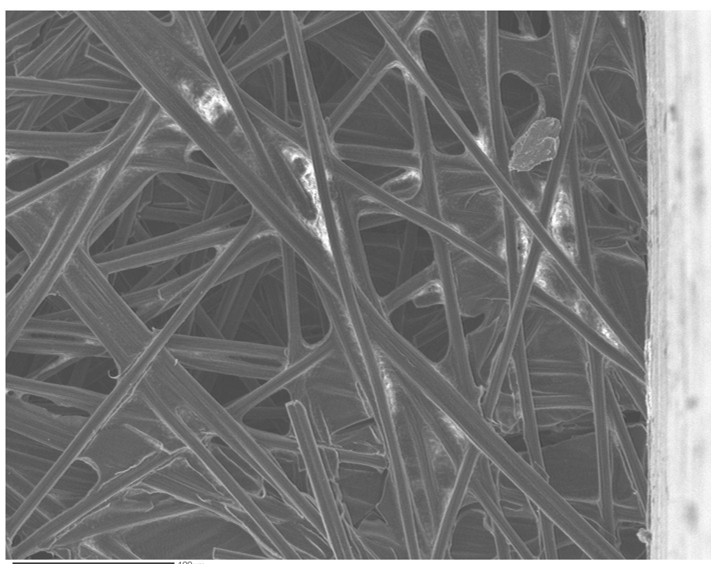

Figure F.30. This image is the sample with no channel affecting the sample at 250x magnification. A small object is visible in the upper right, but is likely a piece of dust or metal shaving and is not part of the GDL. No other damage or shifting is observed.

F.1.8 76.2 μm Compression

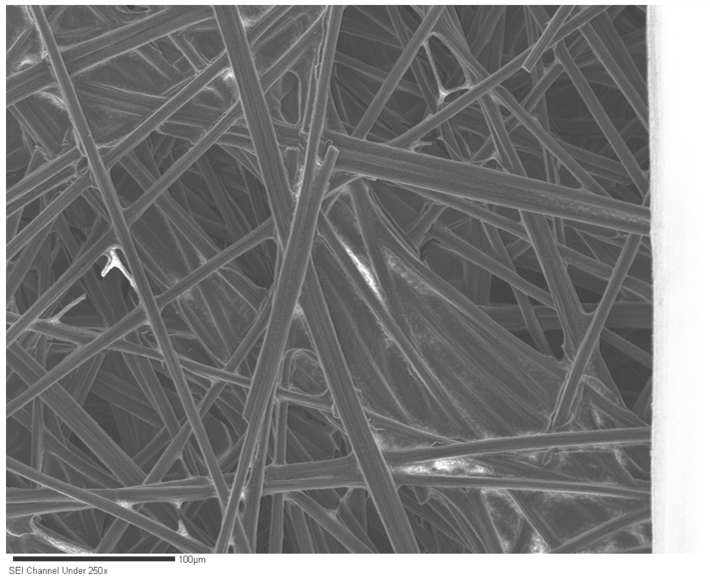

Figure F.31. This image is the sample with a channel running under at 250x magnification. No damage is observed and a very minor shift to the right is seen.

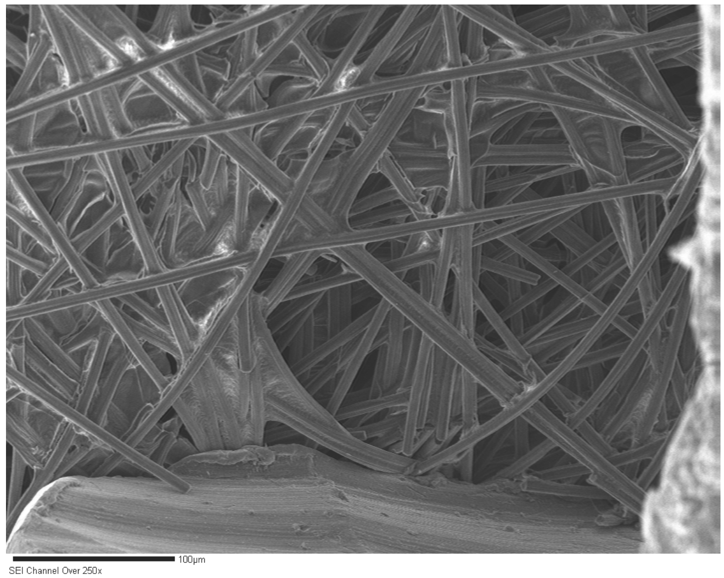

Figure F.32. This image is the sample with a channel above the sample at 250x magnification. Several fibers running vertically down the middle can be seen to be snapped and the snapped ends are seen pushing below the other fibers leading to the bottom edge. Also near the bottom left corner something, possible a developing hole, is seen in the coating over the fiber.

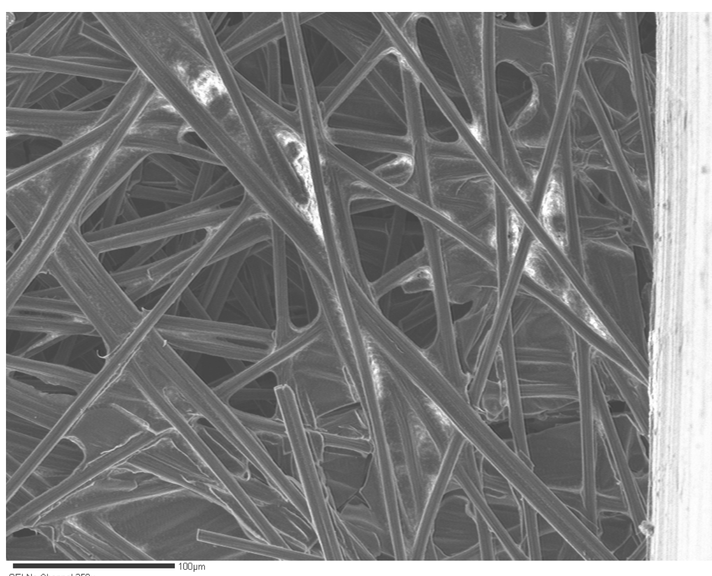

Figure F.33. This image is the sample with no channel affecting the sample at 250x magnification. The particle is gone, and some shifting to the left this time is observed in the sample.

F.1.9 Compression Force and Ring Removed

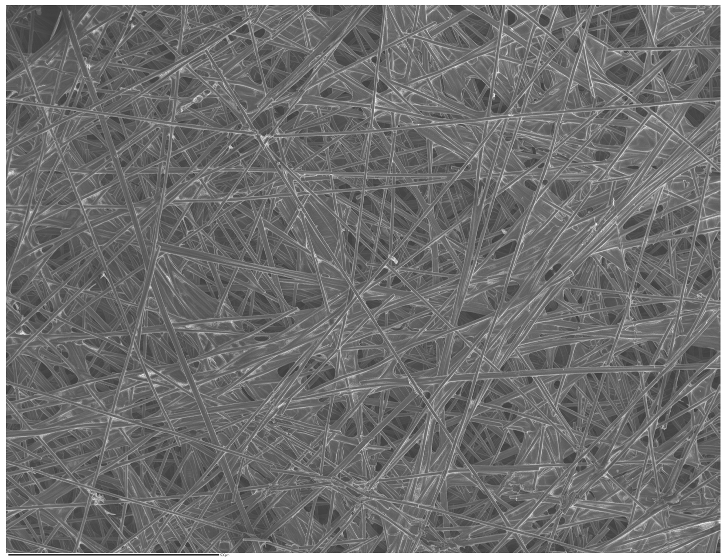

Figure F.34. This image is the sample with a channel running under at 65x magnification. Damage can be observed in the form of snapped fibers, and some loss of depth of field in the image.

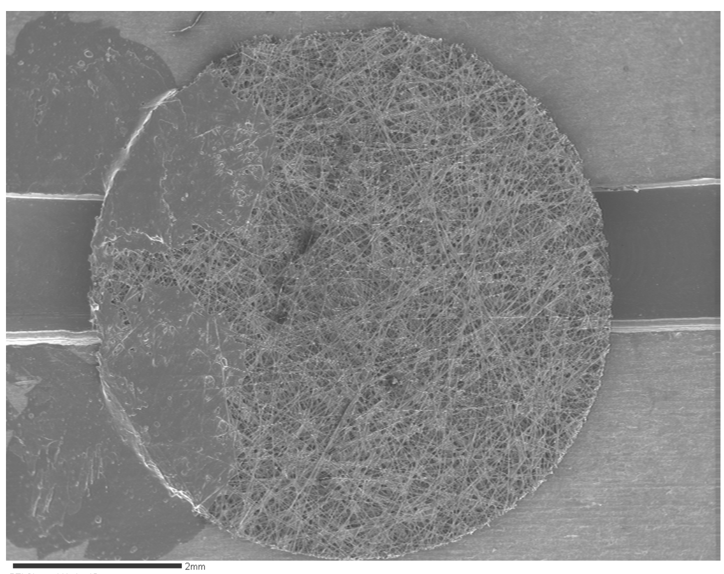

Figure F.35. This image is the sample with a channel running under at 13x magnification. This image was taken for area calculation. The damage line is not apparant in the image.

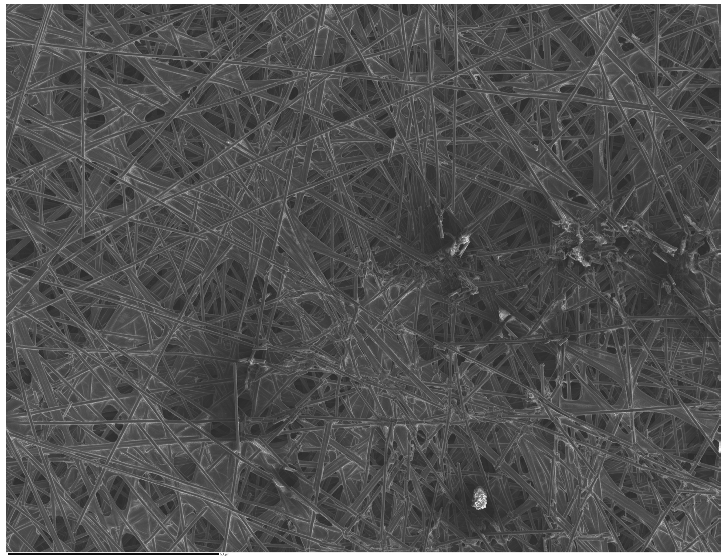

Figure F.36. This image is the sample with a channel above the sample at 65x magnification. A lot of damage can be seen, as many fibers are snapped, and in some areas are so detached they actually begin charging and affecting the image. The bottom right of Figure F.4 corresponds to the large damage cluster in the middle right of this image. The fibers are badly damaged and the materials appear to have torn loose and begun charging.

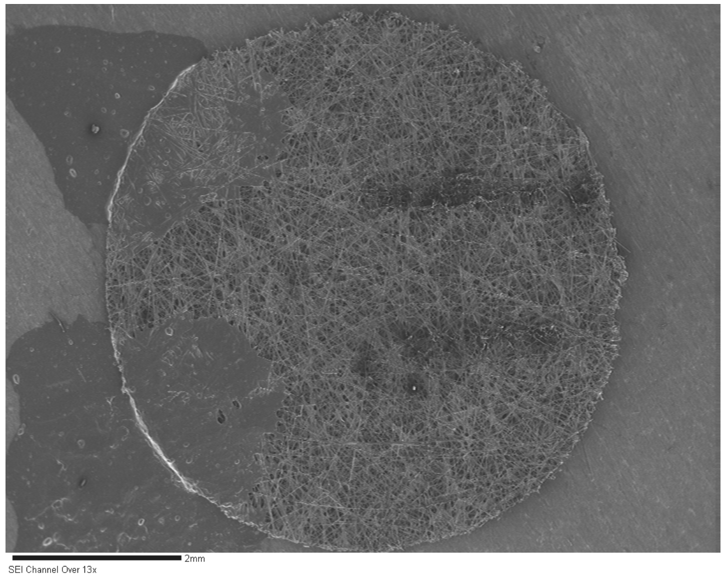

Figure F.37. This image is the sample with a channel above the sample at 13x magnification. This image was used for calculating area, however the area where the channel edges pressed down are readily apparant in the image and the darker charging areas.

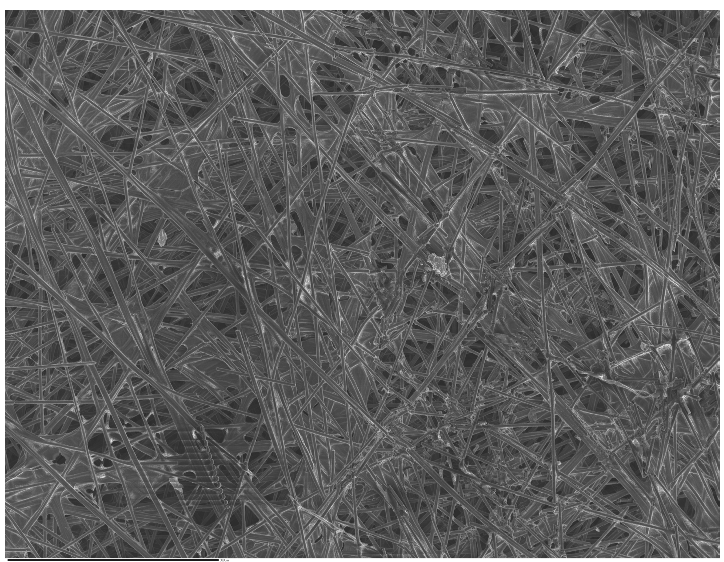

Figure F.38. This image is the sample with no channel affecting the sample at 65x magnification. Again a lot of damage is evident in this image, many long fibers are now snapped in multiple locations and the depth of field appears reduced in most areas. Interestingly their appears to be little charging due to the damage as opposed to Figure F.36.

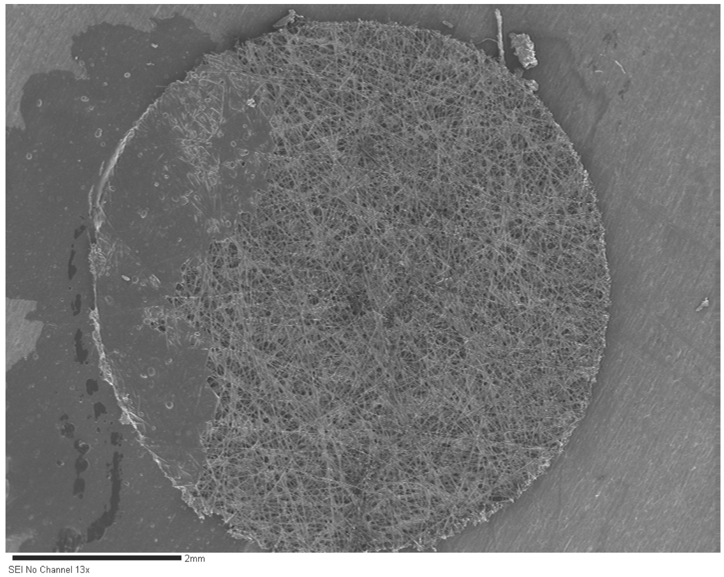

Figure F.39. This image is the sample with no channel affecting the sample at 13x magnification. This image was used for calculating area. A few areas of charging can be seen, but an overall line marking the edge of the ring is not visible.

REFERENCES

[1] Iwao Nitta, Tero Hottinen, Olli Himanen, and Mikko Mikkola. Inhomogeneous compression of PEMFC gas diffusion layer: Part i. experimental. *Journal of Power Sources*, 171(1):26–36, 2007.

[2] Lin Wang and Hongtan Liu. Separate measurement of current density under the channel and the shoulder in PEM fuel cells. *Journal of Power Sources*, 180(1): 365–372, 2008.

[3] Z. Y. Su, C. T. Liu, H. P. Chang, C. H. Li, K. J. Huang, and P. C. Sui. A numerical investigation of the effects of compression force on PEM fuel cell performance. *Journal of Power Sources*, 183(1):182–192, 2008.

[4] P. Zhou and C. W. Wu. Numerical study on the compression effect of gas diffusion layer on PEMFC performance. *Journal of Power Sources*, 170(1):93–100, 2007.

[5] Andreas Wiegmann Jurgen Becker, Volker Schulz. Numerical determination of two-phase material parameters of a gas diffusion layer using tomography images. *Journal of Fuel Cell Science and Technology*, Vol. 5(May 2008), 2008.

[6] A. Bazylak, D. Sinton, Z. S. Liu, and N. Djilali. Effect of compression on liquid water transport and microstructure of PEMFC gas diffusion layers. *Journal of Power Sources*, 163(2):784–792, 2007.

[7] Sylvie Escribano, Jean-Franois Blachot, Jrmy Ethve, Arnaud Morin, and Renaut Mosdale. Characterization of PEMFCs gas diffusion layers properties. *Journal of Power Sources*, 156(1):8–13, 2006.

[8] N. Fekrazad. The effect of compressive load on proton exchange membrane fuel cell stack performance and behavior. *Journal of Heat Transfer*, 129:1004–1013, 2007.

[9] J. P. Feser, A. K. Prasad, and S. G. Advani. Experimental characterization of in-plane permeability of gas diffusion layers. *Journal of Power Sources*, 162(2): 1226–1231, 2006.

[10] C. Lim and C. Y. Wang. Development of high-power electrodes for a liquid-feed direct methanol fuel cell. *Journal of Power Sources*, 113(1):145–150, 2003.

[11] Caishun Lin, Tongtao Wang, Feng Ye, Yong Fang, and Xindong Wang. Effects of microporous layer preparation on the performance of a direct methanol fuel cell. *Electrochemistry Communications*, 10(2):255–258, 2008.

[12] Iwao Nitta, Olli Himanen, and Mikko Mikkola. Contact resistance between gas diffusion layer and catalyst layer of PEM fuel cell. *Electrochemistry Communications*, 10(1):47–51, 2008.

[13] ASM International Handbook Committee. *ASM Handbook Volume 8 Mechanical Testing and Evaluation*, volume 8. ASM International Handbook Committee, 2000.

[14] J. Kleemann, F. Finsterwalder, and W. Tillmetz. Characterisation of mechanical behaviour and coupled electrical properties of polymer electrolyte membrane fuel cell gas diffusion layers. *Journal of Power Sources*, 190(1):92–102, 2009.

[15] Derek Fultz. General motors, compression testing data. *Personal Communication*, September 26, 2008.

[16] Paul Nicotera. General motors, compression testing methods. *Personal Communication*, April 1, 2009.

[17] J. P. Holman. *Experimental Methods for Engineers*. The McGraw-Hill Companies, Inc., New York, seventh edition edition, 2001.